Impulse radio ultra wideband over fiber techniques for broadband in-building network applications

DOI:
10.6100/IR735363

Document status and date:
Published: 01/01/2012

Document Version:
Publisher's PDF, also known as Version of Record (includes final page, issue and volume numbers)

Impulse Radio Ultra Wideband over Fiber Techniques for Broadband In-Building Network Applications

PROEFSCHRIFT

ter verkrijging van de graad van doctor aan de
Technische Universiteit Eindhoven, op gezag van de
rector magnificus, prof.dr.ir. C.J. van Duijn, voor een
commissie aangewezen door het College voor
Promoties in het openbaar te verdedigen
op woensdag 29 augustus 2012 om 16.00 uur

door

Solomon Tesfay Abraha

geboren te Adigrat, Ethiopië

Dit proefschrift is goedgekeurd door de promotor:

prof.ir. A.M.J. Koonen

Copromotor:
dr.ir. E. Tangdiongga

This Ph.D. thesis has been approved by a committee with the following members:

prof.dr.ir. A.H.M. van Roermund(chairman), Technische Universiteit Eindhoven
prof.ir. A.M.J. Koonen(first promotor), Technische Universiteit Eindhoven
dr.ir. E. Tangdiongga(copromotor),Technische Universiteit Eindhoven
prof.dr.ir. P.G.M. Baltus, Technische Universiteit Eindhoven
prof.dr. B. Ortega Tamarit, Universidad Politecnica de Valencia
prof.dr. A. Yarovoy, Technische Universiteit Delft
prof.dr.ir. S. Heemstra de Groot, Technische Universiteit Delft
dr. N. Gomes, University of Kent

A catalogue record is available from the Eindhoven University of Technology Library
Impulse radio ultrawideband over fiber techniques for broadband in-building network applications/ by Solomon Tesfay Abraha
Eindhoven: Technische Universiteit Eindhoven, 2012
Proefschrift.-ISBN: 978-90-386-3212-4
NUR 959
Trefwoorden: Opische telecommunicatie/ radio-over-glasvezel/ magnetron fotonica/ plastic optische vezel.
Subject headings: optical fiber communication/ radio-over-fiber/microwave photonics/plastic optical fiber.

Typeset using LaTeX, printed in the Netherlands

Summary

Essays on Impulse Radio Ultra Wideband over Fiber Techniques for Broadband In-Building Network Applications

In recent years, the demand for high bandwidth and mobility from the end users has been continuously growing. To satisfy this demand, broadband communication technologies that combined the benefit of both wired and wireless are considered as vital solutions. These hybrid optical wireless solutions enable multi-Gbit/s transmission as well as adequate flexibility in terms of mobility. Optical fiber is the ideal medium for such hybrid solution due its signal transparency and wide bandwidth. On the other hand, ultra wideband(UWB) radio over optical fiber technology is considered to be one of the key promising technologies for broadband communication and sensor network applications. The growing interest for UWB is mainly due to its numerous attractive features, such as low power spectral density, tolerance to multipath fading, low probability of interception, coexistence with other wireless services and capability of providing cost-effective $>$ 1 Gb/s transmission. The main idea of UWB over fiber is to deliver UWB radio signals over optical channels, where the optical part serves as a backbone communication infrastructure to carry the UWB signal with a bandwidth of several GHz. This enables multiple novel applications such as: range extension of high speed wireless personal area networks (WPANs), low cost distributed antenna systems, secure and intelligent networks, or delivering broadband services to remote areas. In particular, this thesis deals with novel concepts on shaping and generation of IR-UWB pulses, theoretical and experimental demonstrations over different fiber types, routing of integrated wired/wireless IR-UWB services and effect of fiber types on ranging/localization of IR-UWB-over-fiber systems.

Accordingly, this thesis investigates techniques for delivery of high data rate wireless services using impulse radio ultra wideband (IR-UWB) over fiber technology for both access and in-building network applications. To effectively utilize the emission mask imposed for UWB technologies by the Federal

Communications Commission(FCC), novel pulse shaping techniques have been investigated and experimentally demonstrated. Comparison of the proposed pulses with conventional ones in terms of the compliance to the FCC-mask requirements, spectral power efficiencies and wireless coverage has been theoretically studied. Simple and efficient optical generation of the new pulse has been experimentally demonstrated. Furthermore, performance evaluation of 2 Gb/s transmission of IR-UWB over different types of fiber such as 25 km silica single-mode, 4.4 km silica multi-mode and 100 m plastic heavily-multi-mode fiber have been performed.

To improve the functionalities of in-building networks for the delivery of wireless services; techniques that provide flexibility in terms of dynamic capacity allocation have been investigated. By employing wavelength conversion based on cross-gain modulation in optical semiconductor amplifiers(SOA), routing of three optical channels of IR-UWB over fiber system has been experimentally realized. To reduce the cost of the overall system and share the optical infrastructure, an integrated testbed for wired baseband data and wireless IR-UWB over 1 km SMF-28 fiber has been developed. Accordingly, 1.25 Gb/s wired baseband and 2 Gb/s wireless IR-UWB data have been successfully transmitted over the testbed. Furthermore, to improve the network flexibility, routing of both wired baseband and wireless signals has been demonstrated.

Additionally, the ranging and localization capability of IR-UWB over fiber for in-door wireless picocells have been investigated. The effect of different fiber types (4 km SMF, 4.4 km GI-MMF and 100 m PF GI-POF) on the accuracy of the range estimation using time-of-arrival (ToA) ranging technique has been studied. A high accuracy in terms of cm level was achieved due to the combined effect of high bandwidth IR-UWB pulses, short reach fiber and low chromatic dispersion at $1300nm$ wavelength. Furthermore, ranging/localization using IR-UWB over fiber system provides additional benefit of centralizing complex processing algorithms, simplifying radio access points, relaxing synchronization requirement, enabling energy-efficient and efficient traffic management networks.

All the concepts, design and system experiments presented in this thesis underline the strong potential of IR-UWB for over optical fiber(silica and plastic) techniques for future smart, capacity and energy-efficient broadband in-building network applications.

Contents

Chapter 1

IR-UWB over Fiber: A System Approach

In recent years, there has been growing interest for high capacity, mobility, flexibility, low cost and energy-efficient integration of wired/wireless over a single in-building optical network infrastructure in order to provide both broadband communications and sensor applications. Accordingly, IR-UWB-over-fiber technology, a key enabler for merging of broadband wired and wireless IR-UWB services in high-capacity and energy-efficient in-building networks is the central investigation topic of this thesis.

This introductory chapter starts with discussing the benefits of telecommunication technologies (wired and wireless) and brief overview of trends in different wireless networks in section 1.1. Then, section 1.2, presents a brief overview of the characteristics, benefits and variants of UWB techniques, followed by applications and challenges of UWB technology in section 1.3 and 1.4 respectively. The main motivation and possible applications of IR-UWB over fiber solutions are presented in section 1.5. The scope and contributions of this thesis are presented in section 1.6. Finally, the outline of the thesis is given in section 1.7.

1.1 Emerging Telecommunication Technologies

Since the beginning, communication has been an integral part of human life and the need for better technology to support our evolving communication needs has been growing continuously. Over the centuries, we have witnessed several different methods of communication (both wired and wireless)to overcome the barrier of distance. With people becoming increasingly nomadic, the need for communication with business partners all over the world and with loved ones at home while on the move, has increased. This is the basis of the worldwide success of mobile telephony [1]. Today, in fact, nothing stops us from sending video and audio messages to any place on the earth. Accordingly, migrant workers are able to share information and have voice conversations with their families on the other side of the planet at relatively low cost. At the same time, the mode of communication has become richer and more varied. This rich communication for people on the move is becoming possible due to fast growth of information and communication technology (ICT), which is the merger of telecommunication technologies and informatics. Note that, rich communication is not limited to human interaction. Hence, nowadays, technology is increasingly used to automate many tasks. For example, with home automation, we can, in principle, control every electronic device in our homes. By using sophisticated devices, we can listen to music, watch movies or play games while waiting at the bus stop or at the airport [1]. All in all, telecommunication technologies (wired and wireless) are becoming an integral part our daily lives. They make our daily lives easier by keeping us connected anywhere, at any time with potentially any device.

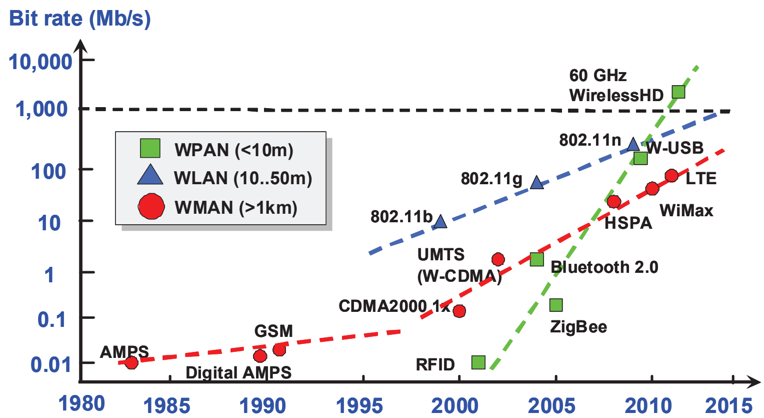

Figure 1.1: Wireless technology trends [2].

Recently, popularization of video-centric hand held devices such as smart phones and computer tablets has led to a sharp increase in the demand for wireless data capacity and coverage [2, 3]. To meet this demand, wireless systems are significantly increasing their capacities as shown in Fig. 1.1. The capacity trend of the key wireless systems deployed today, which are generally classified in terms of the coverage area -namely wireless metropolitan area networks,(2G, 3G cellular, WiMAX, etc), wireless local area networks (WLAN) and wireless personal area networks (WPAN) is shown in Fig. 1.1. From Fig. 1.1, the capacity of WPAN, which is a more recent wireless technology appears to be rising at a much faster rate than the older wireless technologies. This is partly due to relatively smaller coverage and introduction of high bandwidth wireless technologies such as UWB (3.1 – 10.6 GHz) and millimeter-wave wireless technologies using the 60 GHz band, which is capable of multi-Gb/s wireless communication. At the same time, the rapid increase in the capacity of WPAN is a concrete evidence to the critical importance of high-speed wireless access needed by the end users of communication networks. Furthermore, this indicates that in-building coverage and capacity have become critically important due to the known fact that handheld devices are mostly operated from inside buildings as opposed to from outside [2]. Therefore, to avoid the last mile bottleneck problem, a high capacity and energy-efficient in-building networks are becoming necessary. This is one of the main reasons this thesis focusses on broadband IR-UWB over fiber for high capacity and energy-efficient in-building networks. Some general overview of these wireless technologies will be discussed in the following sections.

1.1.1 Trends in WMAN

Trends in Cellular systems

Mobile telephony is a good example of a very successful technology. The first successful large-scale deployment of mobile telephony started in the 1980s as depicted in Fig. 1.1. In less than two decades, mobile communication has developed to a mass-market high tech product, having experienced unprecedented growth that has never been achieved by other technology, whether radio, television or even internet [4]. Accordingly, mobile phones usage has undergone a dramatic change from being a rare and expensive device to a pervasive low-cost personal item for everybody. In many countries, mobile phones now outnumber land-line telephones, with most adults and many children owning mobile phones [1]. Fig. 1.1 shows the global system for mobile communication(GSM), the various forms of 3G networks, such as the universal mobile telecommunication telecommunication systems (UMTS) and long term evolution (LTE). These technologies offer better packet switching support as well as higher data rates with similar support for mobility as shown in Fig. 1.1.

Currently long term evolution (LTE) is leading the mobile telecommunication standard. In general, in the past, the growth was mainly driven by the voice and messaging service (short message service,sms). The growth as today is mainly driven by mobile video and internet.

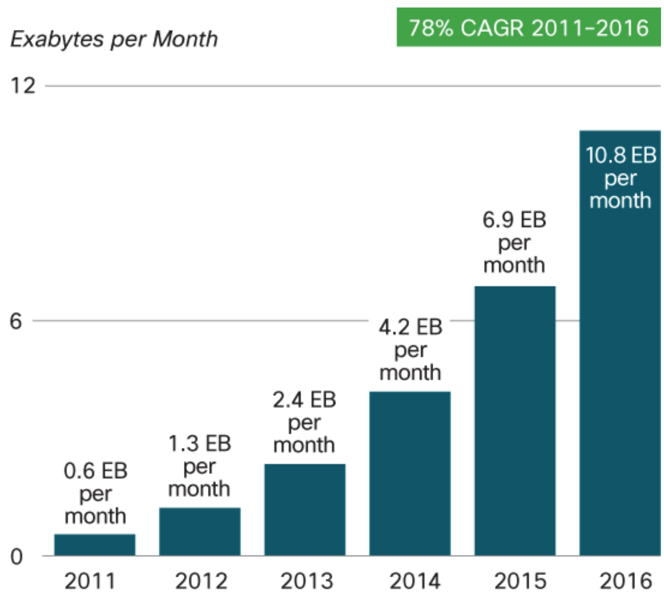

Figure 1.2: Cisco Forecasts 10.8 Exabytes per month of mobile data by 2016 [3].

One of the most significant challenges operators face today is coping with the data deluge [5]. According to the global mobile data traffic forecast update by Cisco Systems provided in [3], global mobile data traffic is expected to increase 18-fold between 2011 and 2016, reaching 10.8 exabytes per month of data in 2016 as shown in Fig. 1.2. Therefore, operators are facing an explosion in mobile data traffic driven by growing penetration of mobile internet (via smart phones) and mobile broadband (via tablets and embedded in laptop) [4]. According to the results reported in [3], laptops and netbooks will continue to generate a disproportionate amount of traffic, but newer device categories such as tablets and machine to machine (M2M) communication will begin to account for a more significant portion of traffic in 2016 as shown in Fig. 1.3. As pointed out earlier, this clearly shows that communication is not limited to only human interaction. The evolution of the cellular wireless systems in terms

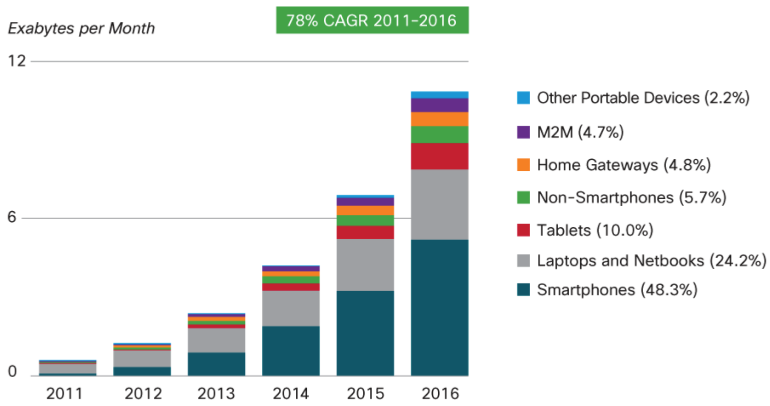

Figure 1.3: Devices responsible for mobile data traffic growth (Laptops and smartphones lead traffic grwoth) [3].

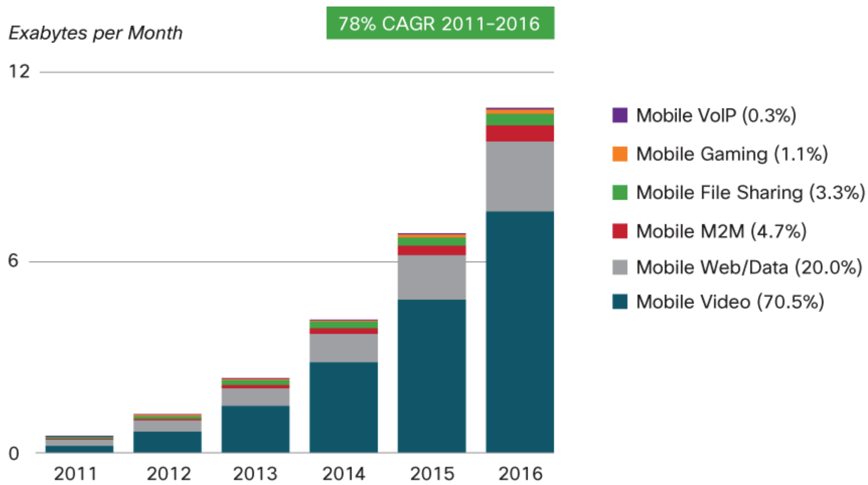

Figure 1.4: Mobile video will generate over 70 % of mobile data traffic by 2016 [3].

of bit rates can be seen in Fig. 1.1. It should be noted that the evolution is not limited in speed but the main future trend is generalized as [4] : 1) flexible, scalable and energy efficient air interface design, 2) maximizing of both peak and especially cell-edge data rates and user capacity, 3) guaranteed ubiquitous coverage in high mobility scenarios.

Trends in WiMAX

Worldwide interoperability for microwave access (WiMAX) has been envisioned by the WiMAX Forum as a single worldwide adopted standard for high-speed WMAN. The initial IEEE 802.16 WiMAX standard was established in the frequency band $10 - 66$ GHz, providing up to 75 Mb/s line-of-sight(LOS) connections for both point-to-multipoint and mesh modes. Then IEEE 802.16a provided non-LOS connection in the frequency band of $2 - 11$ GHz (licensed and non-licensed). IEEE 802.16d is for fixed WiMAX in the frequency range band $2 - 11$ GHz [6]. To offer scalability with regard to both radio access technology and network architecture, another standard has been specified known as IEEE 802.16e standard. It provides various services, for instance, it is able to provide wireless internet and support seamless IP mobility for end users. The data rate is up to 75 Mb/s for frequency range below 6 GHz and coverage up to 10 km. In addition, to provide high data rate connections, the use of space-time coding techniques allows multiple input multiple output (MIMO) antenna techniques and flexible sub-channelization schemes to be employed. Recently, the IEEE 802.16m task group was formed to design next generation Gigabit with coverage up to 100 km, also known as fourth-generation (4G) WiMAX networks. Gigabit WiMAX supports both fixed and mobile by providing up to 1 Gb/s and 100 Mb/s data rates, respectively. In general, there is a clear trend for higher data rates for mobile devices. It should be noted that better battery technology or other miniaturized energy sources and energy harvesting techniques, more computational power and improved radio technology will undoubtedly offer higher data rates, higher quality, and more communication possibilities, enabling a vast range of high quality mobile devices [1].

1.1.2 Trends in WLAN

The evolution of radio communication has also given birth to another trend: medium and short range wireless communication [1]. One of the first successful mass market products in this segment was the wireless local area network (WLAN) standard IEEE 802.11 (IEEE 1999) originally released in 1997 as shown in Fig. 1.1. It was designed to make the LAN wires redundant in an office and was much more successful in this than of any of its predecessors, such as Infrared Data Association (IrDA) [1]. When the enhanced version of IEEE 802.11b came onto the market, its deployment really took off and the so called wireless "hotspots" were installed where an IEEE 802.11b (and later IEEE 802.11g/n) access point could offer wireless internet connectivity with data rates of several Mbps to devices, such as laptops and personal digital assistance (PDAs), within a range of up to about 100 meters. Millions of hotspots have been installed worldwide in strategic locations where people congregate and need to communicate. Examples are airports, train stations, restaurants, hotels and convention centers. In 2007, the IEEE 802.11 very high-throughput (VHT) WLAN study group was set to introduce next-generation Gigabit VHT WLAN [6]. Accordingly, in 2008, the VHT study group formed the following VHT task groups: 1) VHT6: IEEE 802.11ac to operate at frequency band below 6 GHz and 2) VHT60: IEEE 802.11ad to operate in the 60 GHz millimeter-wave (mm-wave) frequency band. In general, an overview of high-data rate WLAN standards can be seen in Table-1.1.

Table 1.1: IEEE 802.11 WiFi standard family

standard	rate (Mb/s)	Spectrum (GHz)
IEEE 802.11	2	2.4
IEEE 802.11*a*	54	5
IEEE 802.11*b*	11	2.4
IEEE 802.11*g*	54	2.4
IEEE 802.11*n*	600	2.4
IEEE 802.11*ac*	Gb/s	< 6
IEEE 802.11*ad*	multi-Gb/s	57-66

One of the major challenges of the IEEE 802.11ac task group is providing backward compatibility with legacy IEEE 802.11a/b/g WLAN as well as HT WLAN operating in the 2.4 GHz and 5 GHz band. On the other hand, the major challenging issue of the IEEE 802.11ad task group is the development of the 60 GHz mm-wave frequency band given its coverage limitations and huge energy consumption [6]. However, both VLT6 and VLT60 aim at supporting future bandwidth-hungry applications such as high-definition (HD) video streaming.

1.1.3 Trends in WPAN

To connect wearable and hand held devices around a person, a much shorter range up to 10 meters is enough [1]. This has led to the development of yet another branch of technologies that cover a wide range of data transmission rates, have low power consumption but limited range. They go under the term wireless personal area networks (WPANs) or just personal area network technologies, of which IEEE 802.15.1 (commonly known as Bluetooth) is currently the most common technology. As can be seen in Fig. 1.1, WPAN is relatively recent technology and shows dramatic increase in its data rate. These technologies interconnect mobile phones, laptops, PDAs, sensors and other personal devices located within 10 meters in a seamless way with low power consumption for normal battery-powered devices. In this segment, very high data rate versions are to be expected in the near future, such as UWB and 60 GHz as shown in Fig. 1.1. It should be noted that, in the future, short-range wireless communications will become one of the dominated wireless communications according to the work reported in [4]. Accordingly, it is predicted that by 2020 there will be 7 trillion wireless devices serving seven billion people [4]. Furthermore, it is expected to be a very diverse range of air interface technologies, network architectures and standards. The air interface technologies could be conventional (narrow band) radio, UWB radio, mm-wave communications and optical wireless communications. In addition, the supported data rate will be diverse from low (1 b/s-100 kb/s), moderate (100 kb/s-10 Mb/s) to high (10 Mb/s-10 Gb/s). However, for the more distant future, data rates in the order of Tbps are the new target for research projects [1]. In short, WPAN in general and UWB in particular are driven by four main points [7]:

1. A growing demand for wireless data capability in portable devices at higher bandwidth but lower in cost and power consumption than currently available

2. Crowding in the spectrum that is segmented and licensed by regulatory authorities in traditional ways

3. The growth of high-speed wired access to the Internet in enterprises, homes and public spaces

4. Shrinking semiconductor cost and power consumption for signal processing

All in all, it is very clear that each part of the network (i.e.,WMAN, WLAN and WPAN), aims to expand network capacity. Fortunately, there are multiple techniques that enable to expand network capacity such as: additional spectrum (large bandwidth), spectral efficient modulation and coding techniques, advanced multiple antenna techniques(MIMO and beam forming) and the use of smaller and more cells [5]. Note that, the simplest approach for improving wireless user access speed is to reduce the size of deployed radio cells, which results in a smaller number of wireless users sharing bandwidth within a given radio cell. This is partly the reason why WPAN are able to offer larger wireless data access speeds. However, the deployment of small radio cell requires the installation of a large number of antennas. In addition, increased antenna densities are also required for improved wireless signal coverage (and capacity) inside buildings, where poor wireless signal propagation causes significant wireless system performance degradation. The dense deployment of antennas requires an extensive high-capacity signal distribution network or backbone. The fundamental reasons that make optical fiber the most ideal technology for feeding antenna of present and future high-speed wireless systems are : large bandwidth, frequency-independent signal loss, low weight, flexible, multi-standard and future proof backbone infrastructure. Hence, this thesis merges the best of the two world wireless (unlicensed high bandwidth IR-UWB) and wired (optical fiber) to provide high capacity and energy efficient in-building networks. The concepts and characteristics of UWB are discussed in the following sections.

1.2 Ultra wideband (UWB) Technology

As mentioned in the previous sections, more and more devices are going wireless every day, it is essential that future wireless technologies can coexist with each other. UWB is a promising solution to this problem which became more popular after the Federal Communications Commission (FCC) in the USA allowed the unlicensed operation of UWB devices in February 2002 subject to emission constraints [8]. Due to its unlicensed operation and low-power transmission, UWB can coexist with other wireless devices and its low cost, low-power transceiver circuitry makes it a good candidate for short-to-medium-range wireless systems such as WSNs and wireless personal area networks (WPANs). Accordingly, considerable attention has been given to UWB technology and it is becoming an emerging technology that has attracted a great deal of interest from academia, industry and global standardization bodies [9].

The definition for UWB, related imposed FCC-mask, the silent features and challenges are discussed in the following.

1.2.1 UWB definition and FCC emission mask

UWB signals are characterized by their very large bandwidths compared to those of conventional narrow-band/wide-band signals [10]. According to the Federal Communications Communication (FCC), a UWB system is defined to have an absolute bandwidth of at least 500MHz or a fractional (relative to the center frequency) bandwidth of larger than 20% [10, 11]. Therefore, the absolute bandwidth is obtained as the difference between the upper frequency f_H of the -10dB emission point and the lower frequency f_L of the -10dB point; i.e.,

$$B = f_H - f_L \tag{1.1}$$

which is also called -10dB bandwidth. On the other hand, the fractional bandwidth (B_{frac}) is calculated as :

$$B_{frac} = \frac{f_H - f_L}{f_c} \tag{1.2}$$

where f_c is the center frequency and is given by:

$$f_c = \frac{f_H + f_L}{2} \tag{1.3}$$

From equations (1.1) and (1.3), the fractional bandwidth B_{frac} in (1.2)can also be expressed as:

$$B_{frac} = 2\left(\frac{f_H - f_L}{f_H + f_L}\right) \tag{1.4}$$

As UWB signals occupy a very large portion of the spectrum, they need to coexist with the incumbent systems without causing significant interference [10, 12]. Therefore, a set of regulations are imposed on the systems transmitting UWB signals. In order to benefit from the advantage of UWB without degrading the performance of other systems, in 2002 modern UWB regulations were introduced by the FCC [12], for an unlicensed frequency band between 3.1GHz and 10.6GHz with an allowable EIRP of -41.3 dBm/MHz and a minimum bandwidth of 500MHz. To put this power level in perspective, this is the same level allowed for the noise emissions of an electronic device [13–16].

Therefore, UWB signaling can be thought of as reusing the noise floor for communication applications. The emission mask imposed for indoor applications is shown in Fig. 1.5. It should be noted that the main challenge is the more severely power-restricted GPS band $(0.96 - 1.61)$ GHz shown in Fig. 1.5.

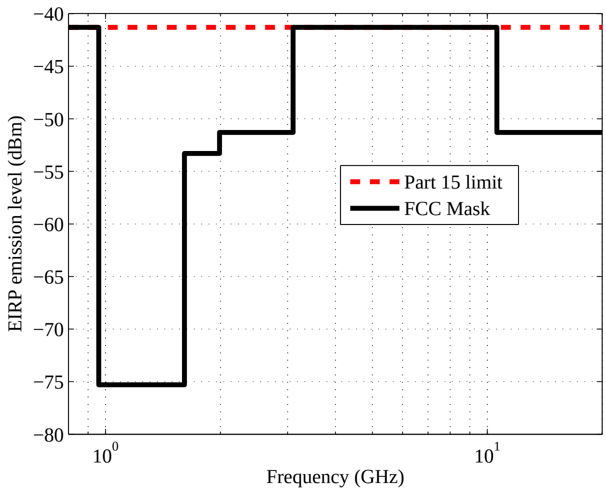

Figure 1.5: FCC emission limit for indoor UWB systems.

On the other hand, it is important to note that for different applications the spectral mask look differently and the totla bandwidth is also different. Furthermore, the mask is different for different regions; in Europe and in Asian countries the regulations are more strict while in the US and Canada they tend to be more relaxed [12]. Fig. 1.6 summarize the bands in which UWB wireless communication is allowed, some of which require detect-and-avoid (DAA) strategies in the UWB transmitter. It can be observed from Fig. 1.6 that across these regulations, the band from $7.25 - 8.5$GHz is the only common spectrum. It should be noted that this is one of the main obstacles for UWB to be successful in the mass market.

1.2.2 Advantage of IR-UWB Signals

UWB have several advantages directly and indirectly related to its huge bandwidth. Some of the advantages of UWB are described in the following.

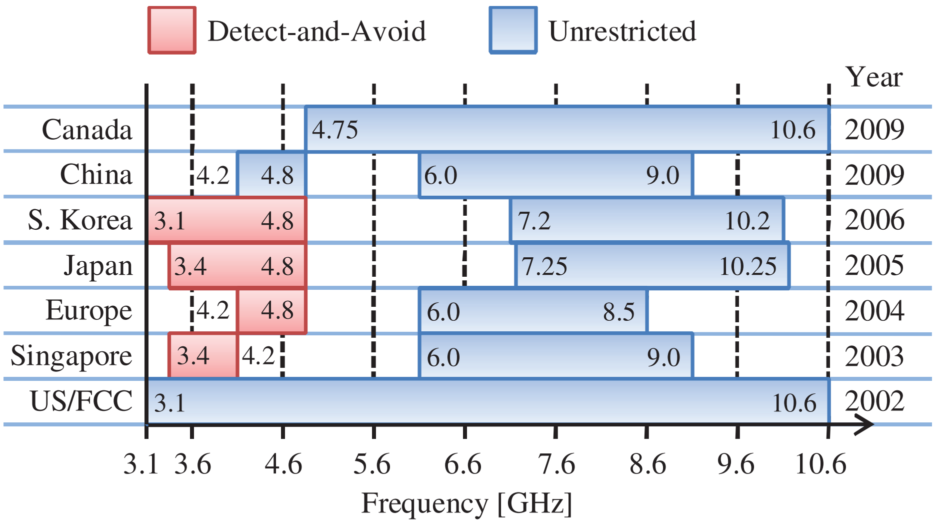

Figure 1.6: UWB intended bands for communications for different regions [12].

Large Channel Capacity

The suitability of UWB signals for high-speed data communications can be observed from the Shannon's capacity formula. For an AWGN channel with bandwidth of $B[Hz]$, the maximum data rate that can be error-free transmitted is given by:

$$C = B \times \log_2 (1 + SNR)\, bits/second \tag{1.5}$$

where C represents the maximum channel capacity, B is the channel bandwidth, and SNR is the signal-to-noise power ratio of the system. As can be carefully observed in equation 1.5, the equation tells us that there are three things that we can do to improve the capacity of the channel. These three things are: increase the bandwidth, increase the signal power, or decrease the noise. According to equation 1.5, capacity C increases as a function of bandwidth faster than as a function of SNR. In other words, equation(1.5) shows that increasing channel capacity requires linear increase in bandwidth while similar capacity increase would require exponential increase in power [11, 17]. Therefore, UWB technology is capable of transmitting high data rates using very low power. As reported in [17], 1.3 giga-pulses per second with support of forward error correction(FEC) encoded data rates in excess of 675 Mb/s have been demonstrated using pulsed UWB systems.

Fading robustness

UWB systems are immune to multipath fading and capable of resolving multipath components (MPCs) even in dense multipath environments. In other words, a UWB transceiver receives a signal with a large absolute bandwidth, and thus resolve many those MPCs. By separately processing the different MPCS, the receiver can make sure that all those components add up in an optimum way, giving rise to a smaller probability of deep fades and thus reduce the fading margin and enhance system performance [9]. This is in particular important for in-building applications in which dense multipath can exist due to the actual scenario of surrounding environment. However, it should be noted that exploiting the multipath for system enhancement adds complexity at the receiver side.

High Precision ranging and localization

One of the most promising aspects of UWB radio (specifically IR-UWB) is their potential for high-precision localization. Due to their large bandwidths, UWB receivers can resolve individual multipath components (MPCs); therefore, they are capable of accurately estimating the arrival time of the first signal path. This implies that the distance between a wireless transmitter and receiver can be accurately determined, yielding high localization accuracy [8, 10, 18]. Such unique aspects of UWB make it an attractive technology for diverse communications, ranging and radar applications such as robotics, emergency support, intelligent ambient sensing, health-care, asset tracking and medical imaging. The potential of UWB technology for future wireless communication network was also recognized by the IEEE, which adopted in the IEEE 802.15.4*a* WPAN standard for creation of a physical layer for short-range and low data rate communication and precise localization [8, 15, 16].

Superior penetration properties

UWB systems can penetrate obstacles and thus operate under both line-of-sight (LoS) and non-LoS (NLoS) conditions. UWB systems can penetrate effectively through different materials (including walls) due to the low frequencies included in the broad range of the UWB frequency spectrum have long wavelength. This property make UWB technology viable for through-the-wall communications and ground-penetrating radars [11]. Note that UWB does not have better penetration than narrowband electromagnetic signals at the same frequency.

Co-existence with other technologies

UWB systems have low power spectral density that allows them to coexist with other services such as cellular systems, wireless local area networks (WLAN), global positioning systems (GPS), etc. As mentioned previously, this is very important as more and more devices are going wireless every day.

1.2.3 Variants of UWB technology

In general, UWB systems can be classified into three different types namely carrier-less UWB, single carrier UWB and multi-carrier UWB [19].

Carrier-less Impulse Radio (IR-UWB): This is the traditional approach to UWB communications. It uses very short, low-duty cycle impulses occupying a single band of several GHz. It should be noted that IR-UWB has the possibility of achieving high throughput, long operating range, low-power consumption, positioning, ranging and low cost implementation. Data is commonly modulated using pulse position modulation (PPM), and multiple access can be realized by time-hopping. In principle, various modulation formats can be used with their own pros and cons. These modulation formats can be pulse polarity modulation (Bi-phase), pulse amplitude modulation (PAM), and pulse shape modulation (PSM) [13, 15, 16]. Recent progress on both the technical and regulatory side of this technology has made the IR-UWB communication more practicable.

Single carrier UWB System Approach: In this scheme, a block of pulse-shaped carrier cycles is bandpass filtered and then transmitted to the antenna. This approach allows a precise control of the spectrum. With a suitable choice of oscillator and mixer, the UWB baseband signal can be converted to a radio signal with the several GHz center frequency. Information can be transmitted using amplitude, pulse position and phase. Multi-user separation can be done by time-hopping codes or direct sequence spread spectrum (DSSS) [19]. In general, DSSS can be used to IR-UWB as well. This is better approach than filtering.

Multi-Carrier UWB (MC-UWB): It uses multiple simultaneous carriers and is usually based on orthogonal frequency division multiplexing (OFDM).

OFDM has been accepted as mature technology for wireless wideband communication and adopted for several technologies: IEEE 802.11a/g, IEEE 802.16a, LTE. This OFDM-based MC-UWB is known as MB-OFDM UWB following the definition of WiMedia [13, 15, 16, 19]. In fact, MB-OFDM based UWB allows the technology to cope with local regulations by dynamically turning off some bands to comply with local rules of operation within the allowed spectrum. In addition, the proposal also allows good coexistence with narrow band systems.

The challenges of UWB in general and the main reasons for selection IR-UWB as research topic for this thesis in particular will be described in the following sections.

1.3 UWB Applications

The trade-off between data rate and range in IR-UWB systems holds great promise for a wide variety of applications in military, civilian and commercial sectors [14]. Accordingly, FCC categorizes UWB applications for radar, imaging and communication. Radar is considered one of the most powerful applications of UWB technology. The fine positioning characteristics of narrow UWB pulses enable them to offer high-resolution radar (with centimeter resolution) for military and civilian applications. As described is section 1.2.3,IR-UWB signals can penetrate various obstacles. This property makes IR-UWB-based ground-penetrating radar (GPR) a useful asset for rescue and disaster recovery teams for detecting a survivor buried under rubble in disaster situations [14].

In particular, the high data rate capability of UWB systems for short distance has numerous applications for home networking and multimedia-rich communications in the form of WPAN applications. UWB systems are suitable for consumer electronics applications, such as laptops, digital cameras, and portable HDTV monitors [14]. Table 1.2 summarizes UWB applications in data communications, radar and localization. Hence, it should be underlined that IR-UWB technology is one of the promising technologies for broadband communication and sensor applications.

1.4 Challenges for UWB Signals

As mentioned in the above, UWB technology has many advantages that makes it very attractive for future wireless communications and many other applications. However, there are some challenges involved in using nanosecond-

Table 1.2: Some UWB applications in military and commercialsectors [14]

	Applications	
	Military and Government	**Commercial**
Data communications	secure LPI/D communications Covert wireless sensor networks (battlefield operation)	Local and personal area networks Wireless streaming video distribution(home networking) Wireless sensor networks (health and habitat monitoring, home automation)
Radar	Through-wall imaging (for law enforcement, fire fighters) Ground-penetrating radar (for rescue operations) surveillance monitoring	Medical imaging (remote heart monitoring) Ground-penetrating radar (detection of electrical wiring, studs, etc. on construction site) Automotive industry (collision avoidance, roadside assistance) Home security (proximity detectors)
Localization	personal identification Lost children Prisoner tracking	Inventory tracking Tagging and identification Asset management

duration pulses for communications. These challenges have opened up many research opportunities in various areas and must be overcome for it to become a popular and ubiquitous technology. Perhaps the most obvious one to date has been regulatory problems. Wireless communication have always been regulated to avoid interference between different users of the spectrum. Since UWB occupies such a wide bandwidth, there are many users whose spectrum will be affected and they need to be convinced that UWB will not cause undue interference to their existing services.

Other challenges include the industry coming to agreed standards for interoperability of UWB devices. There are currently two camps of UWB supporters each with their own standard of UWB design, and currently there is no compromising ground to resolve these issues. This standard battle is a of concern because in the near future consumers will be hesitant to choose which standard to buy and thus limit the potential of UWB market growth. Furthermore, many technical and implementation issues still remain to be solved to meet the promise of low cost devices, low power consumption and high data rate [15].

1.5 Why IR-UWB over fiber?

As mentioned previously, future generations of communication systems will require mobility, flexibility, high data rates, low cost and low power consumption. In this context, broadband wireless digital communication is inevitable. As discussed in previous section 1.2.2, the capacity of the channel is directly related to its bandwidth, hence UWB technologies are advantageous for use in a number applications, especially in short range high data rate networking. In particular, among the three variants, IR-UWB over fiber has been selected as central investigation of topic in this thesis due to silent features to provide many advantages and wide variety of applications. The main benefits of IR-UWB are summarized as follows:

1. *Simple transceiver architecture*: IR-UWB requires fewer RF components than carrier based transmission. For this reason IR-UWB transceiver architecture is significantly simpler and thus cheaper to build. The low complexity and low cost of IR-UWB systems arises from essentially baseband nature of the signal transmission. In other words, the transmission of low-power pulses eliminates the need for a power amplifier (PA) in IR-UWB transmitters. Also, because IR-UWB transmission is carrier less, there is no need for mixers and local oscillators to translate the carrier frequency to the required frequency band; consequently there is no need for a carrier recovery stage at the receiver end [17].

2. *Simultaneous communication and localization capabilities*: Hence, it has been considered suitable for ubiquitous computing. The key elements in a ubiquitous computing environment are identification, location, sensing and connectivity [19]. This is mainly due to its high bandwidth which leads to high time space resolution in localization and thus suitable for ubiquitous computing.

3. *Flexibility*: One of the enormous potential of IR-UWB systems is the ability to trade data rate between the very high data rate(HDR), short link distance and very low data rate(LDR), longer distance applications. In principle, trading data rate for link distance can be as simple as increasing the number of pulses used to carry a bit. The more pulses per bit, the lower the data rate and the larger the achievable transmission distance [16, 17].

4. *High data rate and very low power*: Due to the huge bandwidth mentioned above, IR-UWB systems can achieve high data rate even for low

SNR in noisy environments. The battery life of UWB devices will also be longer because of the very low transmitted power as well as very low power consumption due to the more simple transceiver architecture of UWB device [13, 15–17, 20]

5. *Small form factors and low cost*: An analog front end of a UWB transceiver is noticeably less complicated than that of a narrowband transceiver. This simplicity makes an CMOS(complementary metal oxide semiconductors) implementation of UWB transceiver possible, which entails small form factors and low production costs [17]

In general, IR-UWB has many advantages and wide variety of applications. Hence, it is a vital technology for short range wireless communications. However, due to the FCC's current power limitation on UWB transmissions, the high data rate is available only for short ranges. This thesis aims for reach extension of IR-UWB by using the concept of RoF. Hence, IR-UWB over fiber solution brings additional advantages by enabling multiple novel applications such as: 1) range extension of high speed wireless personal area networks (WPANs), 2) integration with other wired and wireless networks, 3)small cells and low cost distributed antenna systems by centralizing complex functions 4) secure, intelligent, high capacity and energy-efficient networks, and 5) infrastructure capable of delivering broadband to remote areas. More detail discussions about the features of IR-UWB over fiber are provided in the subsequent chapters.

1.6 Scope and Contributions of this Thesis

The research work reported in this thesis has been carried out at Eindhoven University of Technology, within the ALPHA project funded by the EU Seventh Framework Program (FP7). ALPHA stands for Architecture for fLexible Photonic Home and Access networks. The ALPHA project aimed to contribute to the convergence processes taking place between the wireless mobile and broadband networks as well as between different segments of the IP-based networks (for example, access-home). An integrated/converged access and in-building network for delivering broadband and existing and future wireless services was one of the focus points of the project. In particular, the research work reported in this thesis was done within the scope of workpackage four (WP4) of ALPHA project. WP4 targeted the development and integration of next generation technologies required in the physical layer (PHY) of access and in-building networks in order to support a wide range of wired and wireless services bringing them to a wide range of end users. As part of this main goal of WP4, this thesis addresses to techniques for delivery of high data rate wireless services using IR-UWB over fiber technology for both access and in-building networks due to many attractive features of IR-UWB described in section 1.5. In general, the scope of the thesis is limited to shaping and generation, transmission and routing of IR-UWB over fiber.

The results achieved in this thesis have been contributed to two main EU projects: 1) ALPHA an integrated project in EU FP7 and 2) Building the Future of Optical Network in Europe (BONE) in a Network of Excellence project. The thesis has also contributed to different scientific communities and the results have been published in high-impact peer-reviewed major journals, regional and international conferences. In general, the key contributions are summarized according to the following main topics:

1. Design of novel pulses for IR-UWB over fiber systems.
2. Experimental demonstration of new and simple optical generation technique for IR-UWB pulses.
3. Performance comparison of proposed pulses and state-of-the-art IR-UWB over fiber pulse using realistic path-loss model.
4. Multi-Gbit/s transmission of IR-UWB over different optical fibers (silica SMF, MMF and plastic optical fibers) for access and in-building network applications.
5. Integration of wired/wireless IR-UWB over single in-building network infrastructure.
6. Routing of integrated wired/wireless IR-UWB over single in-building network.
7. Investigation of fiber effects on the accuracy of ranging/localization of IR-UWB over fiber systems.

1.7 Outline of the Thesis

Chapter-1 Introduction: This chapter introduces the research domain for broadband IR-UWB over fiber. It discusses the general evolution and recent trends in wireless communication networks. It introduces the basic concepts, characteristics and advantages of UWB systems. The motivation and possible applications of IR-UWB over fiber systems are also described in this chapter. Furthermore, this chapter summarizes the scope, contribution and outline of this thesis.

Chapter-2 Literature Review: This chapter focusses on the literature survey of the state-of-the-art IR-UWB over fiber systems. First, the concept of radio over fiber (RoF) and role of microwave photonics in RoF systems has been reviewed. Then different techniques for photonic generation of IR-UWB and the state-of-the art experimental demonstrations have been summarized. Research problems and challenges have been identified. Accordingly, different solutions are proposed and demonstrated in the subsequent chapters.

Chapter-3 IR-UWB pulse shaping and generation technique: One of main objectives of this chapter is to solve key challenges of shaping and generation techniques of IR-UWB pulses. First, system requirements that need to be satisfied have been identified. Then new and novel pulse shaping concepts have been proposed.A theoretical performance analysis and experimental results have been demonstrated.

Chapter-4 IR-UWB over fiber transmission experiments: This chapter addresses the research problem of reach extension of multi-Gigabit/s IR-UWB using different fiber types. The selection of fiber types depends on several criteria such as cost of installation/maintenance, bandwidth, attenuation and bending losses. Hence, in this chapter the performance of the transmission of IR-UWB over both silica (SMF and MMF) and plastic fibers has been investigated.

Chapter-5 Routing of wired and wireless IR-UWB over fiber: The main goal of this chapter is to address the networking capabilities of IR-UWB over fiber for in-building network applications. It also addresses the integration of wired and wireless IR-UWB over a single optical infrastructure. Then the integrated solutions are finally extended to achieve routing wired and wireless IR-UWB over the same infrastructure to reduce the cost, energy consumption and provide flexibility of in-building networks.

Chapter-6 Ranging/localization using IR-UWB over fiber: This chapter focuses on the effects of fiber on ranging and localization based IR-UWB over fiber systems for future smart and energy efficient in-building networks. Accordingly, in this chapter the effects of different fiber types such as silica and plastic fibers have been studied.

Chapter-7 Conclusion and Recommendations: This chapter summarizes the main conclusions of the work and suggests some future research directions.

Chapter 2

Literature Review: Overview of RoF and IR-UWB over Fiber Systems

This chapter deals with review of basic concepts and techniques of radio-over-fiber (RoF) in general and IR-UWB over fiber in particular. After the introduction, the role of microwave photonics in enabling RoF systems in generating and distributing RF and/or microwave signals will be described. Then RoF architectures will be summarized followed by IR-UWB over fiber concepts. Review of photonic generation of IR-UWB is provided. Then a summary of IR-UWB transmission experiments that include wireless links will be presented. Finally, based on literature review, research problems will be defined and solutions to these problem will be described in the subsequent chapters. A summary of the chapter will be provided at the end[1].

2.1 Introduction

As described in chapter-1, the growth of mobile and wireless communication will continue at an even greater pace in the next decade. Currently available wireless services and standards such as Wi-Fi, GSM, UMTS are concentrated in the lower microwave band. New emerging wireless standards such as WiMAX and LTE will further enhance existing wireless transmission speeds and throughput; however, they still operate within the lower microwave re-

[1]This chapter is partly published in [21]

gions ($2-6$ GHz), causing a heavy burden on the already congested wireless spectrum in the microwave region [22]. This spectral congestion forms the fundamental driver for new wireless technologies with large bandwidth either by using co-existing principle such as ultra wideband (UWB) or by using the large unused spectra of millimeter wave (mm-wave) frequency regions for the provision of future broadband wireless services. One particular band of interest is the unlicensed($3.1-10.6$ GHz) UWB band which allows co-existence with other narrowband services without looking to new free high frequency bands. UWB targeted towards short range in-building high-speed applications, has gained significant popularity. Recently, UWB over fiber based pico-cell architectures have been proposed to provide high capacity and energy-efficient geographical coverage which necessitates a widespread deployment of radio access units (RAU). Hence, this chapter focusses on reviewing IR-UWB pulse shaping techniques as well as experimental transmission results. In addition, a short overview of microwave photonics applications in enabling both RoF and IR-UWB over fiber systems will be presented.

2.2 Microwave Photonics: Enabling for RoF Systems

The broad bandwidth and low loss offered by photonics have led to an ever-increasing interest in design and implementation of photonically assisted solutions for generation, processing, control and distribution of microwave signals [23]. Microwave photonics have been defined as an area that studies the interaction between microwave and optical waves for applications such as radar, communications, sensor networks, warfare systems and instrumentation [23–27]. In past few years, there has been an increasing interest and efforts in finding new microwave photonic solutions for these applications. Recently, microwave photonics found a new application in shaping and distributing UWB signals directly in the optical domain for broadband communications and sensor network applications [27]. The applications of microwave photonics especially in generating high frequency carrier signals and shaping IR-UWB pulses by using microwave photonic bandpass filters will be described shortly in the subsequent sections.

2.2.1 Optical Generation of Microwave Signals

There are several photonic generation techniques of microwave signals, which are used particulary in RoF systems. Each of these techniques have their own pros and cons. Some of the commonly used microwave carrier generation techniques, architectures of radio-over-fiber (RoF) systems and IR-UWB over fiber shaping techniques are presented in the following.

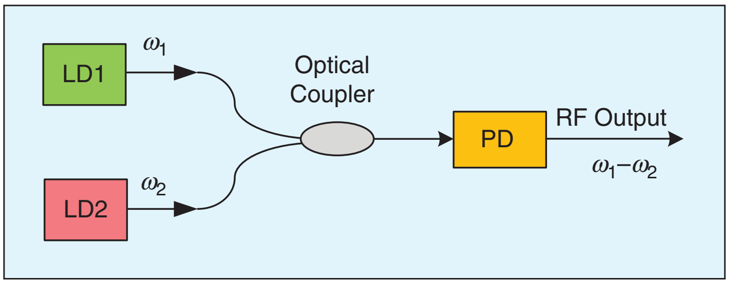

Figure 2.1: Beating of two optical waves at a PD for generation of a microwave signal [23].

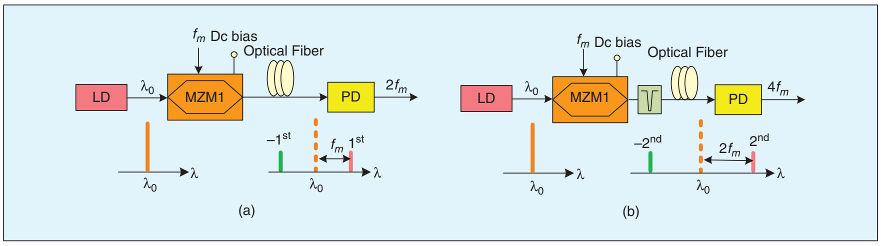

Figure 2.2: Microwave generation based on external modulation [23].

- *Optical heterodyning technique:* A high frequency and frequency-tunable microwave signal can be generated by beating two optical waves at a photodetector (PD). As can be seen in Fig. 2.1, two optical waves with angular frequencies ω_1 and ω_2 beat together at the PD to generate a microwave signal with frequency equal to the frequency difference $|\omega_1 - \omega_2|$ between the optical waves. This technique is capable of generating an electrical signal with a frequency up to THz band, limited only by the bandwidth of the PD [28]. However, beating two optical waves from two free-running laser diodes (LDs) would lead to a microwave signal having high phase noise. This is due to the fact that the phase terms of the two optical optical waves are not correlated, and the beating process will transfer the phase noise of the two optical waves to the generated microwave signal. In the past few years, several techniques have been proposed to generate low-phase-noise microwave signals with two optical waves being locked in phase. These techniques can be classified into three categories: 1) *Optical injection locking* 2) *Optical phase-locked loop (OPLL)* 3) *Microwave generation using external modulation* 4) *Harmonic generation through FM-IM conversion*. In addition, a low-phase-noise microwave signal can be generated using an opto-electronic oscillator(OEO). These techniques have been widely described in the literature and interested readers can find more details in [23, 28, 29].

- *Microwave generation based on external modulation:* Another way of microwave signal generation can be implemented based on external modulation, by which the frequency of a low frequency microwave signal can be increased to high frequency through frequency multiplication [23]. The basic principle of this technique is described using the scheme shown in Fig. 2.2 to achieve frequency doubling using a Mach-Zehnder modulator (MZM). As shown in the Fig. 2.2, a RF signal is applied to the MZM via the RF port. The MZM is biased at the minimum transmission point to suppress the optical carrier. Accordingly, at the output of the MZM, only two first-order sidebands are generated. Then by beating the first-order sidebands at a PD, a frequency doubled microwave signal can be generated. On the other hand, if the MZM is biased at the maximum transmission point, at the output of the MZM, an optical signal with an optical carrier and two second-order sidebands are generated [23]. The optical carrier can be removed using a notch filter so that after beating the two sidebands at the PD, a frequency quadruple microwave signal can be generated. Furthermore, to generate a microwave signal with a higher multiplication factor, a configuration that employs two cascaded MZM can be used. According the work reported in [23], a multiplication factor as high as 12 has been demonstrated.

- *FM-IM conversion technique:* Another interesting technique based on harmonic generation using frequency-modulation to intensity-modulation (FM-IM) conversion has the advantage of generating high microwave and mm-wave carriers with the use a single laser and low frequency electronics [28, 30]. This technique exploits the wide optical spectrum broadening achieved with an optical phase modulator to produce an optical FM signal, which has frequency components at every multiple of the modulating frequency that drives the phase modulator. Since a square-law photodetection of the optical FM signal would only generate a DC component from a constant envelope, an FM-IM conversion is necessary prior to photodetection in order to extract the multiple-order harmonics of the modulating frequency. To make the system more independent of fiber length variation, the FM-IM conversion can also be implemented with a periodical optical bandpass filter, for instance, a delay interferometer or a Fabry-Perot etalon [28]. In general, this technique is very robust against laser phase noise and presents high tolerance against chromatic and modal dispersion impairment in transmission [28].

2.2.2 RoF System Architecture

There are three main RoF systems architectures proposed for commercial in-building wireless deployments as reported in [31]. These architectures are described in the following:

- *RF transmission over fiber*: This architecture deals with RF transmission over fiber directly at the radio carrier frequency. This is the simplest configuration or scheme for transporting RF signals over fiber without any need for frequency translation at the remote base station(BS). The modulated RF signal is generated at the central office (CO) in RF band and directly transmitted to the BS through fiber. At the BS, the modulated signal will be detected by a photodetector (PD) and amplified by RF amplifier before transmitted via an antenna to mobile devices. In particular for mm-wave wireless signal is externally modulated onto optical carrier resulting in an optical double sideband(ODSB)signal. The two sidebands are located at the wireless carrier frequency away from the optical carrier. Upon detection at the BS, the mm-wave wireless can be recovered via direct detection using a high-speed photodetector. In general, RoF transport technique has the advantage of realizing simple BS designs with additional benefits of central control, independence of the air-interface and also enabling multi-wireless band operation. However, one of its major drawbacks is the requirement for high-speed optical modulation techniques that can generate mm-wave modulated optical signal and also high-speed photodetection schemes that directly converted the modulated optical signal back to mm-wave signals in the RF domain.

Another key issue is the significant effect of fiber chromatic dispersion (CD) on the detected mm-wave wireless signals leading to fading of the mm-wave signal [22]. It should be noted that several schemes have been proposed in the literature to overcome the problem of ODSB such as optical signal sideband (OSSB) modulation and OSSB filtering. The idea of incorporating OSSB to combat CD-induced fading is direct and simple: if only one optical sideband is transmitted along the fiber with an optical carrier, then only one mm-wave component is generated at photodetection and thus there is no more signal fading.

- *IF transmission over fiber*: At the CO, the RF signal is down-converted to the IF band and the modulated IF signal is directly transmitted to the BSs through the fiber network. At the BS, the modulated IF signal will be detected by the PD and amplified by the IF amplifier before being up-converted to higher RF band and then transmitted to mobile devices. This can reduce significantly the effect of fiber chromatic dispersion on the optical distribution of the IF signals. Furthermore, IF-over-fiber transport technique has advantage of using low speed optoelectronic components or devices. However, the complexity of the antenna BS hardware increases with IF signal transport in particular for mm-wave wireless access systems. This is mainly due to the fact that a stable mm-wave local oscillator (LO) and high speed mixers are required in the BS for the high frequency translation processes. This could form another limitation when considering the ability to upgrade or reconfigure the wireless network for adding additional mm-wave wireless channels or changing the wireless frequency. The subsequent requirements for a mm-wave LO at the antenna BS can be solved by remotely delivering LO signal optically from the central office (CO) [22].

- *Baseband over fiber*: At the CS, the RF signal is down converted to IF band and the signal is digitized before being modulated and directly transmitted to the BSs through the fiber. At the BS, the modulated signal will be detected by the PD and converted back to analog IF signal before being up-converted to the desired RF band and transmitted to mobile devices. This scheme has the advantage of using mature digital and electronic circuitry for signal processing at the BS [22]. Furthermore, it enables low-speed optoelectronic devices to be used within the BS and the effects of chromatic dispersion are greatly reduced. However, it should be noted that this scheme is dependent on the air-interface which means that the BS must have the intelligence to thoroughly process the wireless signals before sending the baseband information back to the CO. Hence, it requires housing of additional hardware within the BS to perform these tasks which eventually leads to increased complexity of the BS.

The most common configuration is an RF transmission over fiber because it is the simplest design and more economical for implementation. However, it is susceptible to fiber chromatic dispersion that severely limits distance. In addition, optical components required for this configuration need to have low noise and low distortion at high frequency. The laser is the dominant source of noise and distortion in a RoF link and it is quite a challenge to find the right balance between the cost and the performance for this component [26, 31].

In general, RoF technology involves the use of optical components and techniques to allocate RF signals from CO to the BSs. Thus, RoF makes it possible to centralize the RF signal processing function in one shared locations (CO). It also offers the use single mode optical fiber that has a very low signal loss (about 0.25 dB/km for 1550 nm and 0.4 dB/km for 1310 nm wavelengths) to distribute the RF signals to the BSs. Furthermore, RoF systems use of free-space radio path as the final drop to the end users providing flexibility since the end-users do not have to be fixed in location. Such system is important in a number of applications, including mobile communications, WLANs, WPAN, wireless local loop, etc. Rapid development in microwave photonics enabling technologies have fulled an intense effort into the research and development of these networks.

2.3 UWB-over-Fiber Concept

To address the fundamental short-range limitations in UWB wireless communications, the relatively new concept of UWB radio over optical fiber or simply UWB over fiber is proposed [32, 33]. The main idea here is to deliver UWB radio signals over mixed wireless RF and optical channels, where the optical part serves as super-efficient transparent medium to carry the radio signal with a bandwidth of several GHz. This will enable multiple new services and applications such as range extension of WPAN by two to three orders of magnitude and new optical/wireless infrastructures capable of delivering broadband multimedia and above 1000 Mb/s traffic to and from users in the remote areas. Another application is related to security; it collects data from a large number of sensors and cameras equipped with UWB and transmits it over existing optical infrastructures using UWB radio over fiber technologies [4].

The IR-UWB over fiber concept is a new paradigm that extends the state-of-the-art RoF technologies to the short-range communication case. As described above, RoF systems in mobile cellular are motivated by the demand for replacing a central high-power antenna with low-power distributed antenna systems (DAS). RoF technologies are successfully deployed for in-building coverage in 2G/3G cellular networks. In this application, many remote antenna units (RAUs) serving as low-cost base stations(BS) are connected to a single CO. The main difference between UWB radio over fiber and the conventional RoF are:

1. *The state-of-the-art RoF technologies are used in the backbone of the wireless access networks, whereas IR-UWB over fiber address the challenges of range-extended low cost WPANs*

2. *In RoF, which targets the 2G/3G cellular systems, the RF signal bandwidth is only a few tens of MHz and its average power is in the range of several hundred of mW. This requires high-cost photonic components in the CO and medium-cost in the BS. IR-UWB over fiber, on the other hand, targets the PAN market, which is characterized by very-low cost and low-power (tens of mW) access point. In IR-UWB over fiber, the optical fiber is used to carry extremely wide RF signal (several GHz)*

2.4 Overview of IR-UWB Photonic Generation Techniques

To distribute IR-UWB signals over optical fiber, it is highly desirable that the UWB signals can be generated directly in the optical domain without the need for extra electrical-to-optical conversion [32, 33]. Furthermore, the use of optical techniques has many advantages, such as light weight of the fiber cable, small size, large tunability and immunity to electromagnetic interference [33]. Accordingly, several approaches have been proposed for generating IR-UWB signals in the optical domain. However, the commonly used approaches can be broadly classified into three main categories [32, 33]:

1. IR-UWB pulse generation based on first or second-order derivatives of Gaussian pulse.

2. IR-UWB pulse generation based on photonic microwave delay-line filters.

3. IR-UWB pulse generation based on optical spectral shaping and frequency-to-time mapping.

The review and details of each of these techniques will be described in the following sections.

2.4.1 Derivatives of Gaussian Pulse

One way of realizing first or second-order differentiation of Gaussian pulses is to implement an optical differentiator, which acts as a bandpass filter to shape the input Gaussian pulse either to a monocycle or doublet pulse respectively. Note that monocycle and doublet pulses are the first and second order derivatives of Gaussian pulse respectively. Their respective time-domain waveforms can be seen in the subsequent figures as shown in Fig. 2.4 and Fig. 2.6. Various techniques have been proposed for realizing an optical differentiator. Simple techniques based on phase modulation to intensity modulation (PM-IM) conversion have been widely employed. The conversion of phase-modulated Gaussian pulse to intensity-modulation can be achieved by using either a dispersive device (such as SMF fiber) or an optical frequency discriminator [32, 33]. The concept of generating IR-UWB pulse using PM-IM technique is shown in Fig. 2.3. An input Gaussian pulse is applied to phase modulator (PM) RF input and will be shaped to IR-UWB pulse using this PM-IM conversion process. This process is equivalent to a bandpass filter, which shapes a Gaussian pulse either to first or second order derivative of Gaussian pulse called monocycle and doublet respectively. An interesting mathematical analysis of this fundamental principle of PM-IM conversion approach and its associated experimental demonstrations of IR-UWB pulse generation of either first or second order derivatives have been reported in [32, 33]. As an example, a doublet pulse has been achieved using PM-IM conversion principle by employing a 25 km SMF fiber as dispersive element with an input of Gaussian pulse with a full-width half maximum (FWHM) of about 63 ps and a laser diode (LD) at 1550 nm as reported in [32, 34, 35].However, it should be noted that as the SMF fiber length changes the shape of the generated pulse also changes. This is mainly due to the change in the transfer function of the system. Hence, this scheme lacks flexibility for different application areas which requires different length of SMF fiber such as access, in-building and in-home networks.

An alternative to this approach is to use a frequency discriminator instead of fiber as dispersive element. For real implementation, the optical frequency discriminator can be realized using an optical filter, such as fiber Bragg grat-

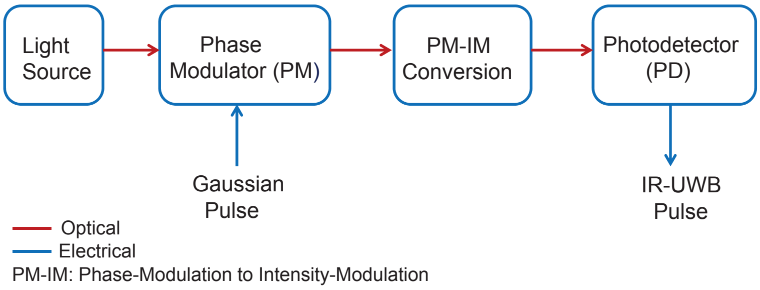

Figure 2.3: Concept of IR-UWB generation based on PM-IM conversion.

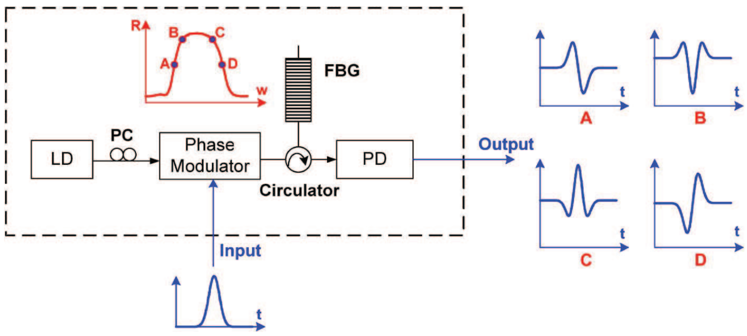

Figure 2.4: PM-IM conversion technique using FBG as frequency discriminator [32].

ing(FBG) as shown in Fig. 2.4. By intentionally locating the optical carrier at either left or right slope of the optical bandpass filter, UWB pulses with different polarities have been generated and reported in [32, 35, 36]. Furthermore, as shown in Fig. 2.4, different portion of the filter transfer function can be exploit for generating either monocycle or doublet pulse. Note that, in principle, several ways of implementing the fundamental principle of PM-IM technique are possible. One such alternative is cross-phase modulation (XPM) instead of phase modulation (PM). Accordingly, all-optical IR-UWB pulse generation systems that generate Gaussian pulses using a femtosecond pulse laser and the phase modulation implemented based on XPM in a length of nonlinear fiber have been proposed in [37, 38]. To control the pulse width, a tunable bandpass filter is incorporated after the femtosecond pulse laser. The generated optical pulse is then injected together with a continuous-wave probe into a length of

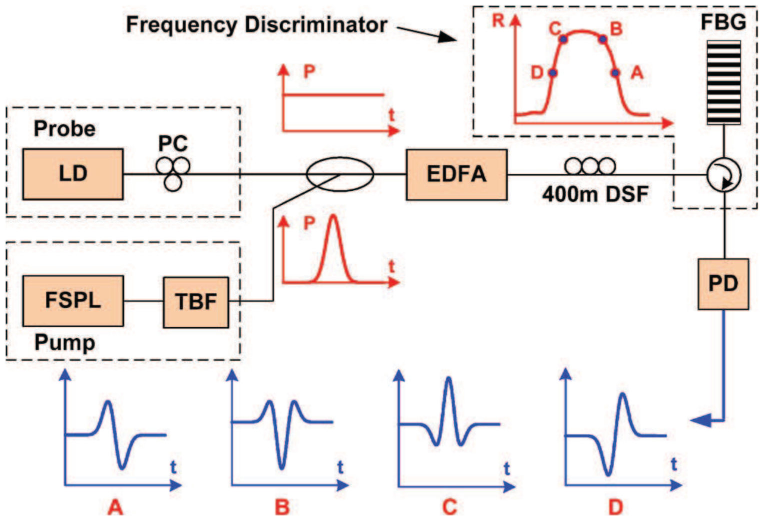

Figure 2.5: PM-IM conversion technique using XPM in nonlinear fiber [32].

dispersion-shifted fiber(DSF) serving as a non-linear element to achieve optical XPM. The phase-modulated signal carried by the probe is then converted to an intensity-modulated signal using an FBG based frequency discriminator. In this particular experiment, the FBG also serves as an optical bandpass filter to remove the residual pump signal and the amplified spontaneous emission noise from the Erbium-doped fiber amplifier (EDFA) [32]. In addition, depending on the location of the probe at the left or right (linear or quadrature) slope of the FBG reflection spectrum, a UWB monocycle or doublet, with or without polarity inversion, is generated [32, 38]. Another approach for monocycle pulse generation is to use XPM in a semiconductor optical amplifier (SOA) together with frequency discrimination using an optical bandpass fiter has been reported in [39]. To reduce the cost, on-chip generation of monocycle pulses using a silicon microring resonator to perform PM-IM conversion has been reported in [40]. In general, the principle to PM-IM is an interesting approach for shaping IR-UWB pulses. However, this approach is limited to generate conventional (monocycle and doublet) pulses, which are not FCC-mask compliant with high spectral power efficiency. Hence, this approach is less flexible in generating other types of pulses. However, the complexity and costs are relatively low as compared to other techniques described below.

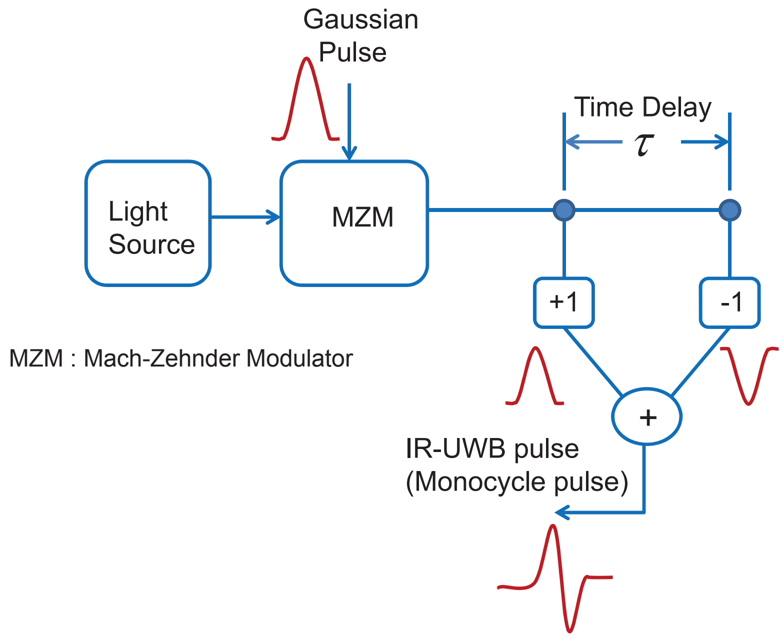

(a) 2-tap delay line.

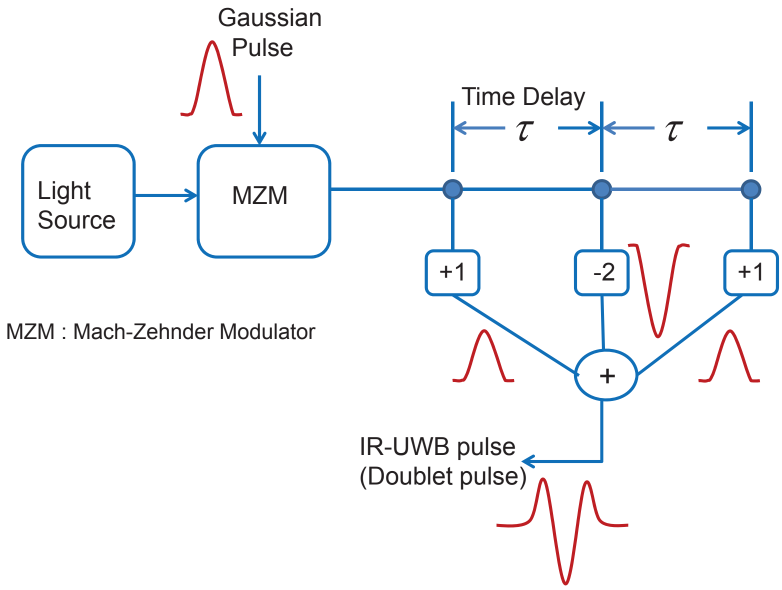

(b) 3-tap delay line.

Figure 2.6: Concept of two- or three-tap delay line generation of an IR-UWB pulse.

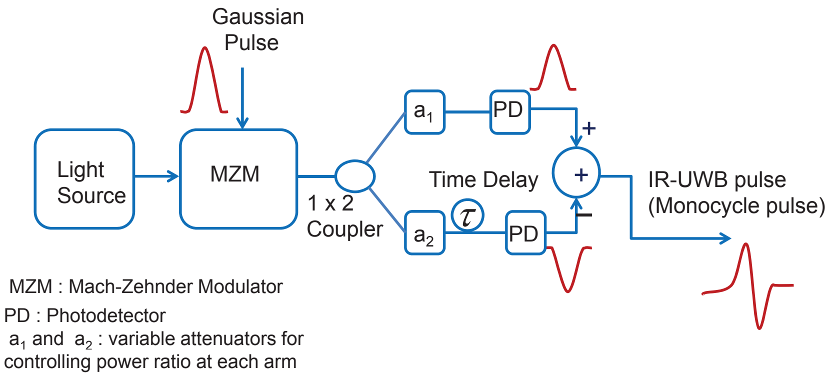

Figure 2.7: IR-UWB generation using differential detection.

2.4.2 Photonic Microwave Delay-line Filter Approach

A Gaussian monocycle or doublet pulse can also be generated by performing the first or second-order differencing of a Gaussian pulse. Mathematically, the first- or second-order derivative can be approximated by a first-or second-order difference [33, 41]. This can be implemented using a two or three-tap photonic microwave delay-line filter with coefficients of $[1, -1]$ or $[1, -2, 1]$ as shown in Fig. 2.6. According to Fig. 2.6a and 2.6b, negative coefficients must be generated. It is well known that, to design a photonic microwave delay-line filter and to avoid optical interference, the filter should operate in the incoherent regime using incoherent detection. A photonic microwave delay-line filter with incoherent detection can usually have positive coefficients only [24, 25]. Based on signal processing theory, an all-positive-coefficient microwave delay-line filter can only operate as low-pass filter [24]. To overcome this limitation, considerable efforts have been taken to design and implement photonic microwave delay line filters with negative or complex coefficients, to achieve bandpass filtering functionality in the incoherent regime [23]. A straightforward solution to generate negative coefficients is to use differential detection as proposed in [42]. As shown in Fig. 2.7, an optical waveform from an LD is modulated by a microwave signal, which is then time delayed by optical delay lines with a time delay difference of τ. The output signals from the fiber delay lines are fed to a differential PD, which consists of two matched PDs with the detected microwave signals combined and subtracted electrically, leading to the generation of positive and a negative coefficient. In particular, if the microwave signal is Gaussian shaped then with appropriate delay τ, a monocycle pulse shape can be generated as shown in Fig. 2.7. The two-tap photonic microwave delay line filter shown in Fig. 2.7 can be extended for n^{th} higher order derivative when the single wavelength source is replaced by an n wavelengths source and the 3 dB coupler is replaced by a $1 \times n$ WDM demultiplexer [23]. It is important to note that in Fig. 2.7, the negative coefficient is not generated directly in the optical domain. The limitation of this technique is that for a filter with "n" taps , "n" PDs are needed, making the filter complicated and costly. Therefore, a few techniques have been proposed to implement all-optical photonic microwave delay line filter with negative coefficients. These are summarized as follows:

1. *Two MZMs that are biased at complementary slopes*: In [43], UWB monocycle generation based on cascaded MZM modulators has been proposed. Depending on the polarity of monocycle needed, the polarity of modulators can be biased on the opposite slopes of the transfer function and by introducing an appropriate delay between the modulators a monocycle pulse can be generated. Similarly, in [44] higher order derivatives have been reported using multi laser source. In this case, part of the lasers are modulated by the positive polarity and the remaining part of the lasers modulated by the second modulator with opposite polarity. The delay is implemented using the chromatic dispersion of fixed length fiber. To further reduce the cost,a broadband laser source wavelength sliced using an AWG is used to replace tunable laser sources and has been reported in [45]. Furthermore, using a similar concept, monocycle and doublet pulses have been generated by implementing the intensity modulator based on a Sagnac interferometer comprising a traveling-wave phase modulator biased at the nonreciprocal quadrature point in [46, 47].

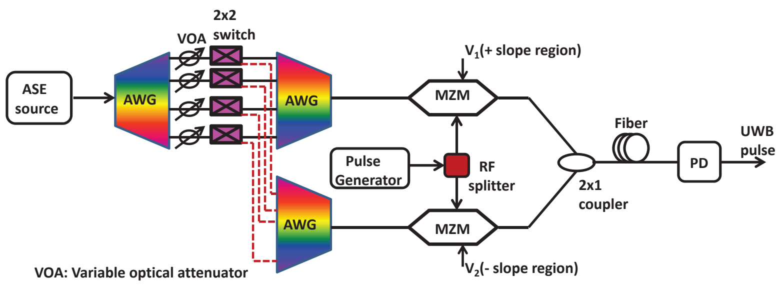

Figure 2.8: Concept of two MZMs biased at complementary slopes [45].

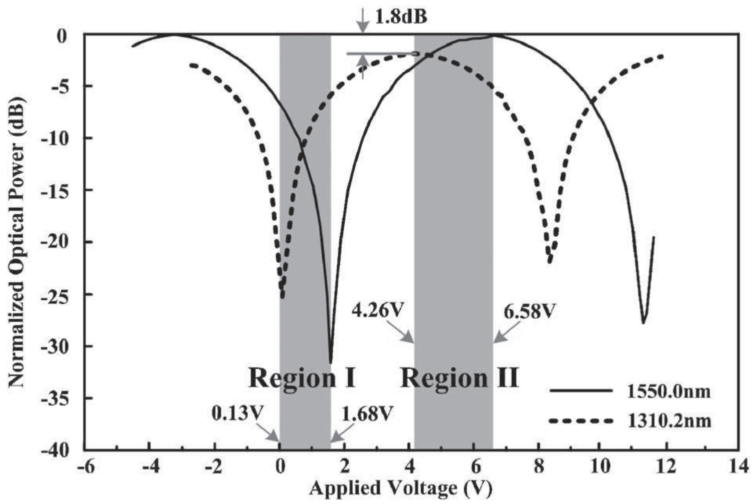

Figure 2.9: Concept of exploiting wavelength dependent transfer function of the MZM [46].

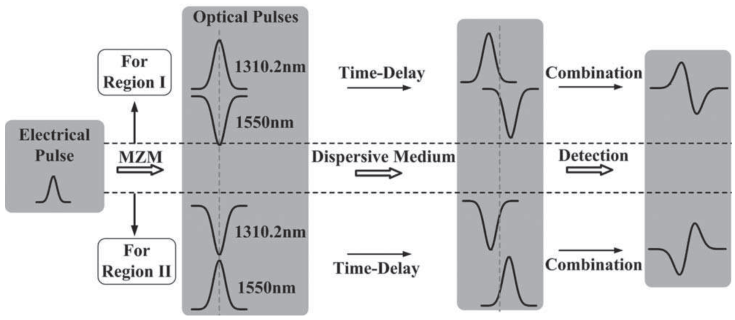

Figure 2.10: Pulse shaping using a wavelength dependent transfer function of the MZM [46].

2. *Using wavelength dependent nature of the transfer function of the MZM*: A similar concept of complementary slopes of MZM but using only a single MZM was proposed in [46]. In this technique by employing a single MZM with dual-wavelength injection at around 1310 and 1550 nm a pair of polarity reversed monocyle pulses have been generated. However, note that reducing the number of MZMs leads to additional laser sources in order to achieve complementary slopes using a single

MZM.

3. *XGM in nonlinear devices*: One of the optical devices which can be used for generation of IR-UWB is a semiconductor optical amplifier (SOA). The function of SOA is to generate a negative coefficient based on cross-gain modulation effect within the amplifier. As proposed in [48], two light waves, one a high-power pulsed light wave called pump, modulated by a Gaussian pulse and the other a lower-power CW light wave called probe, are injected into the SOA. Due to cross-gain modulation, the power of the probe varies inversely with pump power. A pair of complementary optical pulses is thus generated, with one at the pump wavelength and the other at the probe wavelength. By introducing a proper time-delay between the two pulses, a UWB monocycle can be generated. The pulse width of the monocycle can be adjusted by adjusting the time-delay so as to make its spectrum meet the FCC spectrum mask. Therefore, this way a photonic microwave delay line with one negative tap can be implemented. Similarly, by increasing the number of probe sources to two and introducing appropriate delay an UWB doublet can be generated using a three-tap photonic microwave filter with three coefficients $[1, -2, 1]$. Note that, the three pulses can be reflected by three FBGs that are physically separated to introduce a proper time-delay difference. The power ratio $1 : 2 : 1$ of the three powers can be achieved by either tuning the power of the three lasers diodes or designing the FBGs to have reflectivities with appropriate ratios. To overcome slow carrier recovery times in an SOA, aiming at multi-gigahertz repetition rate pulse generation, UWB generation using pump depletion effect in optical parametric amplifier (OPA) has been proposed in [49]. However, these techniques need multi-laser sources and high power for cross gain modulation to occur using either non-linear devices or highly non-linear special fibers.

4. *Cross Polarization modulation (XPolM) in polarization modulator*: In [50, 51], two polarity reversed pulses have been proposed by polarization modulation using a single phase modulator and delayed in polarization maintaining fiber (PMF) with the proper time to generate a monocycle pulse. According the work reported in [52, 53], the monocycle generation technique has been extended to generate doublet pulse by placing a SOA after the monocycle pulse generation to modify the optical pulses using the gain saturation and recovery principle in SOA. On the other

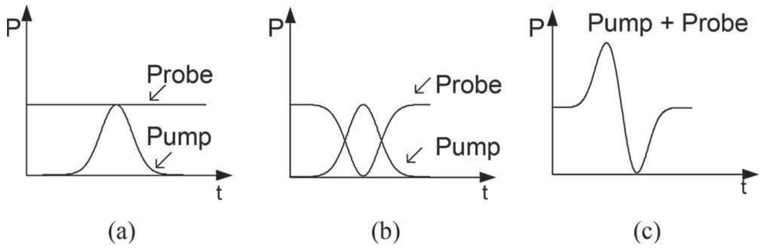

Figure 2.11: Concept of pulse shaping using XGM in an SOA [48]: a) Probe and pump power, b) probe and pump after XGM and c) final pulse shape after appropriate delay.

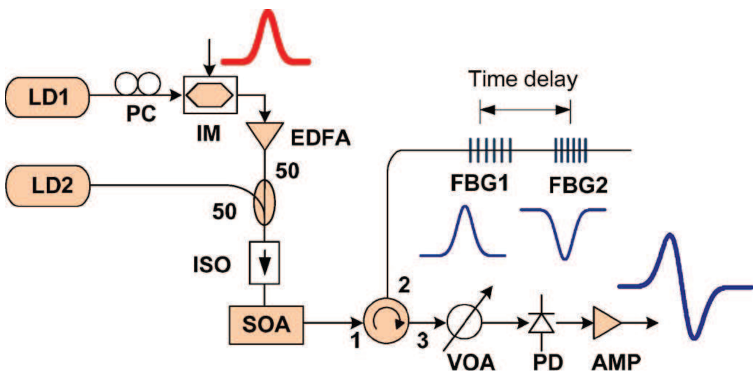

Figure 2.12: General experimental scheme for XGM in an SOA for IR-UWB pulse generation [32, 48].

hand, in [54], a switchable optical monocycle and doublet generation has been proposed based on 2 or 3 tap photonic microwave delay line using polarization modulation together with balanced photo-detectors.

2.4.3 Optical Spectral Shaping and Frequency-to-Time Mapping

IR-UWB pulses can also be generated based on optical spectral shaping and frequency-to-time conversion using a Fourier transform device. Fourier transform optical spectral shaping and dispersive stretching have been implemented to generate adaptive broadband microwave arbitrary waveforms in [55]. All-fiber spectral shaping and frequency-to-time conversion to generate monocycle and doublet pulses have been proposed in [56]. The basic concept of this approach is shown in Fig. 2.13. According to the work done in [56], the optical spectrum of a femtosecond pulse from a passively mode-locked fiber laser (MLFL) is optically shaped by an all-fiber optical spectral shaper, to obtain a spectral shape corresponding to a monocycle or doublet pulse. Then a length of single-mode fiber (SMF) is used to act as a dispersive device to perform the frequency-to-time conversion. Finally, an IR-UWB monocycle or doublet pulse is obtained at the output of a high-speed photodetector (PD). Using a similar fundamental concept, two linearly chirped fiber Bragg gratings (LCFBGs) with resistive heaters and a gain-switched laser, to perform accurate pulse shaping through frequency-to-time mapping have been proposed in [57]. In this method a reconfigurable UWB pulse shaping can be achieved by spectral shaping of a broadband optical source using thermal apodization of LCFBG followed by frequency-to-time mapping. It should be noted that, the frequency-to-time mapping method also holds for incoherent signals. Then, with minor modifications, the Fourier transform pulse shaper and the frequency-to-time mapping method can operate with an incoherent broadband sources, like amplified spontaneous emission (ASE) radiation, instead of a femtosecond laser. However, the main difference with coherent is that the synthesis of the profile of the electrical signal is defined from an average perspective. This implies that there are random, uncontrollable, fluctuations from pulse to pulse, and the target signal is only constructed by collecting a significant amount of pulse profiles and calculating the corresponding statistical average. In other words, the achieved electrical signal is not coherent. In consequence, this incoherent RF arbitrary waveform generation (RF-AWG) cannot be employed for application relying on high waveform fidelity in a single shot. However, by combining incoherent microwave photonic filtering with that of RF-AWG, a coherent electrical signal can be obtained using techniques such as microwave photonics filtering with N discrete taps and multi-wavelength techniques as reported in [58].

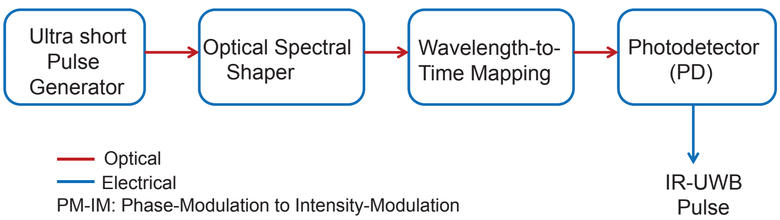

Figure 2.13: Concept of optical shaping and frequency-to-time mapping.

In addition, there are techniques that exploit non-linear transfer characteristics of optical components to shape Gaussian pulses to IR-UWB pulses. Such an example, is a technique proposed in [59], that exploits the non-linear transfer characteristics of MZM by biasing in its non-linear region to generate doublet pulses. In addition, complex IR-UWB waveform generation based on relaxation oscillations of a semiconductor laser and external injection locking of a DFB laser has been proposed in [60]. Recently, there is a tendency towards power-efficient pulses. One of such examples is IR-UWB pulse generation based on incoherent summation of two asymmetric monocycle pulses with inverted polarities achieved using the concept of multiple cross-phase modulation in the HNLF and multiple PM-IM conversions in arrayed-waveguide grating (AWG), which has been reported in [61]. It is also important to note that an IR-UWB pulse can be generated in principle by using the well-known optical pulse shaping techniques for arbitrary waveforms by exploiting the following basic techniques:

1. Direct space-to-time (DST) mapping
2. Line-by-Line pulse shaping
3. Temporal pulse shaping

Direct space-to-time mapping

Arbitrary waveform generation can be realized based on direct space-to-time mapping, in which an arbitrary optical pulse sequence is generated in the optical domain and then applied to a high-speed photodetector (PD) to generate a microwave waveform [62, 63]. By employing this technique, reprogrammable cycle-to-cycle synthesis of an arbitrarily shaped phase- or frequency-chirped waveform can be implemented. This technique can be implemented in free space where a spatial light modulator (SLM) is usually employed to perform temporal or spectral shaping. The key advantage of using SLM in a microwave arbitrary waveform generation system including IR-UWB pulses is its flexibility. An SLM can be updated in real time, making the system reconfigurable. However, a pulse shaping system based on an SLM is usually implemented in free space, making the system bulky and costly. Considering the low loss and small size, a microwave waveform generation system using fiber optic devices is a promising alternative to that implemented based on free space optics.

Line-by-Line Pulse Shaping

Mode-locked lasers generate periodic trains of ultrashort pulses which are characterized in the frequency domain by an evenly spaced series of discrete spectral lines, with the frequency spacing equal to the pulse repetition rate. Pulse shaping techniques, in which phase and amplitude manipulation of optical spectral components allow synthesis of user-specified ultrashort pulse fields according to a Fourier transform relationship, have been developed and widely adopted. Such technique of manipulation of the phase and amplitude of individual spectral lines can lead to a waveform spanning the full time period between mode-locked pulses (100 % duty cycle) known as line-by-line shaping. Note that to manipulate each spectral line a high resolution filter or multiple hyperfine filters are required, hence this technique is not widely adopted for IR-UWB pulse generation due to cost and complexity issues. However, it is sometimes used to generate radio frequency (RF) beat signal by exploiting a single pair of spectral lines using a hyperfine filter. It is essential to note that strong suppression of the deselected spectral lines is critical for accurate waveform generation. Note that, in principle, any periodic waveform can be constructed from a complete set of harmonic (cosine and sine) waveforms [64]. In [65], spectral line-by-line pulse shaping using a phase-modulated CW laser has been proposed with the aim of reducing the cost, complexity and achieving reasonable stability without active control.

Temporal Pulse Shaping

Microwave waveforms can also be generated using temporal pulse shaping (TPS) [63]. A TPS system usually consists of a mode locked laser source, a pair of complementary dispersive elements and a modulator. The modulator can be a Mach-Zehnder modulator (MZM) or a phase modulator. In general, the output signal is a scaled version of the Fourier transform of the input microwave signal. This means based on Fourier transform property, we can generate a high-speed microwave waveform using a relatively low speed input microwave waveform. However, it is important to note that those optical arbitrary waveform pulse shaping techniques are relatively complex and costly and hence they are not widely implemented for IR-UWB systems.

In general, all the above IR-UWB generation techniques used directly or indirectly the principle of microwave photonics filters. Hence, this is an indication of microwave photonics starting to play a key role in generating and distributing UWB signals for broadband and sensor network applications.

2.5 Overview of IR-UWB over fiber transmission concepts

Table 4.2 shows an overview of the IR-UWB over fiber transmission techniques including wireless link demonstrations. The results in the Table 4.2 show how the performance of IR-UWB over fiber wireless systems varies in terms of data rate, range in wireless, modulation format, antenna type and pulse shaping techniques. Furthermore, most of the reported results focused on the access part of the network using SMF fiber for transmission. It is very evident from Table 4.2 that conventional pulse design techniques of monocycle and doublet pulses have limited coverage at high bit rate ($\geq$ 1 Gb/s). It should be noted that modulation formats play a crucial role in the achievable distance. Modulation formats like On-off keying (OOK) can produce unnecessary spectral lines on the basic spectrum of the modulated pulse [66, 67]. These spectral lines have to be suppressed such that the spectral mask is satisfied. This can lead to reduction of SNR and hence limited coverage. A modulation format like bi-phase modulation (BPM) is suitable for range extension due to the smoothened spectrum. However, it needs coherent receivers, which can increase the cost of the system compared to direct detection receivers for OOK modulation format. It is also very clear from Table 4.2 that the choice of an antenna plays an important role on the performance of the system. In particular, a high gain directional antenna at receiver can improve performance of the system at the expense of large size and narrower field of view [68]. Therefore, it is very clear that a power-efficient pulse design technique is one the fundamental points which needs greater consideration for power-limited IR-UWB systems. Furthermore, IR-UWB systems are more suitable for low to medium data rate. The data rate is fundamentally limited by the wireless channel due to the multipath effect. Hence, this shows that there is no reason to push the data rate beyond the actual achievable data rate in the wireless link as there is a tendency of increasing the data rate to 5 Gb/s as reported in [69]. Note that, IR-UWB is suitable for precise ranging and localization due to the large available bandwidth. Accordingly, IR-UWB systems are recognized by IEEE 802.15.4a for relatively low data rate communication and localization applications. Hence, most of the experimental results, which are described in the subsequent chapters are limited to a maximum data rate of 2Gb/s and targeted BER of 10^{-3} due to off-line processing.

Table 2.1: Overview IR-UWB over fiber (SMF: Single mode fiber, MMF: Multi-mode fiber, NZDSF: Non-zero dispersion shifted fiber, OOK: On-Off keying modulation, BPM: Bi-phase modulation, Omni: Omni-directional and NC: Non-conventional pulses).

Data rate (Gb/s)	Fiber type L(km)	Wireless reach (cm)	Modulation	BER	Antenna Directivity	Pulse Shape	Reference
1.70	SMF (24km)	5	OOK	$1e^{-9}$	Tx:Omni Rx:Omni	Monocycle	[70]
1.00	MMF (600m)	90	BPM	$1e^{-5}$	NA	Monocycle	[71]
1.25	SMF (25km) (25km)	45	OOK	$2e^{-3}$	Tx:Omni Rx:Omni	Doublet	[72]
1.25	SMF (20km)	35	OOK	$2e^{-3}$	Tx:Omni Rx:Omni	Doublet	[73]
1.025	SMF (10km)	20	OOK	$1e^{-4}$	Tx:Directional Rx:Directional	Modified doublet	[74]
0.50	SMF (5.46km)	65	OOK	$1e^{-6}$	Tx:Omni Rx:Directional	NC	[75]
1.00	SMF (15km)	100	OOK	$1e^{-4}$	Tx:Omni Rx:Omni	NC	[57]
4.00	MMF (100m)	400	OOK	$2e^{-3}$	Tx:Omni Rx:Directional	5^{th}-derivative	[76]
2.00	MMF (1km)	300	BPM	$2.7e^{-3}$	Tx:Omni Rx:Directional	5^{th}-derivative	[77]
1.00	SMF (23km)	200	OOK	$2.5e^{-4}$	Tx:Omni Rx:Directional	5^{th}-derivative	[78]
2.00	SMF (25km)	400	BPM	$4.9e^{-4}$	Tx:Directional Rx:Directional	5^{th}-derivative	[79]
2.00	NZDSF (20km)	800	OOK	$2e^{-3}$	Tx:Omni Rx:Directional	5^{th}-derivative	[80]
2.00	SMF (46km)	50	OOK	$2e^{-3}$	Tx:Omni Rx:Directional	NC	[81]
1.00	SMF (23km)	40	OOK	$2.5e^{-3}$	Tx:Omni Rx:Directional	NC	[82]

2.6 Research Challenges

Following the discussions in the previous sections on generation and transmission of IR-UWB signals over fiber, the following research problems have been identified. It should be noted that the selection of the impulse signal type is one of the fundamental considerations in designing an IR-UWB radio system, because the impulse type will determine the performance of the system and should be compliant with the FCC power and spectral mask. Furthermore, the key design requirements of UWB systems such as low cost, low complexity, low power consumption and high data rates are very important for IR-UWB over fiber systems. Accordingly, several research challenges have been identified and this thesis tries to address them:

1. *Power-efficient pulse shaping techniques:* Most of the photonic generation techniques focus on the conventional monocycle and doublet pulses. These pulses are not FCC-compliant and very poor in power efficiency. Hence, simple and novel IR-UWB pulses, which are fully FCC-compliant and have better power efficiency should be investigated. Furthermore, a performance comparison of the proposed pulses and conventional pulses must be made using a realistic path loss model.

2. *Simplicity and low-cost:* As mentioned above, the main promise of UWB is simplicity, low-cost, low power consumption and high data rate for WPAN applications. However, as described in the previous sections, most of photonic generation techniques are complex and consume more power. This is mainly due to the need multiple of laser sources, multiple modulators and non-linear devices such as semiconductor optical amplifiers (SOA) to generate IR-UWB signals. Hence, simple optical schemes with potential features of low cost, low complexity, low power consumption and with feasibility to be integrated on a photonic integrated chip should be investigated.

3. *Multi-Gbit/s transmission of IR-UWB over different fiber types:* As mentioned in the previous section, most of the reported results focuses on PON-like access network application and thus SMF fiber is used for transmission. However, there is a very clear trend that optics is also reaching for LAN-like in-building and in-home applications. Therefore, with this application in mind, different fiber types (multimode silica and plastic fiber) can be employed to reduce cost of installation and

transceivers. Hence, performance of multi-Gbit/s of IR-UWB over SMF, MMF and POF should be investigated.

4. *Networking capability of IR-UWB over fiber:* Most of the IR-UWB over fiber research focuses on point-to-point applications. Hence, the networking capability of IR-UWB by exploiting routing and switching should be investigated. In addition, to further reduce the cost by exploiting existing optical infrastructure, co-existence of wired baseband data with wireless IR-UWB in a single fiber should be investigated for integrated, high capacity and energy-efficient in-building network applications.

5. *Ranging/localization using IR-UWB over fiber:* As mentioned in Chapter 1, one of the attractive features of IR-UWB technology is its capability for both communication and localization applications. Due its short pulse, ranging/localization with centimeter-level accuracy can be achieved and thus makes it suitable for indoor applications. In line with the vision of a single fiber-wireless infrastructure for future in-building communication networks, the potential of effective of ranging/localization of IR-UWB over fiber system should be investigated.

2.7 Summary

In this chapter the concept of RoF systems has been described. The application of microwave photonics in terms of generation of RF and microwave signals has been described. In particular, the role of microwave photonics in shaping IR-UWB pulses has been described. An overview of photonic generation techniques of IR-UWB for UWB-over-fiber application has been given. It has been pointed out that most of the photonic generation techniques are focusing on generation of conventional pulses without taking into account the power efficiency, complexity and cost of the system. Hence, it is clear that microwave photonics are playing a key enabler of RoF in general and UWB-over-fiber in particular. However, to be widely accepted in a cost-sensitive application environment such as in-building/in-home communication the integration of microwave components in optical chips should be the next step. Furthermore, more widely exploiting existing infrastructure by integrating wireless is one of way of reducing the cost of the system. However, for better exploiting the FCC-mask novel pulse generation is a key step for successful deployment of IR-UWB-over-fiber systems.

Chapter 3

IR-UWB Pulse Shaping and Generation Techniques

This chapter focusses on shaping and generation of novel IR-UWB pulses. After introduction, a simple IR-UWB signal model will be presented. IR-UWB requirements from Shannon's perspective and FCC-mask will be described. Figure of merit for effective utilization of the FCC-mask or spectral power efficiency of IR-UWB will be defined. Overview of existing pulse shaping techniques will be discussed. Proposed new and novel pulse shaping techniques will be presented. Simple optical generation of the novel pulse will be described. Theoretical performance comparison of conventional pulse shapes and proposed pulse shapes are discussed using figure of merit and realistic path loss model. Furthermore, features of the proposed pulses will be presented.[1].

3.1 Introduction

As mention in the previous Chapter 1, there is a clear demand for broadband wireless services. Users want to share multimedia applications among networked consumer electronics, personal computers and mobile devices accessed at home and perhaps remotely. However, the increasing demand for large bandwidth multimedia wireless services is hampered by the lack of available spectrum [84]. On the other hand, in recent years, there has been growing interest for converged integration of wired and wireless over a single in-building optical network infrastructure to provide both broadband communications and

[1]This chapter is based on the results published in [21, 83–86]

sensor applications. From the indoor wireless perspective, some of the important design requirements are: high data capacity, robustness against multipath fading, low power dissipation, co-existence with other wireless services, low cost and simplicity [21]. UWB technology is considered as one of the most promising techniques for next generation short-range broadband wireless and sensor networks with capabilities of achieving these design requirements [13–16, 20, 87–89]. However, as introduced in Chapter 2, the UWB communication distances are limited, typically less than 10 meters. To increase the coverage area, UWB signals should be carried over wired lines such as coaxial cable or optical fiber. Due to the low loss, large bandwidth and immunity to electromagnetic interference, distribution of UWB signals over optical fiber, better known as UWB-over-fiber is considered a promising solution [32, 33].

One of the fundamental points that require detailed consideration in IR-UWB circuits and systems design is the selection of the impulse signal type as it determines the performance of the IR-UWB system [90]. The techniques for shaping or generating IR-UWB pulses can be broadly classified into two main categories: electrical and optical techniques [83]. In both techniques, Gaussian-based monocycle and doublets pulses are considered as conventional pulses due to better bit-error rates and multipath resilience as compared to different impulse signals [90]. Accordingly, in the past few years, several photonic generation schemes that focused on the generation of the conventional monocycle and doublet employing different schemes have been reported [32–38, 48, 50–54, 59, 91–94]. However, these pulses do not fully satisfy the FCC rules with good spectral utilization and hence limit the achievable wireless distance as described in Chapter 2 and reflected in Table 2.1. Hence, different pulse design pulse shaping techniques in the electrical domain have been proposed [13, 15, 16, 95–100]. As shown in Chapter 2 and Table 2.1, among the complex generation schemes, the 5^{th}-order derivative has been recently adapted for IR-UWB over fiber systems in [76–80]. Recently, photonic generation techniques that focused on nonconventional pulses aimed at enhancing the power spectral efficiency has been reported in [44, 45, 57, 61, 75, 94, 101–103]. However, all previously proposed pulse generation concepts show either increasing complexity and cost due to either multiple laser sources, multiple modulators or non-linear devices.

In this chapter, simple and new pulse generation concepts with the potential of low complexity and cost of the system will be provided. To clearly understand the choice of impulse signal for IR-UWB systems is one of the key issues, a simple signal model and IR-UWB from Shannon's perspective will be described first. Then the shaping, generation and performance evaluation will be explained in the subsequent sections.

3.2 Signal Model

In a UWB impulse radio, each information symbol is conveyed over a train of N_f repeated basic pulses, with one pulse per frame of duration T_f. Each unit-energy pulse $x(t)$ has an ultrashort duration T_p ($T_p \leqslant T_f$) at the nanosecond scale. The equivalent symbol signature waveform is $p_s(t) = \sum_{n=0}^{N_f-1} p(t - c_n T_c - nT_f)$ and has symbol duration $T_s = N_f T_f$, where the sequence $\{c_n\}_{n=0}^{N_f-1}$ represents the user-specific pseudo random time-hopping (TH) code with ($c_n T_c < T_f$), $\forall n \in [0, N_f - 1]$. Let $b_k \in \pm 1$ be independent identically distributed binary data symbols with energy E_s spread over N_f frames. When pulse amplitude modulation (PAM) is used, the transmitted PAM IR-UWB waveform is given by [100]:

$$u(t) = \sqrt{\frac{E_s}{N_f}} \sum_k b_k p_s(t - kTs) \tag{3.1}$$

The power spectral density (PSD) of $u(t)$ is then given by:

$$\phi(f) = \frac{E_s}{N_f} \cdot \frac{1}{T_s} |P_s(f)|^2 \tag{3.2}$$

where $P_s(f)$ is the Fourier transform (FT) of $p_s(t)$ and depends on both $p(t)$ and the TH code $\{c_n\}_{n=0}^{N_f-1}$. Specifically, $P_s(f)$ can be expressed as:

$$P_s(f) = P(f) \sum_{n=0}^{N_f-1} \exp\left(-j2\pi f_n T_f\right) \exp\left(-j2\pi f c_n T_c\right) \tag{3.3}$$

where $P(f)$ is the FT of $p(t)$. Equation (3.2) now becomes:

$$\phi_{uu}(f) = \frac{E_s}{T_s N_f} |P(f)|^2 \left| \sum_{n=0}^{N_f-1} \exp\left(-j2\pi f(nT_f + c_n T_c)\right) \right|^2 \tag{3.4}$$

when the TH code $\{c_n\}_{n=0}^{N_f-1}$ is independent and uniform distributed over$[0, N_c - 1]$ with integer values, $\phi_{uu}(f)$ can be approximated as [100]:

$$\phi uu(f) \approx \alpha |P(f)|^2 \tag{3.5}$$

where $\alpha = \frac{E_s}{T_f}$ is a constant. A similar result is also derived in [104] for pulse position modulation (PPM) UWB waveforms. In both cases, a UWB transmitter can be treated as linear amplifier of the pulse shape $p(t)$. Hence, the UWB pulse design problem is equivalent to designing the basic pulse $p(t)$ to meet the relevant system requirements [100].

3.3 IR-UWB from Shannon's perspective

From the communications theory point of view, the most attractive feature of IR-UWB systems is the wide bandwidth and power-limited operation. This extremely wide bandwidth is the fundamental difference between UWB systems and conventional narrowband wireless systems. Assuming, an additive white Gaussian noise (AWGN) channel, the channel capacity of UWB and narrowband systems has been evaluated using Eq. 1.5 as described in Chapter 1. Accordingly, the capacity of UWB and narrowband systems depicted in Fig 3.1. According to Fig. 3.1, the result show clearly two distinct power and bandwidth limited regimes. More specifically, UWB systems operate in the power-limited regime whereas many narrowband systems available today operate in the bandwidth-limited regime as shown in Fig. 3.1. This fundamental difference has a significant effect on design choices for modulation, pulse shaping and coding techniques. For IR-UWB systems, the bandwidth tends to be much higher than the data rate so that the system can operate at very low signal-to-noise ratios as shown in Fig. 3.2. Notice that Fig. 3.2 indicates that the IR-UWB systems have a potential to achieve high data rates in Gigabit/s with relatively low transmit power. It should be noted that a power efficient pulse shaping and modulation technique is critical for IR-UWB system: a small disadvantage in power efficiency directly translates to a corresponding reduction in throughput as shown in Fig. 3.2. This highlights the importance of comparing the commonly used pulse shaping techniques not only from FCC-compliance perspective but also from power spectral efficiency perspective.

3.3.1 Spectrum-mask utilization efficiency

For quantitative evaluating the spectrum-mask utilization efficiency, the normalized effective signal power (NESP) or spectral power efficiency has been introduced in [100]. NESP is defined as the ratio of power of the synthesized UWB waveform to the total power permissible under the mask. When

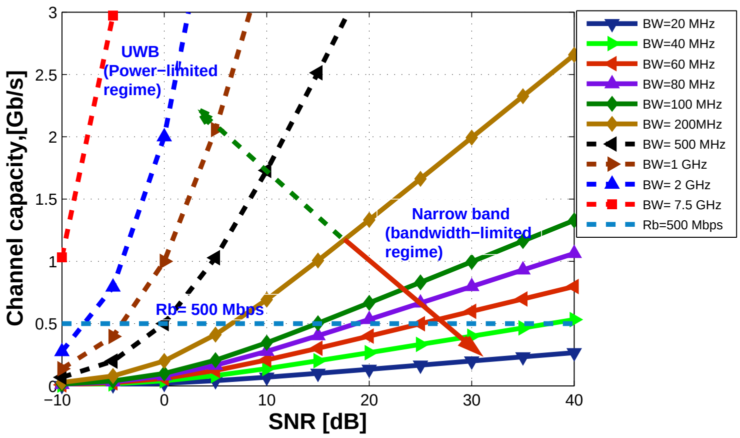

Figure 3.1: Theoretical capacity comparison between UWB and narrow band systems under AWGN channel.

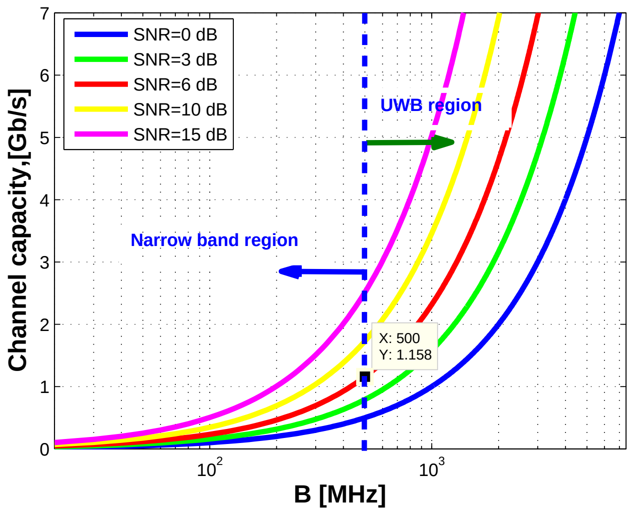

Figure 3.2: Theoretical capacity comparison between UWB and narrow band systems under AWGN channel(another view).

the spectrum mask is given, the total transmission power allowable under the mask is fixed, so maximization of transmitted power is equivalent to maximization of NESP [100]. Therefore, the spectral power efficiency (η) is defined as the ratio between the average power of the pulse within the desired band ($3.1 - 10.6$ GHz) and the total admissible power under the FCC mask within the same band. It is expressed as:

$$\eta = \frac{\int_{f_l=3.1\text{GHz}}^{f_h=10.6\text{GHz}} Y(f)\, df}{\int_{f_l=3.1\text{GHz}}^{f_h=10.6\text{GHz}} P_{FFC}(f)\, df} \times 100\% \tag{3.6}$$

Using the NESP or spectral power efficiency given in Eq. 3.6 different pulse shapes can be compared for effective utilization of the spectrum mask. The higher the spectral power efficiency the better the waveform. Several optimal and complex shaping using optimization techniques based on the principle finite-impulse response (FIR) are proposed in the literature [97, 100]. However, due to the difficulty of implementation with low cost, only Gaussian based derivative are commonly employed in IR-UWB over fiber systems.

3.4 Overview of IR-UWB Pulse Shaping Techniques

As mentioned in section 3.3, UWB systems are power limited systems rather than spectral limited. Therefore, waveform design for the IR-UWB communication is a major issue and the aim is to obtain a pulse waveform that complies with FCC mask as closely as possible and to maximize the bandwidth as well [16]. A typical signal that can be considered as a basis function for IR-UWB transmission is the Gaussian pulse expressed as:

$$p(t) = \frac{A}{\sqrt{2\pi}\sigma} \exp\left(-\frac{t^2}{2\sigma^2}\right) \tag{3.7}$$

where, A and σ denote the amplitude and spread or shaping factor of the Gaussian pulses respectively. As antennas are not efficient at DC, it is preferable to use derivatives of Gaussian pulse which have smaller DC components [13, 15, 16]. Hence, as mentioned earlier, in the UWB systems, the most commonly used waveforms are monocycle and doublet. These pulses are becoming conventional and most widely used in photonic generation of UWB over fiber systems due to the mathematical simplicity, multipath resilience and good BER performance [32, 34–36, 46, 48, 50–56, 66, 67, 70, 91, 92, 105–107].

On the other hand, these commonly used pulses have poor NESP or spectral power efficiency. The PSD of n^{th} derivative of Gaussian pulse can be obtained recursively as provided in [16, 95]. It is obvious that everything can fit FCC mask if the spectral power efficiency is low enough. However, as UWB is a power limited system, the radiating power must be as high as possible without violating the regulation. Therefore, in the Fig. 3.3, I use the first seven derivatives of the Gaussian pulse with an optimal pulse shaping factor for each derivative to make the spectrum as wide as possible [83]. Then PSD of each derivative is normalized and finally scaled to the maximum legally allowed PSD. Notice that the low-order derivatives ($n \leq 4$) are not FCC compliant around the GPS band ($0.96 - 1.61$ GHz) if they are forced to optimize the assigned power and the bandwidth. The main reason for this limitation is that most of their energy or peak frequency lies in the low frequency range. Therefore, in order to respect the FCC mask regulations, higher order derivatives are preferable because of the peak frequency of the pulse is increased with increasing derivation order as shown in Fig. 3.3. For this reason, a fifth order derivative is recommended in [95]. However, it is more complex and not suited for low cost short-range fiber communications.

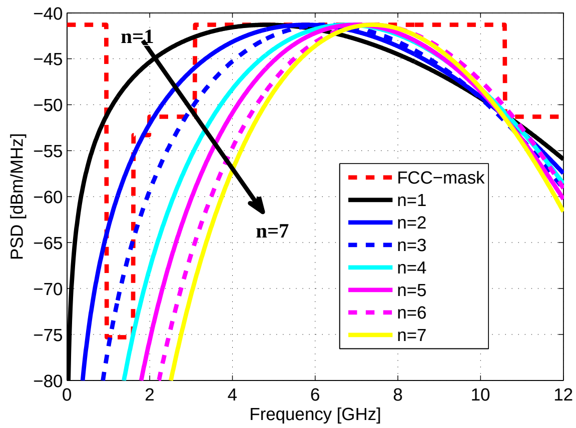

Figure 3.3: PSD of higher order derivatives of Gaussian pulses.

A general relationship between peak frequency f_{peak}, the order of derivation k and the shaping factor σ (ps), by observing the Fourier transform of the k^{th} derivative is given by [13, 88].

$$f_{peak} = \frac{1}{\sigma\sqrt{\pi}}\sqrt{k} \tag{3.8}$$

Variation of peak frequency with pulse shaping factor σ, for the first seven derivatives of the Gaussian pulse is shown in Fig. 3.4. According to the simulation result shown in Fig. 3.4, the smaller pulse shaping factors the higher

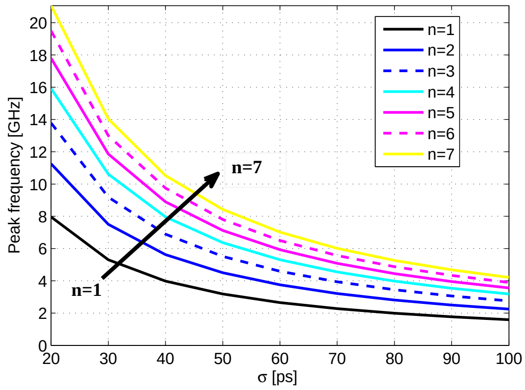

Figure 3.4: Peak frequency versus pulse shaping factor σ (ps).

peak frequency. Furthermore, the bandwidth of the signal increases as the pulse shaping factor becomes smaller due to the time and bandwidth inverse relationship. Therefore, differentiation of the Gaussian pulse influences the PSD; both peak frequency and the bandwidth of the pulse vary with differentiation order and pulse shaping factor as clearly shown in Fig. 3.3 and Fig. 3.4 respectively. It should be noted that, as the order of the derivatives increases, the energy of the pulse moves to higher frequency bands and thus the allocated spectrum is used more efficiently as shown in Fig. 3.4.

The main bottleneck of UWB remote communication is due to electromagnetic interference between UWB systems and the GPS band [83]. The FCC-mask requirement for protecting the GPS band and the low peak frequency of the conventional pulses lead them to be poor NESP pulses. Furthermore, it is very important to note that IR-UWB systems for applications in consumer electronics or short-range fiber communications required low complexity, low cost, low power consumption, high power efficiency and high data rate. Therefore, an IR-UWB pulse design technique must consider both the FCC-mask and the system requirements. All previously reported [13, 15, 16, 95–100] electrical IR-UWB pulse design techniques do not satisfy all the requirements. Hence, a new pulse design approach is required to satisfy all the requirements and also exploits the simplicity, feasibility and good BER performance of conventional pulses employing signal processing techniques.

3.5 Proposed Pulse Shaping Techniques

3.5.1 Linear Combination of Monocycles

In general, shaping the spectrum by modifying the pulse waveform is an interesting feature of IR-UWB. Basically, the spectrum may be shaped in three different ways [13]: *pulse width variation, pulse derivation, and combination of basis functions.* In order to reduce the complexity of the systems, a linear combination of two monocycles using different pulse-shaping values of σ_{11} and σ_{12} is proposed and reported in [83]. The linear sum value $y_{ws1}(t)$ is given by:

$$y_{ws1}(t) = a_{11}x_{11}(t, \sigma_{11}) + a_{12}x_{12}(t, \sigma_{12}) \tag{3.9}$$

where $x_{1i}(t, \sigma_{1i})$ is the first order derivatives of Gaussian pulses, expressed by [15]:

$$x_{1i}(t, \sigma_{1i}) = \left(\frac{-2t}{\sigma_{1i}^2}\right) \exp\left(\frac{-t^2}{2\sigma_{1i}}\right) \tag{3.10}$$

with $i = 1, 2$, $\sigma_{11} = 81.35$ps and $\sigma_{12} = 50.3$ps are the pulse shaping factors used for each monocycles. Furthermore, $a_{11} = 0.81$ and $a_{12} = -1.2$ are the normalized optimal weighting parameters obtained from the simulation result. In practice, the summation of the pulses can be realized by a wideband RF power splitter and combiner that have a flat frequency response in the desired band. In the optimization of the IR-UWB pulse weighting parameters, two searching criterions were used: First, the generated RF spectrum must be fully FCC compliant, the test pass parameter, ζ can be defined as:

$$\zeta = \begin{cases} 1 & \text{if } min\{P_{FCC}(f) - Y(f)\} \geq 0, \forall f \in [0, f_{max}]; \\ 0 & \text{if } otherwise. \end{cases}$$

where $P_{FCC}(f)$ is the normalized FCC spectral density mask and $Y(f)$ is the normalized power spectral density of the designed pulse respectively. The value of the test parameter, $\zeta = 1$ indicates the compliance of the PSD of the pulse with FCC mask requirements. Otherwise, $\zeta = 0$ indicates violation of the FCC mask. The maximum frequency, f_{max} considered during the simulation is 12GHz.

Secondly, as described in the previous section 3.3, IR-UWB systems are power limited systems, the power efficiency or normalized effective signal power (NESP) efficiency of the pulse as defined in subsection 3.3.1 within the useful UWB band should be as high as possible [83]. In other words, the spectral utilization efficiency, η as defined in Eq. 3.6 should be maximized.

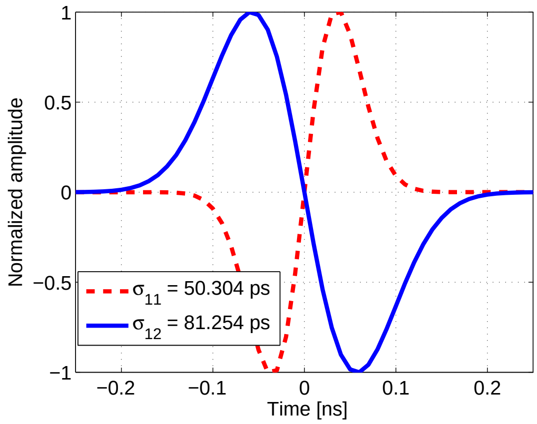

Figure 3.5: Two monocycles with different pulse shaping factor.

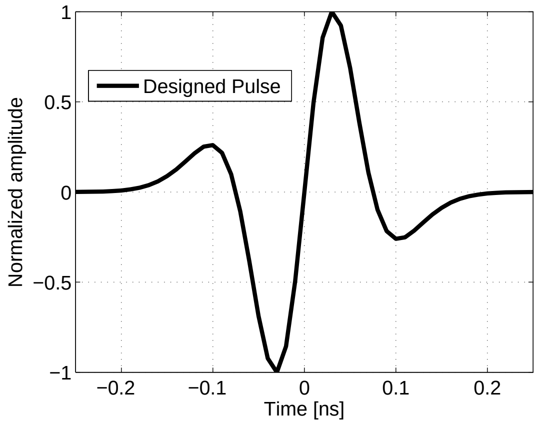

Figure 3.6: Proposed pulse in time domain after linear combination.

Note that, maximizing the power efficiency yields that the bandwidth of the pulse at -10 dB as defined by FCC as large as possible. This in turn helps to achieve high data rates and hence increase spectral efficiency of the system. In short, the pulse shaping parameters, $\sigma_{11}$and σ_{12} mainly determine the bandwidth of the pulse and are selected based on the peak frequency and pulse shaping factor relationship provided in Eq. 3.8. Then the weighting factors are determined when the FCC mask requirement is satisfied (i.e., $\zeta = 1$) and spectral power efficiency is maximized as expressed in Eq. 3.6. The Fourier

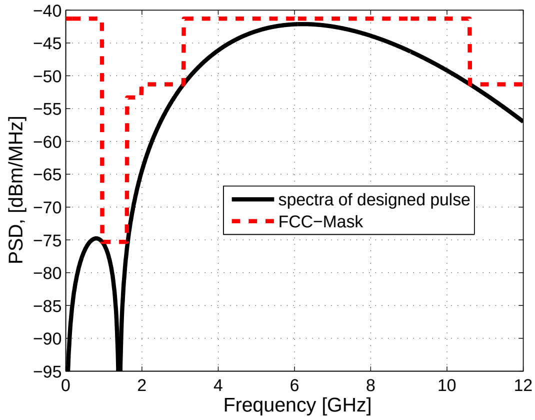

Figure 3.7: PSD of proposed pulse.

transform of $yws1(t)$ is given by:

$$Y_{ws1} = a_{11}X_{11}(f, \sigma_{11}) + a_{12}X_{12}(f, \sigma_{12}) \tag{3.11}$$

where

$$X_{1i}(f, \sigma_{1i}) = (j2\pi f)\, exp\left(-\frac{(2\pi f \sigma_{1i})^2}{2}\right) \tag{3.12}$$

The simulation result of each normalized monocycle pulse is shown in Fig. 3.5. The normalized pulse after linear combinations of the pulses using their corresponding weighting coefficient is depicted in Fig. 3.6 and its corresponding spectral density compared with FCC mask is shown in Fig. 3.7. According to the simulation result shown in Fig. 3.7, the newly designed IR-UWB pulse fits the FCC-mask better than the conventional monocycle and doublet pulses even in the power-restricted GPS band from 0.96 GHz to 1.61 GHz [83]. Furthermore, due to the side lobes created in the basic shape of the monocycle, the designed pulse has more zero crossings compared to the conventional monocycle and doublet pulse, which moves the energy of the pulse to higher frequency ranges with similar effect as higher-order derivatives of Gaussian pulse. Accordingly, the resulted pulse has a central frequency of 6 GHz and a 10 dB bandwidth of 7.5 GHz with fractional bandwidth of 125% as shown in Fig. 3.7 and reported in [83]. Note that antenna response is an important factor as reported in [75, 101]. However, different antenna type and different antenna configuration yields different characteristics. Hence, I use a generic approach to design a pulse which confirms the FCC-mask requirement with high power efficiency by assuming an antenna with flat gain and a linear phase response in the desired band. An antenna with reasonably quite flat response in the desired UWB band is commercially available (Skycross SMT-3TO10M-A) and it has been reported in [66]. Hence, the novelty of this approach lies in employing a linear combination of the lowest derivative of Gaussian pulses in order to provide all the desired features needed for IR-UWB communication systems especially for short-range fiber communications [83].

3.5.2 Linear Combination of Modified Doublet Pulses

To avoid using two different pulse shaping factors as described in the previous section 3.5.1, I have proposed a linear combination of modified doublet with fixed pulse shaping as reported in [84]. A general signal model for the modified doublet,$x(t)$, is expressed as:

$$x(t) = A_2 \left[1 - 4k\pi \left(\frac{t}{\sigma}\right)^2\right] \exp\left(-2\pi \left(\frac{t}{\sigma}\right)^2\right) \tag{3.13}$$

where σ is a pulse shaping factor and $k = 1+\epsilon$ is an arbitrary scaling parameter for ϵ nonzero very small values. Notice that, if $k = 1+\epsilon$ and ϵ are a set of very small positive values, then $x(t)$ results in a family of modified doublet pulses. As a special case, for $\epsilon = 0$, then $k = 1$ and $x(t)$ turns to be the well known conventional doublet [86]. Therefore, a modified doublet pulse is a Gaussian doublet variant in which the amplitude ratio between its positive and negative part of doublet pulse slightly modified as shown in Fig. 3.8. The Fourier transform of the proposed modified doublet pulse is expressed as [21, 86]:

$$X(\omega) = \left[\frac{4\pi(1-k) + k\omega^2\sigma^3}{8\pi\sqrt{\pi}}\right] \exp\left(-\frac{(\omega\sigma)^2}{8\pi}\right) \tag{3.14}$$

The pulse shape and PSD of the modified doublet pulses for $\sigma = 150$ ps are shown in Fig. 3.8 and Fig. 3.9 respectively. It should be noted that a modified doublet has been selected as the basis function due to its notch around GPS band. The level and location of the notch is determined by the scaling parameter k as shown in Fig. 3.9. However, the PSD is still not FCC compliant as shown in Fig. 3.9. Therefore, it is evident that from Fig. 3.9, an additional signal processing equivalent to a bandpass filter is required [21, 86]. Hence, as a second step, I used the linear sum of the modified doublet with

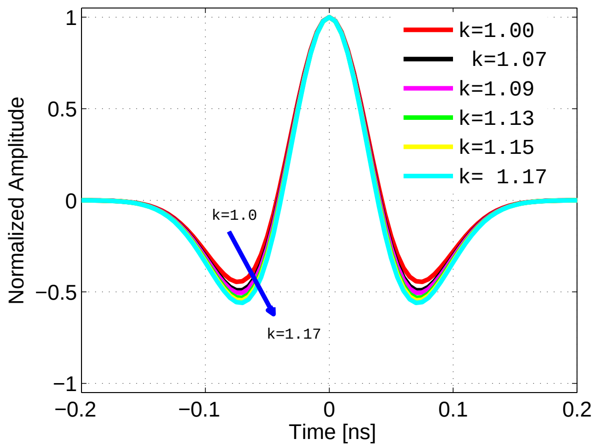

Figure 3.8: Family of modified doublet pulses in time domain.

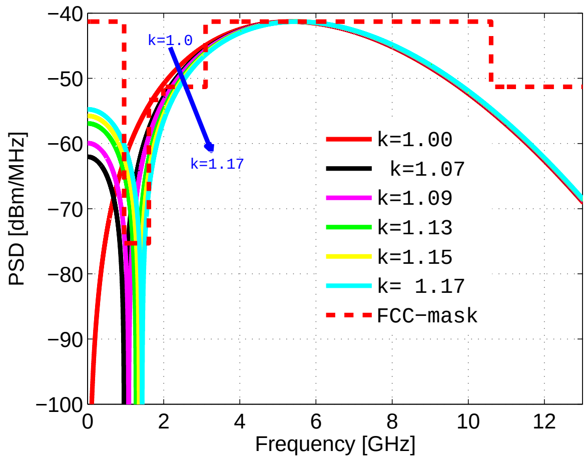

Figure 3.9: PSD of modified doublet pulses before linear combination.

its delayed and inverted form but with a fixed pulse shaping factor, $\sigma = 150$ ps. This linear sum operation, $y(t)$ is expressed as :

$$y(t) = a_{11}x(t) + a_{12}x(t-\tau) \tag{3.15}$$

where $x(t)$ and $x(t-\tau)$ are the modified doublet pulses, one is delayed from the other, $a_{11} = +1$ and $a_{12} = -1$. In practice, it can be considered as a two-tap microwave delay line bandpass filter with coefficients $(+1, -1)$. The

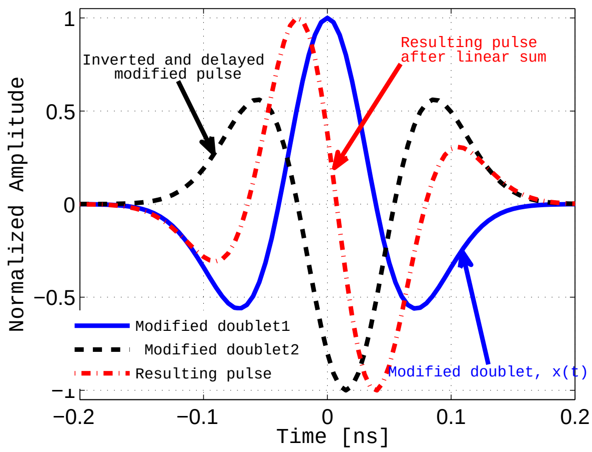

Figure 3.10: Linear sum operation of modified doublet pulses and the resulting pulse shape.

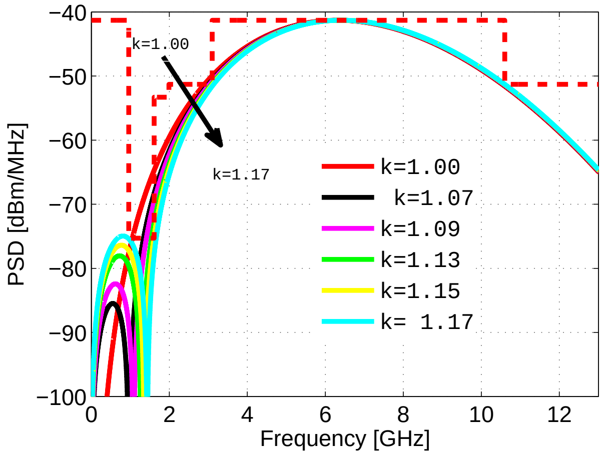

Figure 3.11: PSD of family modified doublet pulses after linear combination.

delay parameter (τ) determines the resulting pulse shape and its PSD. If the delay is too large then the bandpass filter is too narrow and hence distorts the original PSD. If the delay is too small, the bandwidth is large enough that the resulting PSD is wide and hence not compliant to the FCC-mask [86]. Therefore, an optimum delay ($\tau = 37$ps) is obtained by optimizing the power efficiency according to Eq. 3.6. The temporal pulse shape of the resulting pulse and its PSD are shown in Fig. 3.10 and Fig. 3.11 respectively. Due to the linear sum operation given in Eq. 3.15, the resulting pulse has more zero-crossing in temporal response; its low frequency components are further suppressed and its peak frequency shifts to a higher frequency as shown in Fig. 3.11. Hence, this approach produces a novel pulse shape that fits the FCC-mask requirement with low complexity and better NESP or spectral power efficiency. It is important to note that the final novel pulse shape shown in Fig. 3.11 can also be realized using a four-tap microwave photonic delay line approach by considering as scaled and shifted sum of Gaussian pulses. The optical generation of this novel pulse will be discussed in the following section.

3.6 Optical Generation of Modified Doublet Pulse

To realize the optical generation of the novel pulse shape described above, I used basically a two-step approach. In the first step, Gaussian pulse has been shaped into a modified doublet by exploiting an electro-optic intensity modulator (EOM) both as modulator and pulse shaping element. Secondly, the modified doublet is divided into two equal arms and finally combined with its inverted and delayed version using a balanced photo-detector (BPD). By this process, I created a novel IR-UWB pulse shape that has a notch in the GPS band and thus fully compliant to the FCC spectral mask. Note that the shaping and delaying process is performed in the optical domain followed by polarity inversion of one of the pulses using BPD in the electrical domain. To produce a family modified doublet pulses, the amplitude of the Gaussian RF input voltage and the EOM setting has been tuned to achieve the desired pulse.

An EOM has a sinusoidal transfer function as shown in Fig. 3.12 and it can be expressed as [59]:

$$P_{out} = \frac{1}{2}P_{in}\left(1 + \cos[\frac{\pi}{V_\pi}V_{bias} + \frac{\pi}{V_\pi}V(t)]\right) \tag{3.16}$$

where P_{in} and P_{out} denote the input and output optical power, $V(t)$ is the voltage of the electrical modulation signal, V_{bias} is the bias voltage, and V_{pi} is the half-wave voltage of EOM. As shown in Fig. 3.12, an electrical Gaussian pulse applied to the EOM can be shaped to a modified doublet when the EOM is biased on the non-linear portion of its transfer function (i.e., near to the maximum or minimum transmission point) and the amplitude of Gaussian pulse is large enough that the peak part and the pedestal part of the pulse lie in the opposite slopes. As a result, either the pedestal or the peak part of the Gaussian pulse can be inverted. Hence, a modified doublet can be produced by controlling both the bias voltage and the amplitude of the Gaussian pulse as shown in Fig. 3.12. Notice that, by switching the bias point the polarity of the modified doublet can be reversed, which provides a simple method to implement pulse polarity modulation (PPM).

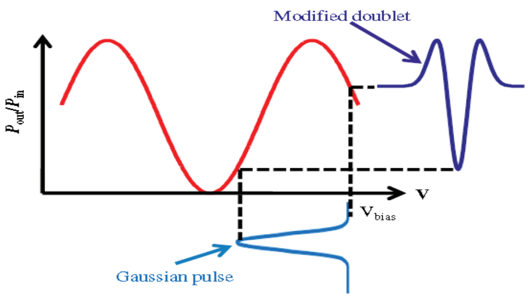

Figure 3.12: Principle of shaping of a Gaussian pulse using the transfer function of EOM.

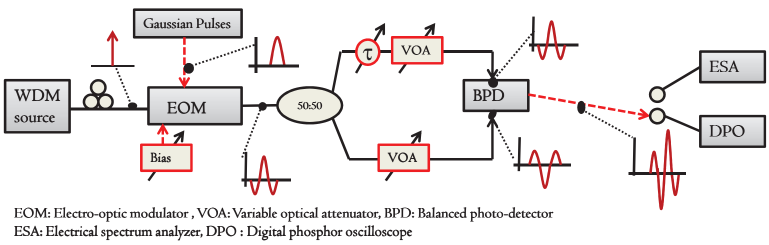

Figure 3.13: Experimental setup of the proposed IR-UWB generator.

The experimental setup is shown in Fig. 3.13. A light wave at 1550nm with an optical power of +2 dBm was generated from a tunable laser source and sent to EOM. An inverted Gaussian-like pulse train with a peak amplitude of 1.302V generated from a pulse pattern generator was applied to EOM to modulate the lightwave. The modulated lightwave signal was further divided into two arms using a 50 : 50 coupler. To equalize the power level in each arm, two optical attenuator were used and then a tunable delay was inserted in one of the arms. Finally, a 12 GHz BPD is used to differentially detect the signals in the both arms in order to perform the linear sum operation given in

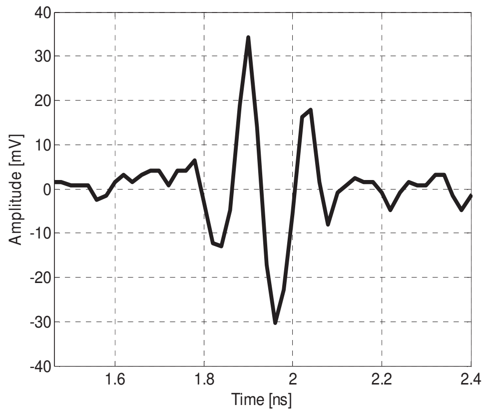

Figure 3.14: Temporal response of experimentally generated IR-UWB.

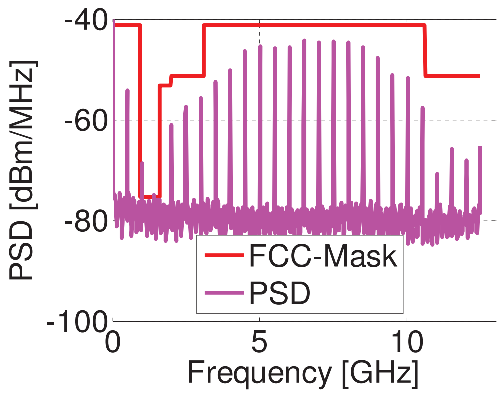

Figure 3.15: PSD of experimentally generated IR-UWB

Eq. 3.15 described above.

In the experiment, an inverted Gaussian-like pulse train generated by pulse pattern generator (AnritsuMP1701A) with a fixed pattern ′1000000000000000′, and a bit rate of 8 Gb/s, which is equivalent to a pulse train with repetition rate of 0.5 Gb/s was applied to EOM. Note that different k-values of the modified doublet are possible by varying both the bias voltage and amplitude of the input Gaussian pulse. Accordingly, I tuned both parameters and then the resulting waveform and PSD was monitored using a high-speed sampling oscilloscope (TektronixDPO72004) and an electrical spectrum analyzer

(R&SFSQ40) respectively. The optimal bias voltage was found to be 3.11V for our EOM with V_π of 2.6 V and a drift from the null point is 0.51 V. This setting achieves a modified doublet-like pulse with duration of about 280 ps. Due to the differential detection by the BPD; pulses at the upper arm are subtracted by pulses in the lower arm, leading to the desired pulse. The resulting pulse from the subtraction process in BPD is depicted in Fig. 3.14. Notice that, it has a similar shape and number of zero-crossings as the simulated result in Fig. 3.10. The PSD of the pulse relative to the FCC mask can be seen in Fig. 3.15. It has a notch around GPS band and fully FCC compliant. However, there is a small deviation between the simulation and experimental result especially at low frequencies ($\leq$ 1GHz). This deviation is a result of the combined effect of the parameters that produces non-optimal modified doublet pulses in each arm of BPD and non-ideal Gaussian-like pulse from pattern generator [86].

In general, based on the discussion on section 3.5.2 and the experiment presented in the above, a new pulse shape has been theoretically investigated and experimentally demonstrated. Note that the scheme need a single lase and single modulator to generate a novel pulse. Furthermore. the proposed scheme can be simplified by photonic integration, which would meet the practical requirements of small size, low cost, and high reliability for UWB communications in short-range applications such as in-building networks.

3.7 Comparison of Conventional and Proposed Techniques

As described in previous Chapters 1 and 2, any IR-UWB systems must meet the power and spectral mask set by the FCC. This spectral mask has a very strong impact on the transmit power, pulse shape and pulse repetition pattern used in an IR-UWB systems. Accordingly, most of the IR-UWB-over-fiber systems reported in the literature differs in terms of their generation techniques, modulation techniques, bandwidth, center frequency, data rate and pulse shapes. For example, the data rate of IR-UWB over fiber varies widely from 500 Mb/s [75] to 5 Gb/s [69]. The wireless demonstrations of IR-UWB-over-fiber systems range from 5cm [70] to 8cm [80]. Furthermore, as summarized in Chapter 2 and Table 2.1, the commonly used pulse shape are monocycle, doublet and 5^{th}-order derivative of Gaussian pulses respectively. This clearly indicates a need for a realistic wireless link budget analysis for IR-UWB-over-fiber systems to determine the achievable data rate versus the wireless range. In addition, it is vital to compare the performance of the proposed pulse shaping techniques with the most commonly used IR-UWB-over-fiber pulses. Hence, a step-by-step derivation and analysis presented in this section is reported in [21]. For uniform representation the Gaussian pulse can be re-written as:

$$p(t) = \frac{A}{\sqrt{2\pi}\alpha} \exp\left(-\frac{t^2}{2\alpha^2}\right) = \frac{A\sqrt{2}}{\sigma} \exp\left(-2\pi\left(\frac{t}{\sigma}\right)^2\right) \tag{3.17}$$

where A and $\sigma = 2\alpha\sqrt{\pi}$ denote the amplitude and spread or shaping factor of the Gaussian pulse, respectively. As described in previous sections, for efficient radiation, a fundamental characteristic of the pulse is to have a zero DC offset [13, 88]. Hence, as described in Chapter 2, the most widely adopted pulse shaping techniques are based on Gaussian derivatives such as monocycle, doublet and 5^{th}-order derivative Gaussian pulse [13, 90, 95]. The time domain expression of these pulses can be obtained by proper derivative of Eq. 3.17. Therefore, the general expression for monocycle is given by :

$$x^{(1)}(t) = A_1 t \exp\left(-2\pi\left(\frac{t}{\sigma}\right)^2\right) \tag{3.18}$$

Using a similar procedure the general expression for second derivative of Gaussian pulse or doublet pulse is given by :

$$x^{(2)}(t) = A_2\left[1 - 4\pi\left(\frac{t}{\sigma}\right)^2\right] \exp\left(-2\pi\left(\frac{t}{\sigma}\right)^2\right) \tag{3.19}$$

The corresponding modified doublet with arbitrary scaling or modifying parameter k is given by [86]:

$$x^{(2m)}(t) = A_{2m}\left[1 - 4\pi k\left(\frac{t}{\sigma}\right)^2\right] \exp\left(-2\pi\left(\frac{t}{\sigma}\right)^2\right) \tag{3.20}$$

The 5th-order derivative of Gaussian pulse is expressed as [95]:

$$x^{(5)}(t) = A_5\left[\frac{-16\pi^2 t^5}{\sigma^4} + \frac{40\pi t^3}{\sigma^2} - 15t\right] \exp\left(-2\pi\left(\frac{t}{\sigma}\right)^2\right) \tag{3.21}$$

where the superscript n shown in $x^n(t)$ is the order of the derivative. The term A_n is the corresponding appropriate amplitudes. The Fourier transform of the n^{th} order derivative of Gaussian pulse is given as [95]:

$$X^n(f) = A(j2\pi f)^n \exp\left(-\frac{(2\pi f)^2}{8\pi}\right) \tag{3.22}$$

Considering the amplitude spectrum of the $n-$th derivative of Gaussian pulse is expressed as:

$$|X^n(f)| = A(2\pi f)^n \exp\left(-\frac{(2\pi f)^2}{8\pi}\right) \tag{3.23}$$

The frequency at the maximum value of Eq. 3.23 commonly referred to as the peak emission frequency, f_m, is given by the critical point of $|X^n(f)|$. Accordingly, a general relationship between peak emission frequency f_m, the order of derivation n and the shaping factor σ , is given by [83, 88]:

$$f_m = \frac{1}{\sigma\sqrt{\pi}}\sqrt{n} \tag{3.24}$$

The normalized power spectral density (PSD) of n^{th} derivative of Gaussian pulse can be expressed as :

$$|P^n(f)| \triangleq \frac{|X^n(f)|^2}{|X^n(f_m)|^2} = \frac{(2\pi f\sigma)^{2n} \exp\left(-\frac{(2\pi f\sigma)^2}{4\pi}\right)}{(4\pi n)^n \exp(-n)} \tag{3.25}$$

Using a similar approach, the amplitude spectrum of the proposed pulse or linear sum, $y(t)$ is give by:

$$|Y(f)| = |X(f)|\sqrt{2 - 2\cos(2\pi f\tau)} \tag{3.26}$$

where the $|X(f)|$ is the amplitude spectrum of the modified doublet. The filtering effect of the microwave delay line can be seen from the band pass frequency response of the second term in Eq. 3.26. For small non-zero values of τ, the linear combination in Eq. 3.15 can be approximated as the derivative of the modified doublet pulses, which leads to higher derivatives of Gaussian pulse called modified third-order derivative of Gaussian pulse, $y(t)$. The corresponding peak emission frequency of this modified third-order derivative of Gaussian pulse is related to the peak frequency modified doublet as described in Eq. 3.24. The approximate value under the assumption that τ is very small compared to the pulse shaping parameter, σ is expressed as [21]:

$$f_m = \frac{1}{\sigma\sqrt{\pi}}\sqrt{\frac{9-3k}{2k}} \tag{3.27}$$

where k is the arbitrary scaling parameter. Note that for $k = 1$, the modified doublet becomes the conventional doublet and the modified third order derivative, $y(t)$ becomes the normal third order derivative of Gaussian pulse.

Therefore, the corresponding normalized PSD of the proposed pulse or linear combination of modified doublet pulse, $|P^n(f)|$, is given as:

$$|P^n(f)| \triangleq \frac{|Y(f)|^2}{|Y(f_m)|^2} = \frac{|X(f)|^2\,(2-2\cos(2\pi f\tau))}{|X(f_m)|^2\,(2-2\cos(2\pi f_m\tau))} \tag{3.28}$$

where the expression for $|X(f_m)|^2$ is given by [30]:

$$|X(f)|^2 = \left[\frac{4\pi(1-k)+k(2\pi f)^2\sigma^3}{8\pi\sqrt{\pi}}\right]^2 \exp\left(-\frac{(2\pi f\sigma)^2}{8\pi}\right)^2 \tag{3.29}$$

Hence, the transmitted PSD of the proposed pulse is given by:

$$|P_t(f)| \triangleq A_{max}\,|P^n(f)| \tag{3.30}$$

where A_{max} is the peak PSD the FCC permits. The parameters k, σ and τ can now be chosen under the constraint of satisfying the FCC mask and maximizing the spectral power efficiency defined as Eq. 3.6:

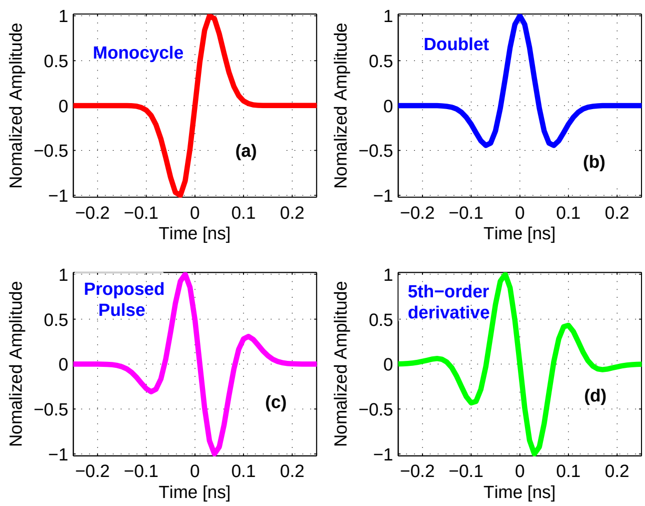

Figure 3.16: Time domain pulse shapes of different pulse shaping: a) Monocycle, (b): Doublet, (c): Proposed pulse and (d) 5^{th}-order derivative.

Fig. 3.16 presents the time domain pulses shapes of the conventional monocycle, doublet and 5^{th} order derivative pulses in comparison to the proposed

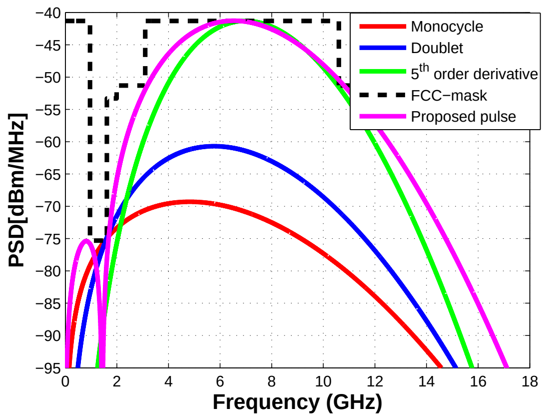

Figure 3.17: Fully FCC-mask complaint PSD of monocycle, doublet, 5^{th}-order derivative and proposed pulse.

pulse. Notice that the proposed pulse is similar to the third-order derivative pulses with three zero-crossings more than monocycle and doublet but less than the 5^{th} order derivative. This clearly indicates that the peak frequency is within the peak frequency of doublet and the 5^{th} order derivative as shown in the PSD of the pulses in Fig. 3.17. According to the simulation result in Fig. 3.17, the proposed pulse shape outperforms the conventional monocycle and doublet pulses. It also shows that the power spectral efficiency is better than the 5^{th} order derivative due to its larger 3-dB bandwidth, as shown in Fig. 3.16. In addition, Table 3.1 summarizes the key parameters of the pulses and it is evident that as the order of the derivative increases the peak frequency increases and the 3 dB bandwidth decreases under the constraint of the FCC-mask. Thus, the proposed pulse has a simple pulse shape but has better FCC-mask compliance and better power spectral efficiency. It should be noted that the proposed pulse can be easily realizable using the microwave photonics delay line approach.

3.8 Realistic IR-UWB Path Loss Model

As described in section 3.3, UWB signals should be able to carry high data rates as shown in Fig. 3.1. The theoretical channel capacity versus distance was evaluated for IR-UWB systems using the free-space path loss model with

Table 3.1: Summary of the key parameters of the pulses (σ: pulse shaping factor, f_{peak}: peak frequency, f_{frac}: fractional bandwidth, $B_{-3\mathrm{dB}}$: bandwidth, η: spectral power efficiency)

Data rate (Gb/s)	σ (ps)	f_{peak} (GHz)	f_{frac} (%)	B_{-3dB} (GHz)	η
Monocycle	117	4.79	109.48	5.53	0.09
Doublet	138.3	5.78	109.39	4.76	0.53
5^{th} order derivative	180.8	7.01	91.2	3.67	50.75
proposed pulse	**150**	**6.46**	**108.40**	**4.20**	**57.40**

a single center frequency GHz in [80]. In [7] the distance as a function of throughput was analyzed for PAM IR-UWB systems. However, the analysis was not performed using a more realistic pulse shaping technique and the path loss was considered constant over the bandwidth of the signal. Therefore, for an IR-UWB system, the bandwidth is larger and hence the frequency dependence of the system should be considered [13, 16]. In addition, a realistic pulse should be considered for evaluation of the performance of IR-UWB systems. To highlight the effect of the pulse shaping technique on the performance of the IR-UWB systems, we perform a comparison among monocycle, doublet, 5^{th} order derivative and the proposed pulse. For fair comparisons, I assumed that the transmitted and received antennas are an isotropic antenna with unity gain. The general scheme used for the analysis in Fig. 3.18. It is assumed that the optical link in Fig. 3.18 does not produce any distortion of the desired IR-UWB pulses. In addition, all the electrical components involved in the system have enough bandwidth to support the whole IR-UWB bandwidth. Noise of the system at the receiver is assumed to be additive white Gaussian noise (AWGN). The operating environment of the system is assumed to be free-space with a power decaying exponent, $\gamma = 2$. Furthermore, it is also assumed that here is no multipath scenario, which can cause inter-symbol interference (ISI) for the system. In the calculations, the noise spectral density is taken with the form $N_0 = k \cdot T_0 \cdot NF \cdot LM$ dBm/MHz, where k is the Boltzmann's constant 1.3810^{-23} Joules/K, K is room temperature. Noise figure of $NF = 6$ dB and a link margin, of $LM = 5$ dB are assumed.

The Friis transmission formula may give misleading or incorrect results

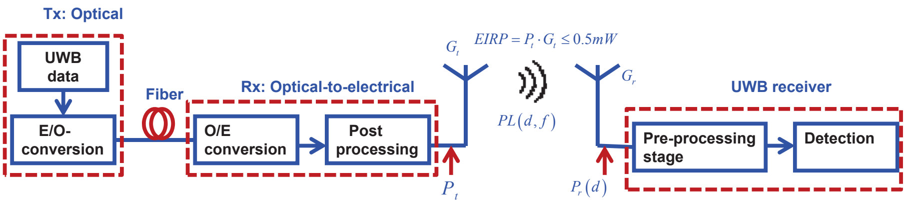

Figure 3.18: General schematic for link budget analysis.

when applied to UWB systems [95]. The Friis transmission formula or path loss formula used for most communication system link design predicts that the received power will decrease with the square of increasing frequency. The equation is given as the following:

$$P_r(d) = P_t G_t G_r \left[\frac{c}{4\pi d f_c} \right]^2 \tag{3.31}$$

where P_t is the transmitted power, G_t and G_r are the transmitted and received antenna gains, respectively,f_c is the carrier frequency and c is the speed of light. It is important to note that for narrowband systems, this change in received power over the signal bandwidth is usually ignored as it has a negligible effect. However, IR-UWB systems can occupy large bandwidth in terms of several GHz. Therefore, the frequency dependence of the Friis appears to have a filter with its transfer function proportional to the inverse of the square of the frequency (i.e.,$H(f) \propto \frac{1}{f^2}$). The main source of this frequency dependence is due to the implicit assumption in the Friis equation that the antenna had a constant gain. In reality, the antenna can be either constant gain or constant aperture. It is possible to have antenna configurations based on the combinations of constant gain/constant aperture antennas. Based on the configuration of the antenna systems, the received power can be either increased by the square frequency, decreased with the square of the frequency or independent of the frequency [7] . In general, it is extremely important to note that antenna is a crucial component for IR-UWB systems. It can distort the spectrum of the IR-pulses and affect the performance of the overall system [103]. In other words, if the antenna gain response is not reasonably flat within the required band then the antenna frequency response should be considered during the pulse design stage to maximize the spectral efficiency as reported in [103]. For this analysis, both the transmitter and receiver antennas are assumed to be omni-directional with relatively constant gain antennas in keeping with commercially available (Skycross SMT-3TO10M-A) antennas and as has been reported in [66]. To account for variations across the band-

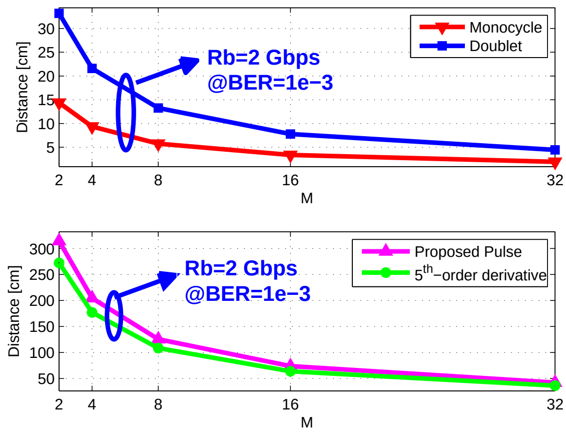

Figure 3.19: Transmission range for M-PAM ($BER = 1e^{-3}$).

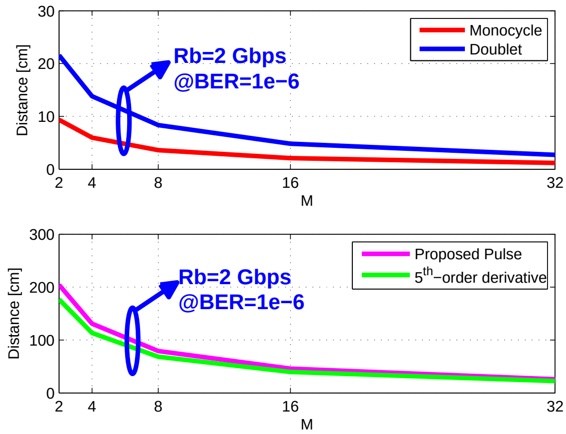

Figure 3.20: Transmission range for M-PAM ($BER = 1e^{-6}$).

width of the IR-UWB signal, Eq. 3.31 should be modified. In particular, the transmitted and received power should be calculated using the integral of the PSD within frequency range and the total transmitted power should be within

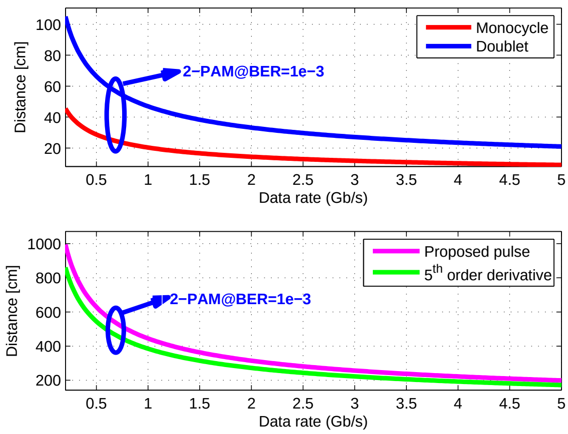

Figure 3.21: Transmission range for 2-PAM for different data rate using different pulse shaping technique ($BER = 1e^{-3}$).

the FCC mask restrictions. Therefore, the transmitted power is given by:

$$P_t = \int_{-\infty}^{\infty} |P_t(f)|\, df = \int_{-\infty}^{\infty} \left|P^{(n)}(f)\right| df \tag{3.32}$$

where $|P^{(n)}|(f)$ is defined for conventional pulses in Eq. 3.25 and proposed pulse in Eq. 3.28, $|P_t(f)|$is defined in Eq. 3.30 and $A_{max} = -41.3$ dBm/MHz is the maximum PSD permitted. If we assume that the received signal occupies a band from f_L to f_H , the received power at distance d becomes:

$$P_r(d) = \int_{f_L}^{f_H} \frac{A_{max}\left|P^{(n)}(f)\right|}{PL(d,f)} df \tag{3.33}$$

where $PL(d,f)$ is the wideband path loss with center frequency in Eq. 3.31 replaced by the variable f. Accordingly, the received power becomes:

$$P_r(d) = \frac{A_{max}G_tG_rc^2}{(4\pi d)^2} \int_{f_L}^{f_H} \frac{\left|P^{(n)}(f)\right|}{f^2} df \tag{3.34}$$

The parameter involved in the analysis can be observed from the general scheme in Fig. 3.18. The received power in Eq. 3.34 necessary at distance d to achieve a target SNR can be computed from the relation given below [95]:

$$P_r(d) = SNR + P_N + LM \tag{3.35}$$

where LM is the link margin of the system and P_N is the received noise power, and is equal to :

$$P_N = N_0 \cdot B \tag{3.36}$$

where B is the noise equivalent bandwidth of the receiver. N_0 is the noise spectral density. If the symbol rate is assumed to be equal to the pulse repetition rate, a single UWB pulse is transmitted for each data symbol, and the energy per information symbol equals to the energy per pulse. Then, the average output SNR is given by :

$$SNR = \frac{\frac{E_s}{T_s}}{N_0 B} = \frac{E_s R_s}{N_0 B} = \frac{E_b}{N_0} \cdot \frac{R_b}{B} \tag{3.37}$$

where E_s is the received symbol energy, T_s is the symbol duration and R_s is the symbol rate. For uncoded and M-ary modulation scheme, the symbol rate is related to the bit-rate as follows:

$$R_s = \frac{R_b}{\log_2 M} \tag{3.38}$$

Similarly, the received symbol energy is related to the energy per bit using the following expression:

$$E_s = E_b \cdot \log_2 M \tag{3.39}$$

For a target error probability, P_{eb}, the required $\frac{E_b}{N_0}$ for PAM can be obtained using the following equation [16]:

$$P_{eb} = \frac{2}{\log_2 M} \left(\frac{M-1}{M} \right) Q \left(\sqrt{\left(\frac{E_b}{N_0} \right) \cdot \frac{6 \log_2 M}{M^2 - 1}} \right) \tag{3.40}$$

Therefore, the compact relationship between the distance and the data rate can be represented as :

$$d = \frac{c}{4\pi} \sqrt{\frac{A_{max} G_t G_r}{(\frac{E_b}{N_0}) \cdot R_b \cdot k \cdot T_0 \cdot NF \cdot LM} \cdot \int_{f_L}^{f_H} \frac{\left| P^{(n)}(f) \right|}{f^2} \, df} \tag{3.41}$$

Fig. 3.19 and Fig. 3.20 show the achievable distance for 2 Gb/s IR-UWB for various M-level PAM modulation format employing different pulse shaping techniques. For these results, the target BER is set at 10^{-3} and10^{-6}, respectively. The simulation results confirm that, the proposed pulse and 5^{th} order derivative outperform monocycle and double pulses in terms of the achievable distance. The main reason is that the proposed pulse and 5^{th}order derivative are relatively power efficient pulses with their power spectral efficiency of 57.40% and 50.75%, respectively. Furthermore, the transmission distance decreases for higher modulation levels. This is due to the fact that PAM is a spectrally efficient modulation technique but not power efficient. Furthermore, the non-conventional pulses proposed in [61, 75, 83] have better performance than monocycle and doublet pulses due to their reported better power efficiencies. Results in Fig. 3.20 show the expected distance for different IR-UWB rate for 2-PAM for targeted BER of 10^{-3}. In general, the simulation result in Fig. 3.20 shows the monocycle and doublet pulses have limited coverage in terms of few centimeters for data rates > 1 Gb/s. For BER=10^{-3}, the proposed pulse and 5^{th} order derivative pulse can achieve a distance longer than 2-m for data rates < 2 Gb/s.

3.9 Features of Proposed Techniques

1. ***Simplicity and Cost***: To fit the FCC mask with good power efficiency, a fifth-order derivative in the electrical domain was recommended in [95]. However, as the order of derivative of Gaussian pulse increases, the system complexity and cost increases as well. This is mainly caused by the proportionally increase in the number of components such as filters which are needed to shape the Gaussian pulse. Recently, photonic generation schemes aiming at increasing the power efficiency of IR-UWB pulses have been reported in [44, 45, 57, 61, 75, 94, 101–103]. However, these photonic schemes are either complex or expensive especially for in-building applications. The proposed approaches utilize the linear combination of lowest possible order derivative of Gaussian pulse, which has the potential of being simple and cheap as described in section 3.6.

2. ***Radiation Efficiency***: As antennas are not efficient at low frequencies, the UWB pulses with low frequency or DC components cannot be used [13, 15, 16]. It is shown that the conventional pulses are good candidate waveforms in terms of radiation efficiency because they do not have a DC component. However, most of their energy lies at low frequencies close to DC. Similar to the conventional pulse, the designed pulse does not have a DC component as can be easily observed in Fig. 3.16. Furthermore, unlike the conventional pulse, most of the energy of proposed pulse as shown in Fig. 3.17 occupies higher spectral regions within the regulation mask. Hence, our pulse design together with the pulse de-

sign techniques reported in [44, 61, 75, 101, 102] can achieve a relatively good radiation efficiency compared to the conventional pulse in [32, 34–36, 46, 48, 50–56, 66, 67, 70, 91, 92, 105–107].

3. ***Compliance with FCC-Mask***: UWB signal spectrum is one of the major issues confronting the industry and governments for commercial use. UWB systems cover a large spectrum and interfere with other existing wireless services. In order to keep this interference to a minimum, the FCC and other regulatory bodies specify spectral masks for different applications, which allow power output for specific frequencies [13, 15, 16]. In Fig. 1 an example is shown of the FCC spectral mask for indoor UWB systems. A large contiguous bandwidth of 7.5 GHz is available between 3.1 and 10.6 GHz at maximum radiation power of -41.3 dBm/MHz. The major reason for extremely low allowed power in the frequency bands $0.96 - 1.61$ GHz is due to the pressure from groups representing existing services such as mobile telephony, GPS and military usage [44]. This causes the primary concern in UWB communication due to electromagnetic interference between UWB systems and GPS band. Hence from this viewpoint, the conventional monocycle and doublet pulses reported in [32, 34–36, 46, 48, 50–56, 66, 67, 70, 91, 92, 105–107] are not suitable for UWB transmission with good spectral power efficiency. However, the pulse design techniques reported [44, 61, 75, 101, 102] and our proposed pulse are fully FCC compliant even in severely power restricted area around GPS band as shown in Fig. 3.17 with a significant improvement in power efficiency.

4. ***Power Efficiency***: The FCC spectral mask limits the maximum permissible radiated power by the transmitter antenna in UWB systems; that is, the effective isotropic radiated power (EIRP) must remain below the specified spectral mask. Compared to more conventional (narrow band) systems, pulse-shaping techniques can be used to optimize the largest legally allowed transmission power to enhance power-limited IR-UWB systems [101]. The conventional pulses based on monocycle and double used in [32, 34–36, 46, 48, 50–56, 66, 67, 70, 91, 92, 105–107] are not power efficient with respect to the FCC mask requirements especially in the GPS band [101]. According to the result shown in Table 3.1, the proposed pulse has much better spectral power efficiency compared to the commonly used IR-UWB pulses depicted in Table 2.1. In addition, the proposed pulse outperforms the conventional pulses in terms the wireless

coverage using a realistic path loss model for IR-UWB as shown in the simulation results in Fig. 3.19, 3.20 and 3.21 respectively.

3.10 Summary

In this chapter, an overview of different pulse shaping techniques employed in IR-UWB-over-fiber systems has been discussed. The high capacity potential of IR-UWB and the need for better spectral power efficiency have been discussed using both the Shannon's channel capacity theory and the realistic pathloss model. Accordingly, new and novel pulse shaping techniques as well as simple optical generation scheme have been proposed and experimentally demonstrated. Furthermore, theoretical comparison between the pulses used in the state-of-the-art IR-UWB-over-fiber systems and the proposed pulses has been investigated using the realistic path loss model. The feature of the proposed pulse has been discussed. In general, the simulation results show the proposed pulse outperform in performance the conventional pulses.

Chapter 4

IR-UWB over Fiber Transmission Experiments

This chapter focusses on experimental demonstrations of multi-Gb/s transmission of IR-UWB over different fiber types for access, in-building and in-home network applications respectively. After introduction, using the novel pulses proposed in Chapter 3, 2 Gb/s transmission of IR-UWB over 25 km SMF fiber for access network applications will be presented. Then results of 2 Gb/s transmission over 4.4 km MMF fiber for in-building network applications will be presented. Finally, for in-home applications, 2 Gb/s transmission of IR-UWB over 100 m PF GI-POF will be described.[1].

4.1 Introduction

In recent years, we are witnessing a strong worldwide push towards bringing optical fiber to individual homes and business, leading to the fiber to the home/fiber to the premises (FTTH/FTTP) networks [112]. In FTTx networks, fiber is brought close or all the way to the end user, whereby x denotes the discontinuity between optical fiber and some other, either wired or wireless, transmission medium. For instance, cable operators typically deploy hybrid fiber coax (HFC) networks where fiber is used to build the feeder network while the distribution of the network is realized with coaxial cable. Another good example for wired fiber-copper access networks are hybrid fiber-twisted copper-pair networks which are widely deployed by telephone companies to

[1]This chapter is based on the results published in [21, 83, 84, 108–111]

realize different variants of digital subscriber line (DSL) broadband access solutions. However, the trend in most of today's green field deployment is that fiber rather than copper cables is installed for broadband access [6, 113]. This is mainly due to optical fiber providing an unprecedented bandwidth that is far in excess of any other transmission medium. In addition, optical fiber has advantageous properties such as low attenuation, longevity and low maintenance costs which eventually makes fiber the medium of choice in wired/last mile access networks [6, 113]. To further reduce the costs of both green-field and brown-field deployment, promising and user friendly new fiber types are emerging such as hole-assisted fiber, which maintain sufficient reliability, even when it is bent at 90^o angles, clinched, or knotted [6, 113, 114]. Note that hole-assisted fibers have excellent bending loss. In these fibers, several air holes arranged around the fiber core confine the field distribution to the core and their bending loss is greatly suppressed compared with that conventional single-mode fibers (SMFs) [115]. Another interesting enabling technology is the so-called plastic optical fiber (POF) which is well suited for simple wiring of low cost optical home networks. POF provides consumers with user-friendly terminations, easy installation and tolerance of dirty connections [113]. In general, the overview characteristics of candidate fiber types for access, in-building and in-home are shown in Table 4.1. The choice of a particular type for particular application will be described in the subsequent sections.

Table 4.1: Characteristics of various kinds of optical fibers (SMF: silica single mode fiber, MMF: silica multi-mode fiber, POF: plastic optical fiber,HAF: hole assisted fibers, GI: graded index, SI: step index) [114]

	SMF	MMF	POF	HAF
λ (to be use)	$850 - 1600$ nm	$850 - 1300$ nm $1240 - 1550$ nm	$850 - 1300$ nm for PF GI-POF $650nm$ for PMMA POF	$1530 - 1565$ nm (C-band)
Loss (dB/km)	< 0.4 in ($1300 - 1600$ nm) < 0.25 @ 1550 nm	< 3@850nm < 0.8 @ 1300 nm	< 40 for GI-POF < 160 for SI-POF	< 0.5 @ 1550 nm
Macro bending loss	$\phi = 30$ mm < 0.25 dB/10 turns @ 1550 nm	$\phi = 75$ mm < 0.5 dB/100 turns @ 850&1300 nm	$\phi \geq 40$ mm GI-POF $\phi \geq 60$mm SI-POF	$\phi = 15$ mm < 0.1 dB/10 turns

FTTH networks are expected to become and already are proving to be the next major success story for optical communications system [113, 116]. Future FTTH networks will not only enable the support of a wide range of new and emerging services and applications but also unleash their economic potential and societal benefit by opening up the first /last mile bandwidth bottleneck between bandwidth hungry end users and high-speed backbone networks [113, 116]. As discussed in the introduction part of this thesis in Chapter 1, end users are looking for mobility as well as high speed. Hence, future broadband access networks need to be bimodal, capitalizing on the respective strength of both technologies and smartly merging them in order to realize future-proof hybrid fiber/wireless networks. In other words, as mentioned in Chapter 1, by combining the capacity of optical fiber networks with ubiquity and mobility of wireless networks, a powerful, flexible, future proof, capacity and energy efficient platform of hybrid fiber/wireless for the support and creation of emerging as well as future unforeseen applications and service can be realized. Accordingly, in this chapter, the transmission of multi-Gb/s IR-UWB over different types of fibers will be described for access,in-building and in-home applications respectively.

4.2 IR-UWB over SMF fiber

As mentioned in the previous Chapters 1, 2and 3, a way to enlarge IR-UWB radio coverage distance is to use a transparent radio-over-fiber(RoF) system to distribute IR-UWB signals to several access nodes. Therefore, IR-UWB signals can modulate an optical carrier which is transported over several hundreds of meters even kilometers, taking benefit of fiber low attenuation (shown in Table 4.1) and large bandwidth. As described in Chapter 2 and shown in Table 2.1, IR-UWB over fiber systems based on single-mode fibers(SMF) have been demonstrated, but these demonstrations used either expensive directly modulated distributed feedback (DFB) single mode lasers or external modulators. Nevertheless, a key advantage of SMF systems is the possibility to implement broadband optical signal processing functions such as all-optical generation of IR-UWB [32, 33, 38, 44, 48, 50, 54, 59, 75, 86, 92, 94, 101, 102, 106] or optical frequency conversion of IR-UWB signals to 24 GHz and 60 GHz band for vehicular short-range radar and future millimeter wave IR-UWB communications applications [117, 118]. Hence, most of the transmission results reported in Table 2.1 were using SMF, which is in fact the dominating fiber type for access networks. To realize multi-Gb/s IR-UWB over fiber for access networks with improved spectral power efficient IR-UWB pulses,I have proposed and investigated the novel pulse creation techniques introduced in the previous section 3.5.1 of Chapter 3 over 25km SMF fiber. In particular, a pulse shaping technique based on a linear combination of moncycles with different pulse shaping factors has been employed and reported in [83]. The experimental setup and achieved results are presented in the following.

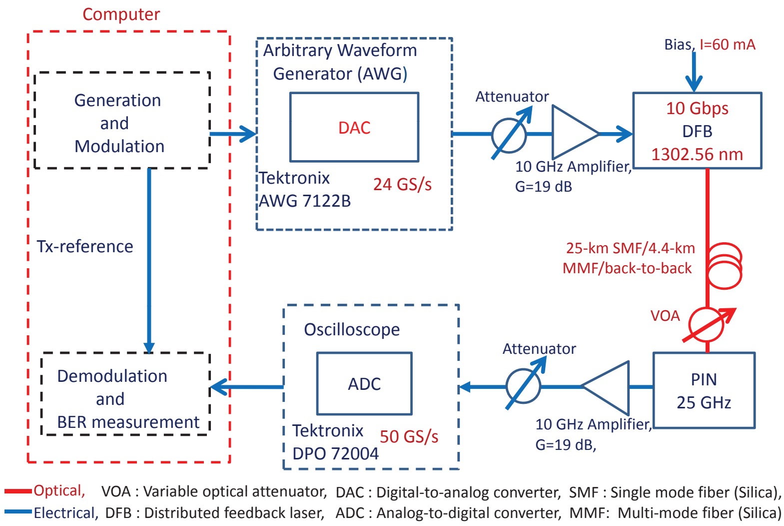

Figure 4.1: Experimental setup.

4.2.1 Experimental Setup

To demonstrate high speed IR-UWB over fiber systems for access network applications, the experimental setup depicted in Fig. 4.1 was employed. The novel IR-UWB pulse proposed in Chapter 3 and section 3.5.1 was modulated by on-off keying (OOK) modulation using PRBS of $2^{13}-1$ data. The modulated pulses were constructed off-line in MATLAB. For electrical waveform generation, the modulated pulse was sent to a Tektronix arbitrary waveform generator (AWG 7122B) with effective RF bandwidth of 9.6 GHz as can be seen in Fig. 4.2, running at 24 GSamples/s. To achieve this sampling speed, the two output ports of the AWG are interleaved with the zeroing option enabled and hence IR-UWB generation was possible due to high effective RF bandwidth of AWG as depicted in Fig. 4.2. However, the maximum output peak to peak voltage(V_{pp}) from the AWG was limited to 0.5 V when zeroing option was enabled. Hence, to increase and control the peak-to-peak current swing for modulating the DFB laser, a variable attenuator cascaded with 10 GHz amplifier was employed as shown in Fig. 4.1. The employed DFB laser, with a wavelength of 1302.56 nm and maximum output power of 10 dBm, was specified for up to 10 Gb/s OOK transmission, maximum forward current of 150 mA and has an electrical small-signal modulation bandwidth of approximately 12 GHz. The biasing current was set at 60 mA in order to obtain a better optical modulation depth and simultaneously ensure the peak-to-peak current swing caused by generated IR-UWB fully lies in the linear portion of the power versus current (P-I) characteristics of the DFB. Accordingly, the distortion of the pulse shape caused due to the non-linearity of the laser characteristics was minimized. The resulting intensity-modulated optical signal was transmitted over 25 km SMF during transmission case or directly coupled to optical attenuator in the back-to-back measurement case as shown in Fig. 4.1. After the optical attenuator, the received optical signal was detected by a 25 GHz multi-mode fiber-coupled photo-detector (NEW FOCUS 1414) with a photosensitive area of 24μm in diameter and an integrated coupling lens. As shown in Fig. 4.1,the received electrical signal was then amplified and captured using a 20 GHz real-time digital phosphor oscilloscope (Tektronix DPO72004DPO) running at a sampling rate of 50 GSamples/s for measuring the time-domain waveform and collect data for offline processing such as demodulation and BER measurements. Finally, an RF spectrum analyzer was employed to present the electrical spectrum of our pulse and compare it to the FCC mask requirement.In general, a computer was used for generation, digital IR-UWB modulation and demodulation in MATLAB, as shown in Fig. 4.1. This also include off-line synchronization, detection and evaluation of transmission performance such as BER measurement. Therefore, the output of AWG was a real electrical waveform of the combined pulse presented in Chapter 3. However, for cost reduction and real-time deployment of the system, a dedicated electronic device could replace the AWG.

4.2.2 Experimental Results

Several modulation formats can be used for IR-UWB communication [13, 15, 16]. The overview of modulation formats for IR-UWB can be find in the Appendix Aof this thesis or interested readers are recommended to refer to books [13, 15, 16]. Recently, a comprehensive study on the implementation of multiple modulation schemes in IR-UWB over fiber system has been reported in [66]. A general theoretical model to analyze the PSD of IR-UWB signals was developed to investigate the transmission performance of different modulation formats in [67]. However, mostly OOK modulation was used in IR-UWB over fiber systems for simplicity and low-cost implementation issues as can be easily seen in the Table 4.2 of Chapter 2. Therefore, it should be noted that

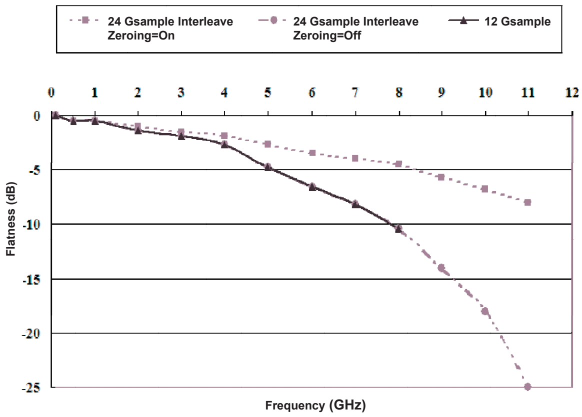

Figure 4.2: Output frequency response of AWG7122B [119].

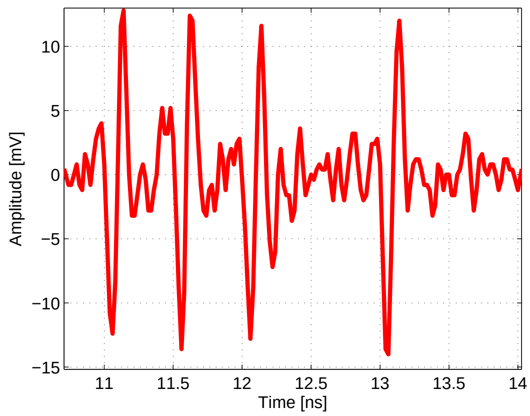

Figure 4.3: IR-UWB pulse sequence in optical back-to-back.

in the entire thesis, I used OOK modulation formats. Fig. 4.3 shows some part of the transmitted data taken during the optical back to back measurement and clearly shows the OOK modulation of a binary sequence of 6 bits "**1 1 1 0 1 0**". Notice that, as shown in Fig. 4.1, the ac-coupled amplifier used in the detection part of experimental setup removes the dc-part of the detected signal. Hence, both the negative and positive part of the designed pulse were observed as shown in Fig. 4.3. The spectrum of the generated IR-UWB was fully compatible with the FCC mask, which had a central frequency of 6 GHz and a -10 dB bandwidth of 7.5 GHz as depicted in Fig. 4.4. Notice that the spectrum shown in Fig. 4.4 has both continuous and discrete spectral components. The discrete spectral lines, called comb-lines, were caused by the modulation format of OOK. Similar results of PSD have been reported in the literature [61, 66, 67, 102]. The comb-lines appear at the locations which are the multiples of the inverse of the pulse repetition interval (PRI) [13, 15, 16]. Hence, in this case, they appear at multiples of 2 GHz which was exactly equal to the bit-rate of the transmission system. As mentioned previously, these spectral lines are not favorable regarding the FCC mask due to the interference that can be made to other operating wireless systems [13, 15, 16]. Hence, the comb-lines are undesirable as they limit the total transmit power. One method to reduce the spectral lines is to use randomly delayed pulse position modulation (TH-PPM) [16]. In this particular measurement case, the comb-lines were forced to remain below the FCC mask to avoid interference to other operating wireless systems. Finally, the results depicted in Fig. 4.3 and 4.4, confirm the signal was not distorted during the optical back-to-back case. This shows the over-all system linearity and bandwidth was adequate enough for 2 Gb/s IR-UWB transmission.

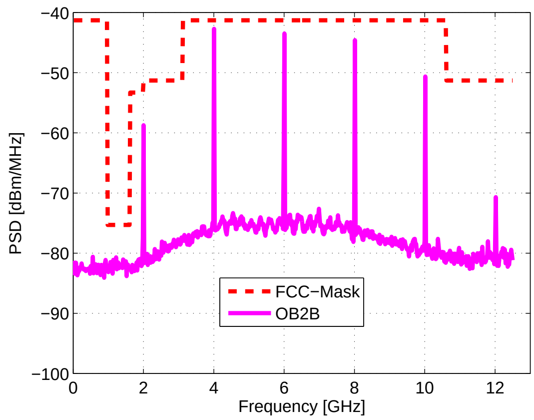

Figure 4.4: PSD of IR-UWB pulse during optical back-to-back.

All in all, SMF offers a very wide bandwidth, very low attenuation (as show in Table 4.1 and Fig. 4.11) and high linearity [120]. However, it should be noted that the whole system linearity mainly depends on the laser transmitter as well as photodiode receiver. Hence, IR-UWB over SMF fiber has been considered as an attractive solution for the distribution of high definition audio and video content in fiber-to-the-home (FTTH) networks [121]. However, as mentioned above, the relatively high cost of UWB over SMF fiber is attributed to the

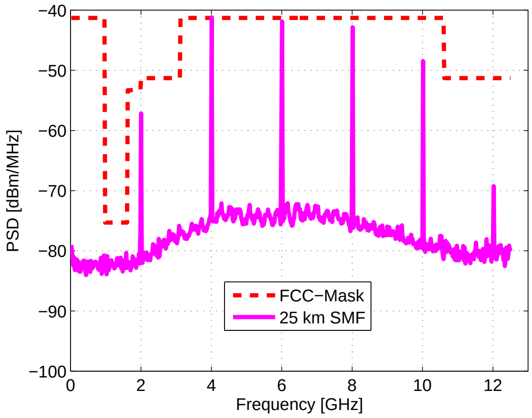

Figure 4.5: PSD of IR-UWB pulse after 25km SMF fiber.

cost of optical transceivers. To lower the cost of IR-UWB over SMF, the IR-UWB signal processing can be centralized in order to simplify IR-UWB base stations [121]. In the cheapest case, an intensity-modulated direct-detection (IM-DD) system can be employed for the IR-UWB transceiver. Therefore, in this particular experiment shown in Fig. 4.1, I employed an IM-DD technique using a directly modulated high speed DFB and a standard single mode fiber for access network application. After 25 km SMF transmission, the PSD of the pulse is shown in the Fig. 4.5. The results clearly show the successful transmission of 2 Gb/s without any significant distortion in the frequency domain mainly due to operation near zero dispersion wavelength at 1300 nm, high linearity and high transmission capacity of the SMF.

Fig. 4.6 shows the bit-error-ratio (BER) results of 2 Gb/s IR-UWB signal transmission over 25 km SMF and optical back-to-back scenario. For each BER measurement points, 8191 bits following a $2^{13} - 1$ PRBS pattern were transmitted and recorded using a 50 GSamples/s digital oscilloscope. The BER was subsequently computed using a DSP algorithm in a bit-by-bit comparison between the transmitted and received data. The DSP algorithm distinguished between binary **1** and **0** by comparing the average power within the central window of each bit slot to an adaptive decision threshold. This approach is expected to provide more accurate results than BER estimates from the eye diagram Q-factor as reported in [122]. According to the result of the BER measurement shown in Fig. 4.6, no power penalty was observed for $BER = 10^{-4}$ up to 25 km SMF transmission. As mentioned above, this

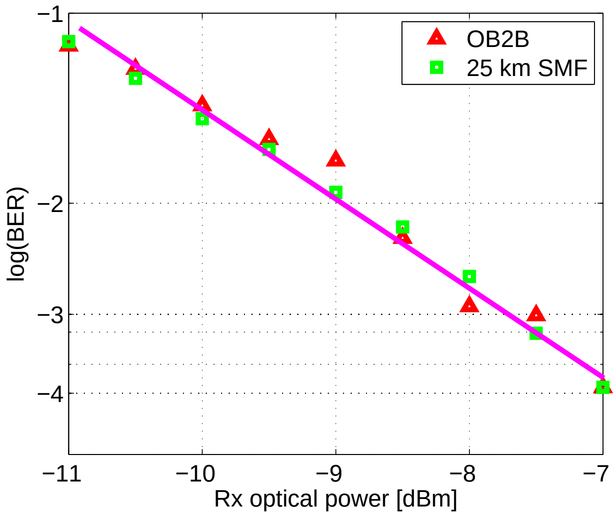

Figure 4.6: BER performance measurement of 2 Gb/s IR-UWB over 25 km SMF transmission.

was mainly due to the combined effects of high capacity, high linearity and low signal dispersion of SMF fiber around 1300 nm [83, 108]. In general, the experimental results show a successful transmission within the forward error correction (FEC) limit of multi-Gb/s of IR-UWB over 25 km SMF for access network applications.

4.3 IR-UWB over silica MMF

In recent years, multimode fiber has increasingly been investigated for RF signal transmission as an alternative to SMF. Its main attraction comes from wide availability in buildings and on campuses, potentially low overall system cost, reuse of existing infrastructure, and higher tolerance due to large fiber core sizes, greater durability and the use of low-cost light sources. Hence, it is considered to be a fiber of choice in applications such as enterprise in-building, intelligent highway systems, fiber-to-the-desk but also short-distance server/computer interconnects. Furthermore, unlike single-mode fiber, the large core diameter of the MMF allows large alignment and dimensional tolerance in transceiver components, thereby lowering installation, maintenance, and component costs [123]. Accordingly, MMF fiber continues to be deployed in significant quantities inside buildings and it is predicted that the fastest growing part of the optical communication market will be that of legacy multimode fiber for installed lengths up to 300m [124]. Note that multimode fibers are identified by the physical size of the core as measured in microns (μm) and the applications for which they are typically used. The term multimode refers to the way the light travels down the fiber. For each pulse of light launched into the fiber by light source (transceiver), the light signal travels within the fiber core along multiple paths, or modes.

Table 4.2: Over view of MMF fiber types(Min. OFL: Minimum overfilled launched bandwidth and Min. EMB: Minimum effective modal bandwidth)

MMF Fiber Type	Wavelength (nm)	Max. cable loss (dB/km)	Min. OFL (MHz · km)	Min. EMB (MHz · km)
62.5/125μm (OM1)	850	3.5	200	–
	1300	1.5	500	–
50/125μm (OM2)	850	3.5	500	–
	1300	1.5	500	–
50/125μm (OM3)	850	3.5	1500	2000
	1300	1.5	500	–
50/125μm (OM4)	850	3.5	3500	4700
	1300	1.5	500	–

Although, extensively used, especially for data communications in local area networks (LANs), MMF suffers a significant bandwidth limitation compared with single-mode fiber (SMF) due to modal dispersion [125]. The main limitation of MMF comes from differential mode delay (DMD), which describes the relative propagation delay of the mode groups of multimode fiber. In the time domain, these effects can be seen as the different modes experience different delays through the fiber link. As many modes have similar group delays, they are often assigned into mode groups. This observation of the delay spreads from these mode groups has become more apparent with the increased use of lasers for higher bandwidth links, as fewer mode groups are excited [125]. However, depending on the fiber design, large variations of DMD can be observed in practice. In general, MMF for data communication is designed with a graded-index (GI) profile where the refractive index decreases gradually from the center of the core to the cladding. There are two main types of MMF: old legacy fibers with a 62.5/125μm and modern high-bandwidth fibers with 50/125μm core/cladding dimensions. They are not easily compatible due to the mismatch of the core sizes when interconnected, which potentially leads to high losses. The 62.5/125μm fibers were developed for low data rate systems using light-emitting diodes (LEDs) and have a specified distance-bandwidth product of 200$MHz \cdot km$ at 850 nm or 500 MHz · km at 1300 nm. This type of fiber is called OM1 fiber. The distance-bandwidth product of this fiber type is only guaranteed if an LED light source launches into the fiber, which is called over-filled mode launch since all mode groups are fully excited. If used with laser source, the actual bandwidth may decrease. For RF signal transmission, especially millimeter wave signal transmission, 50/125μm is much better choice due its higher bandwidth. In order to show the capacity of MMF, the general characteristics and progress of multimode fibers are summarized as shown in Table 4.2. OM2 fiber, with a guaranteed distance-bandwidth product of 500 MHz · km at 850 nm and 1300 nm, and OM3 fiber, with bandwidth larger than 2000 MHz · km at 850 nm are suitable for RF signal transmission. Note that there exist commercial products with minimum bandwidth of even 4700 MHz · km as shown in Table 4.2. Such fibers are much more suitable for RF system design. It should be underlined that there are several product types MMF with different bandwidth. For example, a Draka Comteq MMF fiber has a distance bandwidth product of 8925 MHz · km at 1300 nm. In short, the actual bandwidth depends on the specific fiber core variations, caused by fluctuations in production processes, which are unknown in practice. It should be noted that OM1 and OM2 intended for use with LED sources at speed of 10 or 100 Mb/s. Their standard performances are specified by minimum overfilled launch (OFL) bandwidth that is measured when a light source with approximately uniform emission in all direction. OM3 and OM4 are laser optimized for use with VCSEL light source. OM3 and OM4 are designed to get the best performance out of VCSEL and their measured bandwidth are specified using minimum effective modal bandwidth.

On the other hand, the bandwidth of multimode fibers in general depends on the launching conditions because of excitation-dependent modal group delay [126]. It has been shown that the bandwidth of standard multimode fibers can be increased using mode-selective excitation with a slight misalignment from center launch [126]. It is important to note that the high-bandwidth fiber, with its more optimized index profile, has a much smaller variation in modal group velocities and is therefore less affected by an offset [126]. It has been observed experimentally that the transmitter characteristic of a standard fiber exhibits dips at certain frequencies due to interference between different mode groups with different group delays. Hence, it is well known that MMF has bandpass characteristics beyond the -3 dB bandwidth of the fiber link [127]. It has been also proposed and demonstrated that this passband frequency region above can be exploited for signal transmission and hence significantly increase the fiber transmission capability at higher frequencies [30, 127]. However, it should be noted that these bandpass regions and transmission nulls in the frequency response of the MMF are caused by constructive or destructive interference of few modes that originally were excited by mode-selective laser launch. Therefore, uncontrolled mode coupling at discontinuities, will lead to variation of this performance. In other words, these bandpass regions are not stable and also vary with time. Hence, special care needs to be taken for exploiting RF transmission. However, it is better to rely on the low-pass region of the MMF frequency response. Furthermore, it is also important typically for the lasers to be biased at least 10 mA (rather than only 1 mA) above its threshold current. This is due to the fact that efficient direct modulation of a semiconductor laser cannot occur above its relaxation oscillation frequency, which is typically low at threshold but increases as the square root of the bias current above threshold. For efficient modulation of a DFB at 10 GHz, for instance it is often necessary to apply a bias that is $40 - 60$ mA above threshold [128]

As described above, in-building radio over fiber systems using distributed antennas to provide coverage and capacity can make use of this installed legacy multimode fiber (MMF) [124]. Accordingly, the design of low cost multimode fiber fed indoor wireless network and its link budget analysis in order to optimize a remote antenna unit (RAU) design and predict maximum coverage range for WLANs, GSM900, GSM1800 and UMTS has been reported in [129, 130]. At short wavelength where component costs are less, a 300m link comprising 850nm VSEL and high bandwidth MMF has been demonstrated with a spurious-free dynamic range (SFDR) of 94dBHz$^{2/3}$ in the frequency range of $1 - 8$ GHz [131]. The SFDR of a system is the range between the smallest signal that can be detected in a system (i.e., a signal above the noise level of the system), and the largest signal that can be introduced into a system without creating detectable distortions in the bandwidth of concern. In general, the distance-bandwidth product governs the MMF transmission distance that can be achieved with significant performance loss. Nowadays, MMF with a specified distance bandwidth product of > 4500 MHz $\cdot$ km is commercially available as can bee see in Table 4.2. Note that selected fiber samples can achieve even higher values, or mode-selective launch could be used to improve distance-bandwidth values. As mentioned above, MMF is a cost-effective and robust alternative to single-mode fiber. Therefore, IR-UWB over MMF is an attractive solution for in-building networks applications. Accordingly, I have proposed IR-UWB over MMF and the experimental setup and results will be described in the following sections.

4.3.1 Experimental Results

To transmit 2 Gb/s transmission of IR-UWB over fiber a similar experimental setup shown in Fig. 4.1 was used. However, the optical attenuator and the fiber were replaced by their corresponding multimode attenuator and fibers respectively. In this particular experiment, Draka Comteq graded-index MMF fiber was used. This particular type of fiber has a high numerical aperture (NA) with bandwidth length product of 8925 MHz · km and a loss of 0.45 dB/km at 1300 nm, which allows the transmission of 2 Gb/s IR-UWB over 4.4 km MMF without severe distortion. The time-domain waveform is shown in Fig. 4.7. There is no significant degradation after 4.4 km MMF transmission; Fig. 4.8 finally shows the spectrum of the received IR-UWB signal after 4.4 km MMF transmission. The signal spectrum is still very nicely fitting into FCC mask with very small periodical notch observed in the spectrum, which signifies the mode coupling leading to interference between guided mode and other modes, which are delayed with respect to its own signal

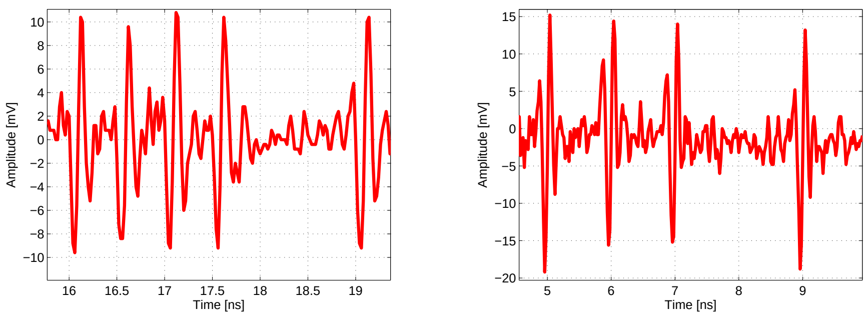

(a) OB2B case.

(b) After transmission.

Figure 4.7: 2 Gb/s IR-UWB pulses transmission (OB2B and 4.4 km GI-MMF).

On the other hand, the performance of a multimode fiber transmission link can be serious degraded by modal noise when a laser diode with a narrow spectral width is employed [132, 133]. A rigorous quantitative analysis of the

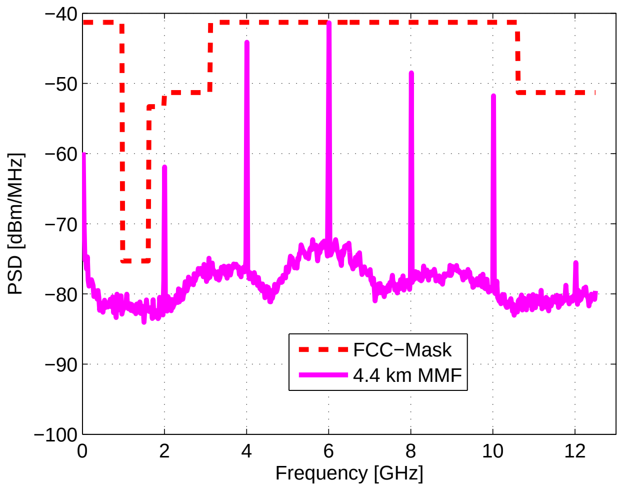

Figure 4.8: PSD of IR-UWB over fiber after 4.4km MMF fiber.

degradation of the BER performance of a digital transmission link caused by modal noise in the multimode fiber link has been reported in [132]. The measured noise distribution for both full and restricted launch cases has been reported in [133]. It was found that the noise statistics for a restricted launch were significantly different than for a full-mode launch. In particular, the variance of the noise distribution was larger than in the over-filled launch case leading to a degradation in the SNR and hence the performance. According to the work done in [132], it was observed that the BER degrades with : 1) increase in mode-selective losses, 2) increase in source coherence, 3) decrease in fiber dispersion (short link) and 4) decrease in number of guided fiber modes. In general, the SNR due to modal noise leads to a BER floor.

Fig. 4.9 shows the BER results of 2 Gb/s IR-UWB signal transmission over 4.4 km MMF and optical back-to-back. As discussed above, for each BER measurement point, 8191 bits following a $2^{13} - 1$ PRBS pattern are transmitted and recorded using a 50 GSamples/s digital oscilloscope. The BER is subsequently computed using a DSP algorithm in a bit-by-bit comparison between the transmitted and received data. The DSP algorithm distinguished between binary **1** and **0** by comparing the average power within the central window of each bit slot to an adaptive decision threshold. According to the result of the BER measurement, the 4.4 km MMF transmission shows a penalty of almost 3 dB due to the combined effect of intermodal dispersion, mode mixing, and

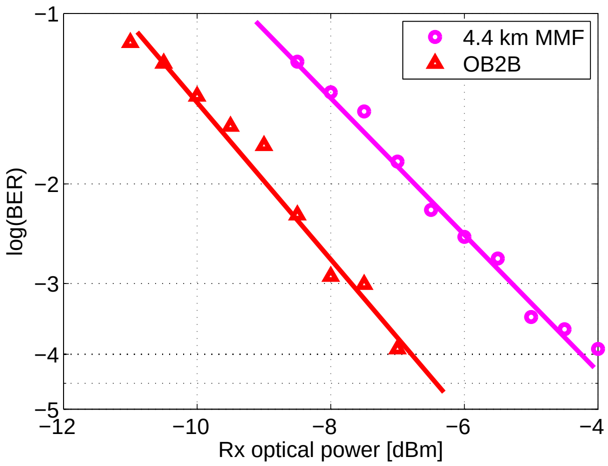

Figure 4.9: BER performance of 2Gb/s IR-UWB over 4.4-km MMF transmission.

modal noise at the receiver side. In general, the experimental result shows a successful transmission within the forward error correction (FEC) limit of IR-UWB over 4.4 km multimode fiber.

4.4 IR-UWB over POF

Single-mode glass optical fiber (SMF) is used extensively, becoming the indispensable information transmission medium in the form of large information pipelines connecting large cities and countries [134, 135]. However, the core diameter of SMF is very small (10μm), and extremely precise techniques and expensive devices are required for connecting the fibers to signal transmitting and receiving devices. For this reason, it would be difficult to install the SMF in in-home networks. These difficulties are recognized as the problem of the "last few meters" for optical infrastructure. In order to overcome the problem, graded-index plastic optical fiber (GI-POF) has been proposed as a solution [134]. Notice that the generic term polymer optical fiber (POF) does not specify a single type of fiber, but a variety of fibers that have in common the use of plastic material for core and cladding, and usually have a large diameter [114]. Among the many available material options, only two are very interesting for home networking [114]: polymethylmethacrylate (PMMA) POF and perfluorinated graded index (PF GI-POF). However, POF has two important weaknesses: it has significantly lower bandwidth than glass optical fiber (GOF) and its attenuation is far higher as can be seen in Fig. 4.11. Recent developments conquering both of these issues make POF a strong candidate for optical data transmission over the last hundred meters [134]. In general, GI-POF is sufficiently flexible and large in core diameter which allows an easy connection with other devices via inexpensive connectors (or no connectors at all ,just butt-joining bare fibers). Therefore, it can be installed at low cost. Moreover, the bandwidth of the GI-POF can be enhanced by controlling its radial refraction index profiles. According to [135], PF GI-POF has been used in offices or schools as high-speed data transmission medium in Japan. This type of fiber has better bandwidth and lower attenuation compared to PMMA POF as shown in Fig 4.11 and reported in [114]. According the results reported in literature for data center application, 47.4 Gb/s PF GI-POF transmission over 100m has been reported using discrete multitone modulation (DMT) based on rate-adaptive bit-loading algorithm in [136–138]. Very recently, 112 Gb/s transmission over 100 m of GI-POF has been demonstrated by exploiting polarization multiplexing (PolMux) and quadrature phase shift keying (QPSK) based on offline digital signal processing(DSP) in [139]. On the other hand, many studies have been conducted concerning Gigabit Ethernet over SI POF, mainly in Europe. Although the bandwidth of SI POF is theoretically limited to several hundred megahertz over 100 m, transmission rates exceeding 1.0Gbps have been achieved by adopting discrete multitone (DMT) modulation in links using SI-POF [114, 140, 141].

As discussed above, for large-scale short-range applications, multimode fibers (MMF) offer the advantage of easy installation as their large core diameter and numerical aperture allow large alignment tolerance. More importantly, plastic optical fibers (POF) can enable short-range low-cost broadband transmission links, best suited to in-home and in-building networks environments. When compared to silica MMFs, graded-index POF (GI-POF) offers further advantages such as smaller bending radius (< 5 mm), better tolerance to tensile load and stress, and simpler connector [136–139, 142]. Therefore, IR-UWB over PF GI-POF provides an attractive solution for simple and low cost in-building networks. Hence, I proposed IR-UWB over PF GI-POF for the first time and reported in [84, 110, 111], the detailed experimental setup and achieved results will be presented in the subsequent sections. Note that the choice of IR-UWB over PF GI-POF rather than over PMMA is due to PF GI-POF having improved optical characteristics such as lower attenuation as shown in Fig. 4.11 and higher bandwidth, espcially in the infrared region.

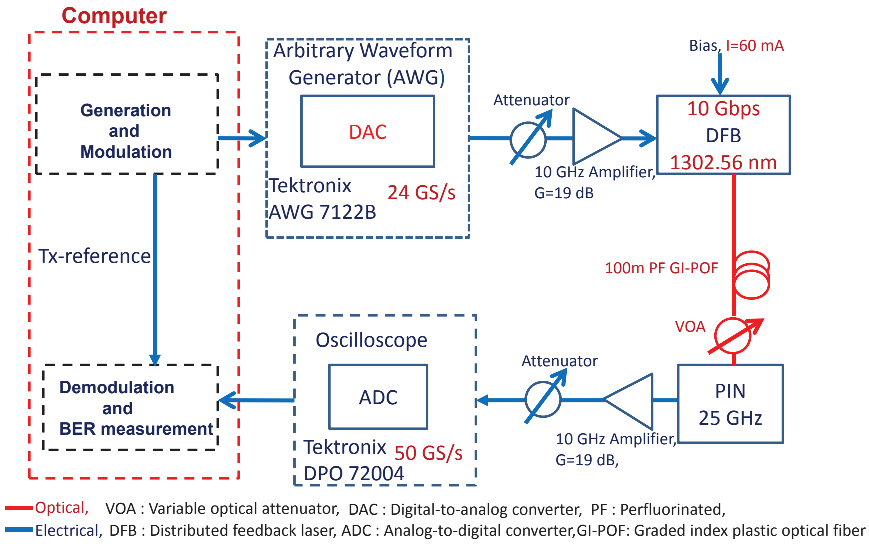

Figure 4.10: Experimental setup.

4.4.1 Experimental Setup of IR-UWB over PF GI-POF

To evaluate the performance of IR-UWB over PF GI-POF an experimental setup is shown in Fig. 4.10. The pulse design technique was based on a linear sum of modified doublet pulse introduced in the previous Chapter 3, section 3.5.2. Then IR UWB pulse was constructed off-line using MATLAB and sent to the arbitrary waveform generator (AWG) running at 24 GSamples/s. The generated electrical IR-UWB pulse from AWG was used to directly modulate a DFB laser at 1302.56 nm wavelength, which was biased at 60 mA. The modulated signal was transmitted over 100 meters of 50μm core PF GI-POF and detected by a 25 GHz photo-detector (PD) with a photosensitive area of 25μm. A real-time oscilloscope running at a sampling rate of 50 GSamples/s was employed to show the time-domain waveform and data for BER measurement. Finally, the electrical spectrum of the pulse was measured using the spectrum analyzer for an FCC mask compliance test.

4.4.2 Experimental Results

As introduced in the previous sections, several modulation formats can be used for IR-UWB, however for simplicity and low-cost, on-off keying (OOK) was employed to directly modulate the DFB laser. After optical-back-to-back (OB2B) and 100 m PF GI-POF transmission, a sample of the received time-

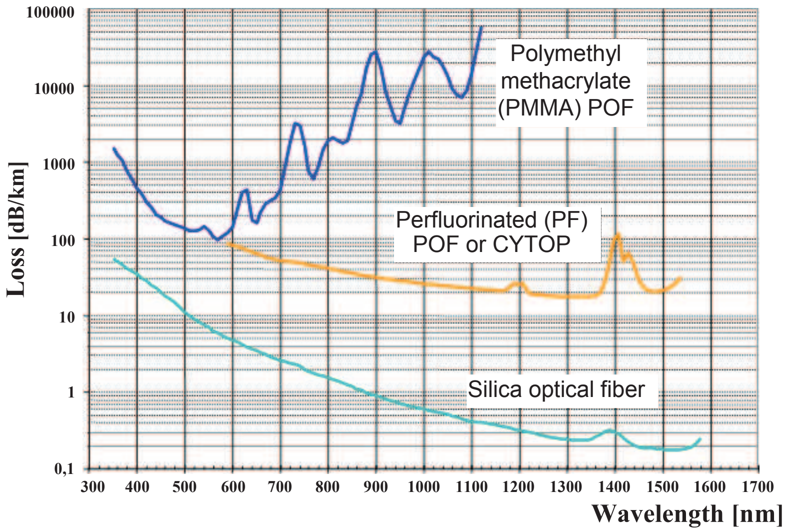

Figure 4.11: Attenuation characteristics of silica, PMMA POF and POF [137].

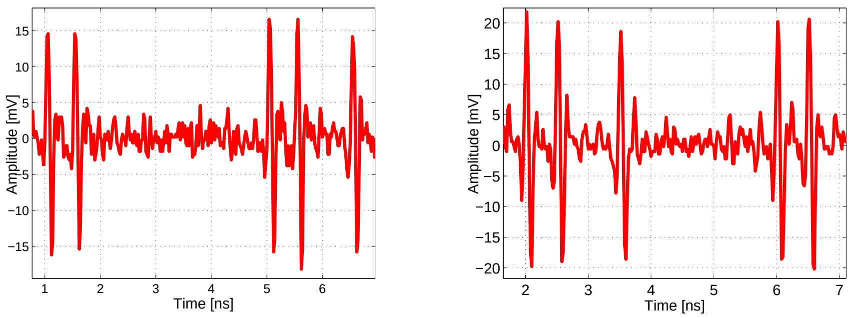

(a) OB2B case.

(b) After transmission.

Figure 4.12: 2 Gb/s IR-UWB pulses transmission (OB2B and 100 m PF GI-POF).

domain waveforms are shown in Fig. 4.12a and Fig. 4.12b respectively. The PSD of IR-UWB in the case of optical-back-to back and after transmission of 100 m PF GI-POF are shown in Fig. 4.13 and Fig. 4.14 respectively. Due to the periodic OOK modulation scheme, the discrete spectral comb-lines appear in the spectrum of IR-UWB data as shown in Fig. 4.13 and Fig. 4.14. As

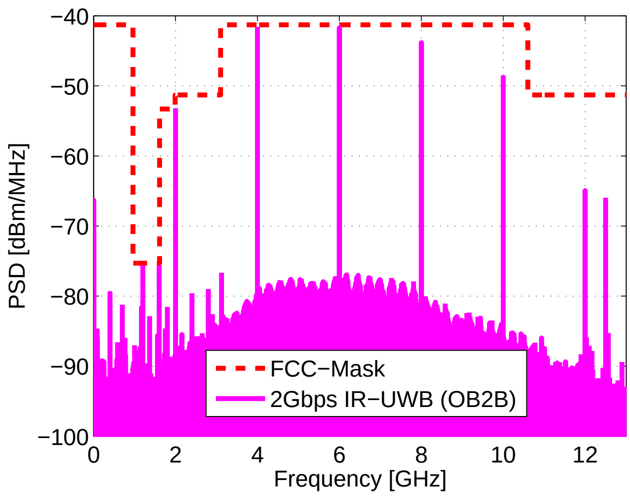

Figure 4.13: FCC mask and PSD of 2 Gb/s IR-UWB pulses during B2B case.

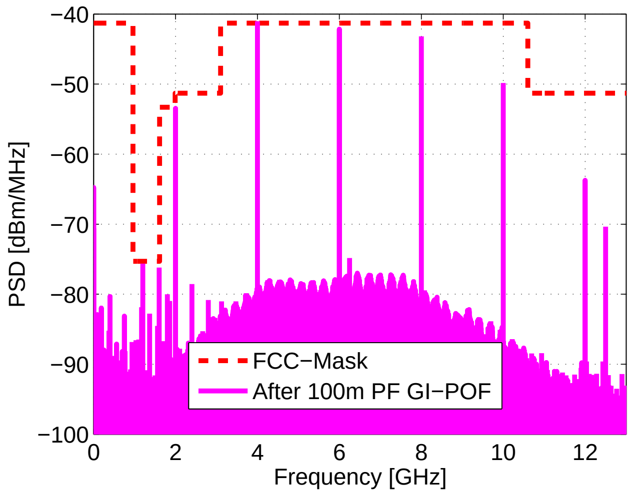

Figure 4.14: FCC mask and PSD of 2 Gb/s IR-UWB pulses after 100 m PF GI-POF.

mentioned in previous sections, the spacing between the comb-lines is 2 GHz which corresponds to the bit-rate of the transmission system.

Fig. 4.15 shows the BER results of the 2 Gb/s IR-UWB signal transmission.

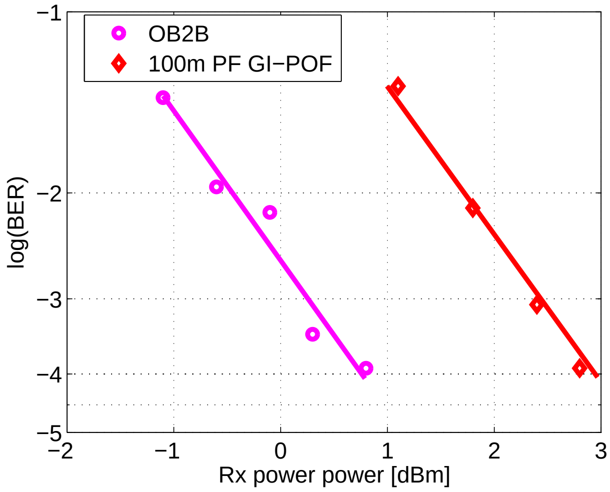

Figure 4.15: BER performance measurement of IR-UWB over 100 m PF GI-POF.

For each BER measurement point, 8191 IR-UWB bits following a $2^{13}-1$ PRBS pattern are transmitted and recorded using a 50 GSamples/s DPO. The BER was subsequently computed using a DSP algorithm in a bit-by-bit comparison between the transmitted and received data. According to the result of the BER measurement, the 100 m PF GI-POF transmission shows a penalty of around 2 dB, due to dispersion, the random mode mixing and modal noise at the receiver.The results clearly show successful transmission of 2 Gb/s without any significant distortion which is mainly due to the high bandwidth of the PF GI-POF fiber. Hence, IR-UWB over PF GI-POF is an attractive solution for future in-home applications.

4.5 Summary

In this chapter, the performance of transmitting multi-Gbit/s IR-UWB signals over different fiber types using offline BER evaluation has been presented. All the transmission experiments employ novel pulse shaping techniques introduced in the previous Chapter 3. The choice of a particular fiber type depends on the actual application requirements such as: low cost, high capacity, low bending loss and low attenuation. Accordingly, 2 Gb/s transmission of the IR-UWB over SMF, MMF and PF GI-POF has been experimentally demonstrated for access, in-building and in-home applications respectively. All these demonstrations show reach extension of high-speed IR-UWB transmission over several order of magnitude in length.

Chapter 5

Routing of Baseband Wired and Wireless IR-UWB over Fiber

This chapter deals with the optical networking aspects of flexible delivery of IR-UWB signals over fiber-based in-building network. First, today's and envisaged in-building networks will be described. Then multicast experiments of IR-UWB over fiber will presented. Then experiments of integration of 2 Gb/s wireless IR-UWB and 1.25 Gb/s wired baseband services over a single optical in-building network infrastructure will be discussed. Finally, based on the experimental results, routing of integrated 1.25 Gb/s wired baseband and 2 Gb/s wireless IR-UWB signals over shared single optical infrastructure will be described[1].

5.1 In-building Networks

5.1.1 In-building Networks Today

As described in Chapter 1, users for telecommunication services are demanding instant access everywhere and anytime. It should be noted that the aggregate amount of traffic inside home can exceed access line capacity as has been reported in [145]. As argued earlier in this thesis, sufficient coverage and a high capacity in-building network to provide both wired and wireless access for existing, emerging and future unseen services is critically important.

[1] This chapter is based on the results published in [21, 85, 143, 144]

Furthermore, it should be noted that, satisfying requirements such as: high energy-efficiency, low-cost, simplicity for maintenance/service upgrading and flexibility of in-building networks are also very important.

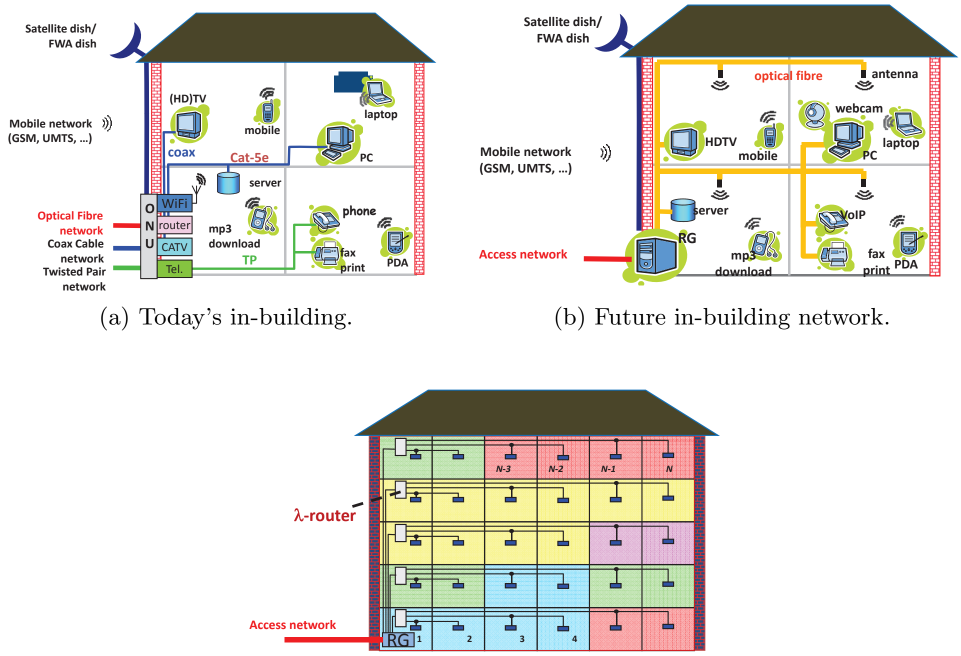

(a) Today's in-building.

(b) Future in-building network.

(c) Dynamic routing concept.

Figure 5.1: Overview of in-building networks [146].

However, as shown in Fig. 5.1a, today's in-building networks consist of a mixture of separate networks, each optimized for a specific set of services [147]. As shown in Fig. 5.1a, the services delivery method inside the building can basically be divided into two approaches: wired and wireless. In principle, the wireline could be unshielded twisted pair (UTP), coax, power line communications (PLC) and optical fiber links [147, 148]. These wired approaches provide potentially higher data rates and better Quality-of Service (QoS), but no flexibility in terms of mobility. Among the wire media, optical fiber with its huge bandwidth, immunity to electromagnetic interference (EMI), signal format transparency, small dimension and low weight and with potentially do-it-yourself capability (e.g., 1-mm core POF) is an attractive medium for future in-building networks. The second approach is using a wireless approach that provides diverse radio solutions such as: WLAN (IEEE 802.11 families), Bluetooth, UWB, GSM, UMTS, HSDPA and LTE. The wireless approach allows a user to have finite range mobility accompanied by a medium and varying channel quality [140, 148]. To provide truly broadband services to the end user, the fiber's vast capacity should be extended into the home itself [149]. In short, to meet the above-mentioned capacity demand and simultaneously satisfy in-building network requirements, a mixture of networks shown in Fig. 5.1a, is expected to disappear and eventually be replaced by a single in-building network as shown in Fig. 5.1b.

5.1.2 Future In-building Networks

As discussed above, wireless communication systems offer mobility and flexibility, while optical fiber-based systems offer large bandwidth, QoS, security and lower power consumption for transport of telecommunication signals [150]. Hence, none of the two technologies separately can satisfy the demands of user for ubiquitous, high speed and affordable access to information services. Therefore, integration of wired optical and wireless systems can offer solutions that combine the best of both technologies. Hence, recently, there is an increasing research effort towards single integrated in-building networks as shown in Fig. 5.1b.

To allow more flexibility, use the resources more efficiently and thus reduce congestion probability of the network, unused network capacity should be directed to those places where an actual high demand exists [146]. This can be done by routing of multiple wavelength channels in the network and accordingly setting different network connection patterns for different types of services. As shown in Fig. 5.1c, wavelength channels may be assigned dynamically to clusters of apartments, where within a cluster the capacity is shared. The dynamic assignment in response to varying traffic requests can yield a more efficient usage of the network's resources and thus an improved network throughput [146]. By changing the cluster size, the granularity of the capacity allocation can be changed to meet the demand. However, the smaller the cluster becomes, the more complex the wavelength router becomes and thus its costs increase. According to the work reported in [146], a cluster size of four apartments may be a good compromise between complexity and network throughput improvement.

In general, optical signal processing of point-to-multipoint (P2MP) and multipoint to-multipoint (MP2MP) network solutions with dynamically adaptable signal routing, where optical signal processing is applied in the nodes in order to change the wavelength paths upon external control has been considered as one of future trends of in-building networks [146, 151]. Furthermore, it should be underlined that, there is also a clear trend towards higher network capacity, higher network flexibility and integrated approach of wired/wireless. As demonstration of optical routing, all-optical multicast routing of RoF signals by cross-gain wavelength conversion in a single SOA followed by an arrayed waveguide grating router has been reported in [152]. In addition, very recently, a wavelength routing concept has been demonstrated for dynamically allocating mm-wave radio signals, by employing integrated tunable microring resonators in the add-drop nodes per apartment together with tunable cross-gain wavelength conversion in an SOA [153]. In line with above trend, for the first time, I have proposed and experimentally demonstrated all-optical flexible multicast of IR-UWB signals and routing of both integrated wired baseband/wireless IR-UWB services as reported in [21, 85, 144]. The corresponding experimental setup and achieved results will presented in the subsequent sections.

5.2 Multicasting IR-UWB over fiber

As mentioned in the previous Chapters 2, 3 and 4 to increase the coverage area of IR-UWB, distribution of IR-UWB signals over optical fiber is considered as a promising solution [32, 33]. Accordingly, in the past few years, there has been increasing interest in generation, modulation and distribution of IR-UWB signals over an optical fiber using various modulation formats employing different generation techniques [32, 33, 44, 61, 83, 84, 86, 101, 102, 109, 154–156]. Recently, there is an increasing interest for convergence of IR-UWB over fiber technology with other wired/wireless services over emerging WDM-PON access networks [81, 82, 122, 155–159].The main reason of integrating IR-UWB with WDM-PON is to reduce the cost of the overall systems by exploiting the existing infrastructure of access networks. This integration concept is quite important for wide deployment of IR-UWB systems and thus can be exploited for high capacity and energy-efficient in-building networks.

However, all previously proposed pulse generation concepts and distribution techniques of IR-UWB over fiber focus on static point-to-point communication links [32–34, 36, 46, 48, 53, 54, 61, 66, 67, 70, 75, 76, 83, 84, 101, 102, 109]. For increased flexibility, point-to-multipoint using all-optical multicast is another potentially useful networking function in the optical networks [160]. Multicast using all-optical wavelength conversion followed by a wavelength selective device can be used for emerging bandwidth-intensive applications (such as video conference and video-on-demand services) over high-speed optical networks. Hence,this section focuses on the networking capability of IR-UWB by all-optical routing for in-building fiber networks. This centralized optical multicast aspect provides many features such as: dynamic adjustment of optical connectivity and capacity, enhanced security, reduction of unnecessary power consumption and flexibility in operation and reconfiguration of the network [152]. The proposed technique is a low-cost solution because it uses the simplest routing scheme based on cross-gain modulation (XGM) of a semiconductor optical amplifier (SOA) without any additional assist light apart from the pump and probe signals.

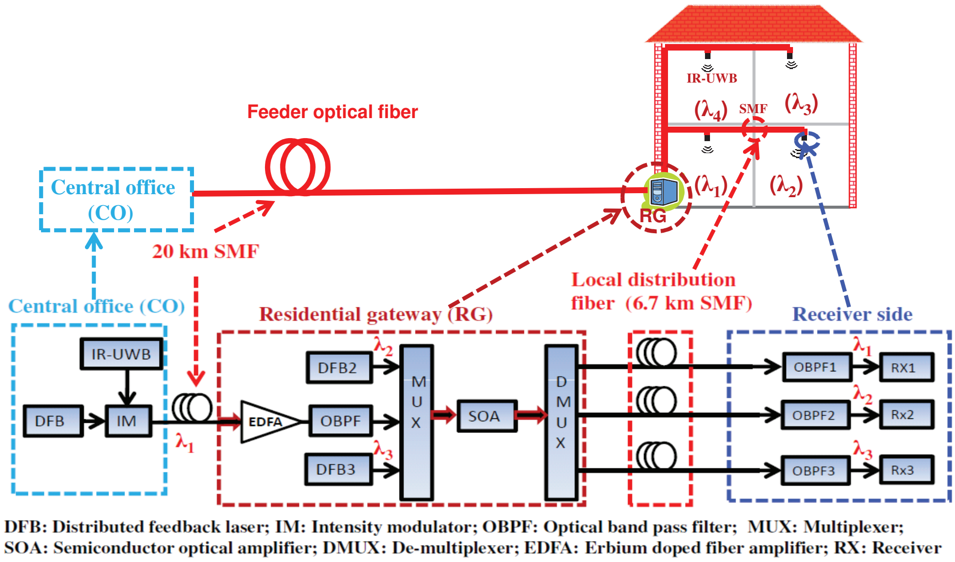

Figure 5.2: Experimental setup.

5.2.1 Experimental Setup

To realize multicast of IR-UWB over fiber for in-building network application, the experimental setup depicted in Fig. 5.2 was employed. A continuous wave (CW) pump signal at 1550.92 nm assumed to be located in the central office (CO) was externally modulated using a 10 GHz $LiNbO_3$ modulator driven by the electrical IR-UWB data at 1 Gb/s. The IR-UWB signal was generated based on a pulse generation technique that employed a linear combination of

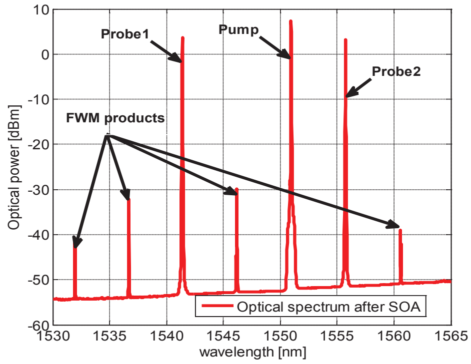

Figure 5.3: Optical spectrum after SOA.

a modified doublet with inverted and delayed forms as discussed in Chapter 3 and reported in [84]. The choice of this pulse shape was due its attractive features compared to the conventional pulses of monocycle and doublet pulses as described in Chapter 3. Then the pulse train was coded with data using a $2^{13}-1$ PRBS pattern, generated by an arbitrary wave generator. The central office connects to the in-building network using standard single mode fiber (SMF) as shown in Fig. 5.2. According to Fig. 5.2, a 20 km standard single-mode fiber (SMF − 28) was employed to distribute the modulated optical signal from the central office to the residential gateway (RG), which connects the in-building network to the incoming access network. Note that the choice of the 20 km was due to the availability in our laboratory during the experiment and also as proof-of-concept demonstration.In the RG, the pump signal was boosted by an erbium-doped fiber amplifier (EDFA) in order to compensate for the insertion loss of the external modulator and the fiber loss incurred after 20 km of fiber. Furthermore, the pump signal was filtered using a 1 nm tunable optical band pass filter (OBPF) to minimize the amplified spontaneous emission (ASE) noise introduced during the amplification process. As shown in Fig. 5.2, two CW probe signals were generated locally inside the RG using laser diodes (DFB-2 and DFB-3) at wavelengths of 1541.35 and 1555.75 nm respectively. In principle, to serve more than two destinations, more wavelengths are possible because of the scalability of the experimental scheme. The pump and two probe signals were multiplexed within the RG using a wavelegth multiplexer (MUX) and co-propagated to the input of a SOA for the XGM. To obtain good conversion performance at individual probe signals, the injected powers into SOA for these CW probes and pump signal were optimized and set to 0, 4.3 and 6.2 dBm respectively. After the XGM process, the data signal was copied to the two probe signals and thus multicast of the services by all-optical routing of IR-UWB was obtained via this process. For routing, the optical signals are wavelength de-multiplexed (DMUX) and finally distributed in-building using 6.7 km SMF fiber. In practice, the choice of this local distribution fiber also depends on the size of the actual building under consideration. Typically, a fiber length in the order of 500 m is enough. In fact, the considered fiber was much longer than a typical in-building network size and can be considered for large in-building networks such big air-ports. It can also be considered as a worst case scenario for evaluating the performance of the system. Note that both the MUX and DMUX in the RG were using an arrayed waveguide grating (AWG). Finally, the spectrum of the received electrical signal was analyzed using a RF-spectrum analyzer and the performance analysis was done using a digital signal processing (DSP) based bit-error-ratio (BER) measurement.

5.2.2 Experimental Results

Fig. 5.3 presents the spectra of all optical channels and the products from four-wave mixing (FWM) at the SOA output. The FWM products were yielded by the high input power of the optical signals and the SOA nonlinear effects. As shown in Fig. 5.3, these unwanted products were about 30 dB or more weaker than the desired converted channels and were filtered out by the AWG during de-multiplexing processes to the appropriate port. Fig. 5.4a, 5.4b and 5.4c show received time domain IR-UWB pulses from the pump signal as well as the two probe channels. The results clearly show OOK modulated of 1Gb/s of IR-UWB pulses without any significant impairments except for the inversion of the IR-UWB pulses of the two probe channels due to the cross gain modulation (XGM) effect. The PSD of the received IR-UWB from the main pump channel after 26.7 km SMF $-$ 28 fiber was fully compatible with the FCC mask as shown in Fig. 5.5a. Note that the noise floor is above -75 dBm which is mainly attributed to cascaded amplification of signal and noise itself. The PSD of the multicasted IR-UWB from both the probe signals during optical back-to-back case are shown in Fig. 5.5b and Fig. 5.5c respectively. As mentioned in Chapter 4, due to the OOK modulation scheme, all the PSDs show discrete spectral lines called comb-lines where the spacing between each comb lines was 1 GHz and exactly equal to the bit-rate of the transmission system. The PSDs of the multicast signals after the distribution fiber of 6.7 km SMF are shown in Fig. 5.6a, 5.6b and 5.6c respectively and also fit the FCC mask

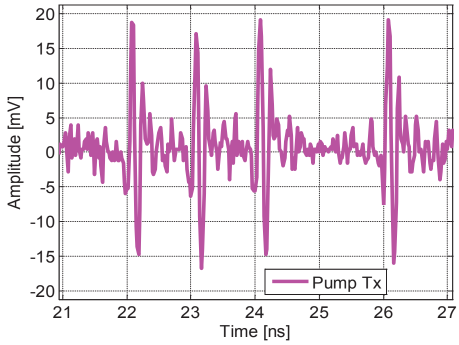

(a) Pump.

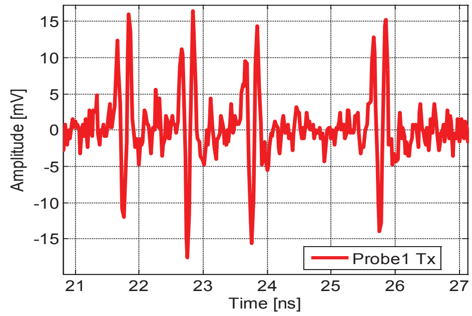

(b) Probe1.

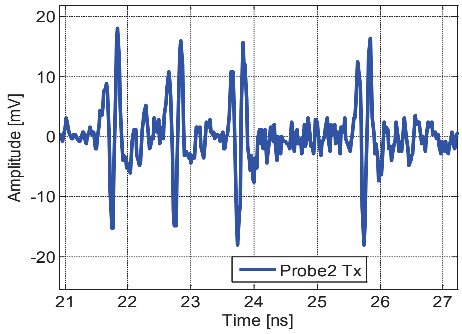

(c) Probe2.

Figure 5.4: Time domain results after transmission.

requirements. In general, the received PSD after transmission show attenuation of the frequency components like low pass filtering due to the accumulated chromatic dispersion of the fiber.

The BER performance was measured to evaluate the quality of the multicasted signals, as shown in Fig. 5.7. The BER was subsequently computed using a DSP algorithm in a bit-by-bit comparison between the transmitted and received data. As mentioned in Chapter 4, the DSP algorithm distinguished between binary "1" and "0" by comparing the average power within the central window of each bit slot to an adaptive decision threshold. The measurements were performed for the pump signal at 1550.92 nm, two other probe signals at 1541.35 and 1555.75 nm respectively. The BER measurement considers both optical back-to-back and transmission over 26.7 km and 6.7 km of SMF fibers for the pump and two probe channels respectively. The

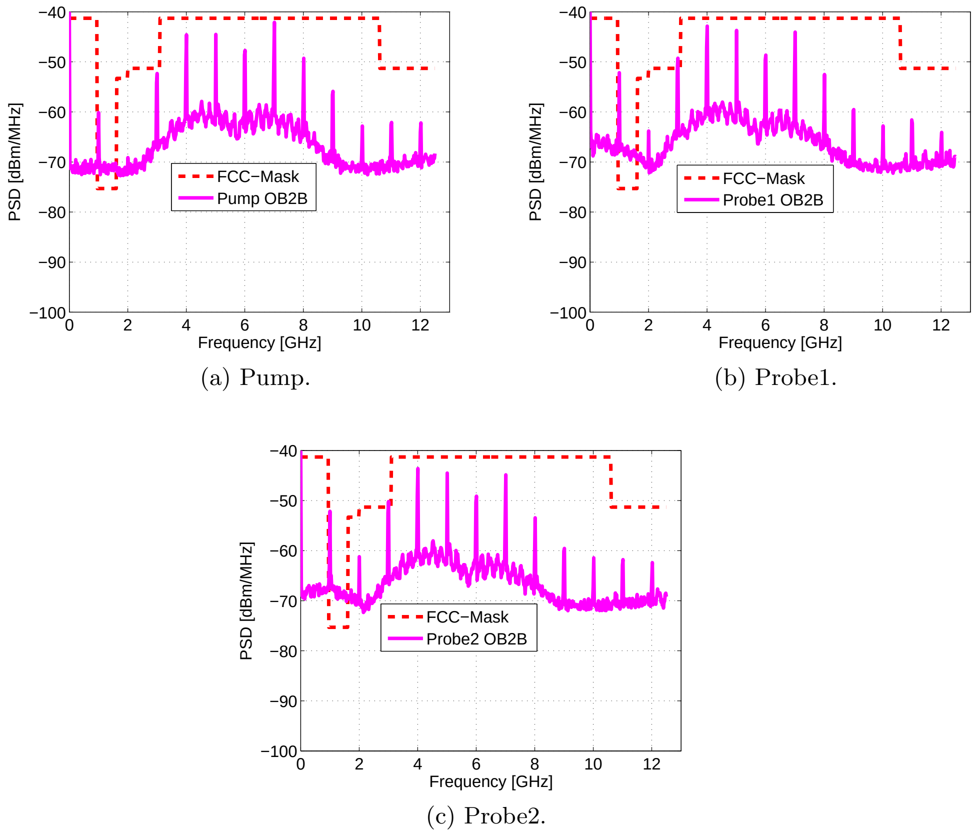

Figure 5.5: FCC-mask and PSD of 1 Gb/s IR-UWB during OB2B case.

results show that the probes were successfully modulated with IR-UWB data and power penalties of 2 and 4 dB were observed compared to pump signal as shown Fig. 5.7. These power penalties resulted from the combined effects of chromatic dispersion of the fiber, ASE noise accumulation from amplifiers, the cross-gain competition between the probe channels, wavelength-conversion penalty and the nonlinearity of the SOA gain profile [152]. In general, the experimental results show a forward error correction(FEC) limit for successful routing of IR-UWB over standard $SMF-28$ fiber transmission for in-building network application. With the experimental results presented in this section, I demonstrated, for the first time, service multicasting by all-optical routing of 1 Gb/s of IR-UWB based on multi-wavelength conversion using XGM in a

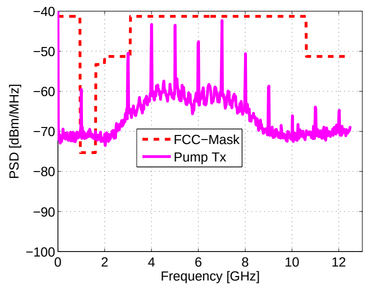

(a) Pump.

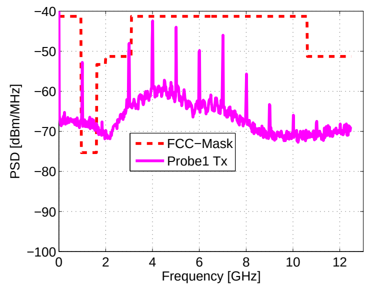

(b) Probe1.

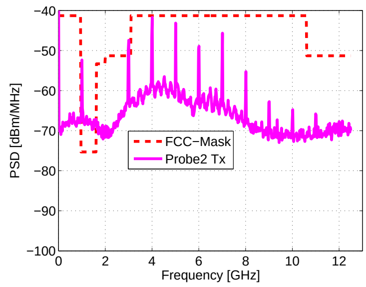

(c) Probe2.

Figure 5.6: FCC-mask and PSD of 1 Gb/s IR-UWB during transmission case.

single SOA as reported in [85]. This proof-of-concept experiment shows that centralizing key features such as signal generation, modulation and routing, which are the main advantages of RoF and in particular for IR-UWB are feasible to achieve low cost and flexible in-building networks.

5.3 Integration of wired/wireless IR-UWB over fiber

Recently, as mentioned above, there is an increasing demand to simultaneously transport wired and wireless broadband services over emerging WDM-PON access network [155, 156, 158]. A similar trend is emerging for in-building optical networks with an increased interest in an integrated optical/wireless network that provides high speed wireless data transfer and entertainment in homes in an energy-friendly way [143]. The in-building network has an optical fiber backbone that connects a central processor called residential gateway (RG) lo-

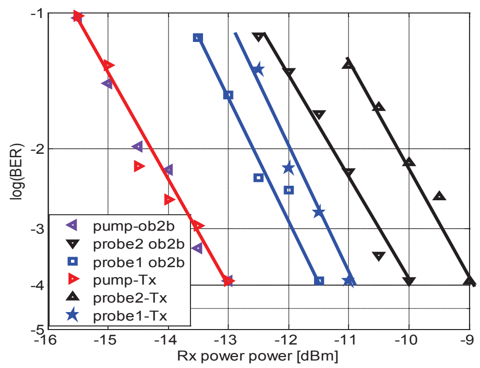

Figure 5.7: BER performance for all channels.

cated somewhere in a house to different rooms served by one or more wireless access points. Operating at multiple wavelengths together with an appropriate configuration management techniques, allows the topology, capacity, coverage and quality of in-home services to be matched to the locally fluctuating demands [143]. Furthermore, an intelligent in-building network can feed one or multiple antennas in each room, thus advanced techniques such as MIMO and adaptive beam steering can be realized for an efficient data transfer [161]. Accordingly, I have proposed and experimentally demonstrated a single integrated optical in-building network system that simultaneously provided 2 Gb/s IR-UWB wireless and 1.25 Gb/s wired services on a single wavelength. Then both signals (wired baseband data and wireless IR-UWB data) were combined electronically and modulated the optical carrier for transmission and were distributed through 1 km SMF to provide wireless and wired services for advanced in-building networks. The experimental setup and the achieved experimental results will be described in the following sections.

5.3.1 Experimental Setup

To realize converged integration of wireless IR-UWB and wired baseband services using a single optical carrier, an experimental setup depicted in Fig. 5.8 was used. A continuous wave (CW) pump signal at 1557.36 nm was externally modulated with combined wired baseband and wireless IR-UWB data using a $LiNbO_3$ modulator. The optimal bias point of the modulator for the combined RF of wireless 2 Gb/s IR-UWB and 1.25 Gb/s wired services without significant distortion of the signals was found at 3.30 V. The IR-UWB

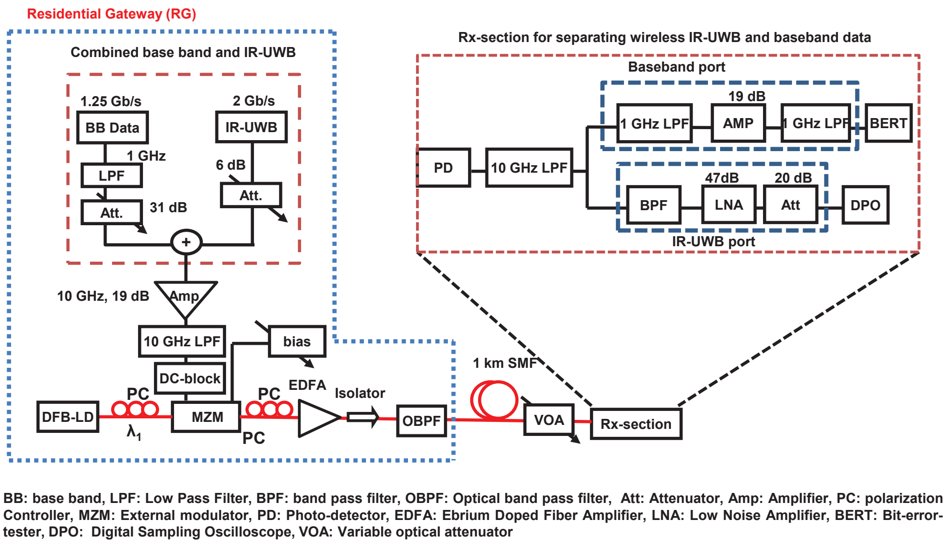

Figure 5.8: Experimental Setup.

pulses were coded with data using a $2^{13} - 1$ PRBS pattern, generated by an arbitrary wave generator (Tektronix AWG7122B) with high bandwidth option enabled as described in Chapter 4. The baseband data was generated using $2^{23} - 1$ PRBS from a 3 GHz pattern generator (HP 70841B). As described in section 5.1.1, generation, filtering and modulation of the optical signal of both wired and wireless signals were performed using the central station called residential gateway(RG). The RG hosts all local functions and establishes a bridge between the in-building network and the access network as shown in Fig. 5.1b and Fig. 5.1c respectively. Furthermore, in the RG, the modulated optical signal was boosted by an erbium-doped fiber amplifier (EDFA) in order to compensate for the insertion loss of the external modulator. To minimize the ASE noise introduced during the amplification process and reduce reflections, a 1 nm tunable optical band pass filter (OBPF) and an isolator are used respectively as shown in Fig. 5.8. The optical spectrum after the OBPF was shown in Fig. 5.9. Finally, the optical signal was detected using a 10 GHz photo-detector (PD) and then a 10 GHz LPF filter was employed after the PD to reduce the noise. Furthermore, appropriate electrical BPF and LPF filters were employed to separate the signals in the electrical domain. Then a performance analysis were done using a DSP-based BER measurement for

IR-UWB data as described in Chapter 4 and a bit-error-tester (HP 70842B) for baseband data. Furthermore, an electrical spectrum analyzer (R&S FSQ 40) was employed to measure the signals in the frequency domain. In general, as it is easily noticeable from Fig. 5.8, the optical fiber link acts as shared optical medium, which delivers integrated wired /wireless signals over a single optical carrier from the residential gateway (RG) to end users within a single room of the building as shown in Fig. 5.1b. This is one of the key advantages of RoF in general to enable a shared infrastructure for multiple operators and to provide a common infrastructure for all wireless channels [125].

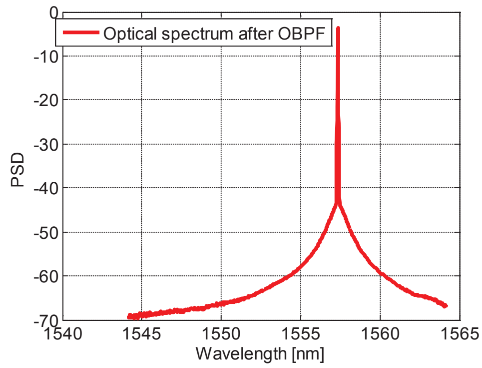

Figure 5.9: Optical power spectrum after OBPF.

5.3.2 Experimental Results

To meet the FCC-mask requirements and efficiently use the available spectrum of IR-UWB, I employed a novel pulse shaping of IR-UWB pulse described in Chapter 3 and reported in [21].The available free spectrum (< 2 GHz) of an IR-UWB PSD is shown in Fig. 5.10a. Therefore, the baseband data spectrum must be limited below 2 GHz to avoid any interference with wireless IR-UWB data. Hence, the higher side lobes resulted from NRZ signaling format as shown in Fig. 5.10b must be filtered out without causing any significant information loss. Thus, a LPF filter of 1GHz was employed to filter out these higher side lobes. The filtered NRZ data spectrum is shown in Fig. 5.10c. Therefore, the spectrum of the wired and wireless IR-UWB can be shared in an efficient manner as shown in Fig. 5.10d without any significant spectrum overlap, which avoids interference of the two systems. Hence, it leads to successful transmission of 2 Gb/s of wireless IR-UWB and 1.25 Gb/s wired

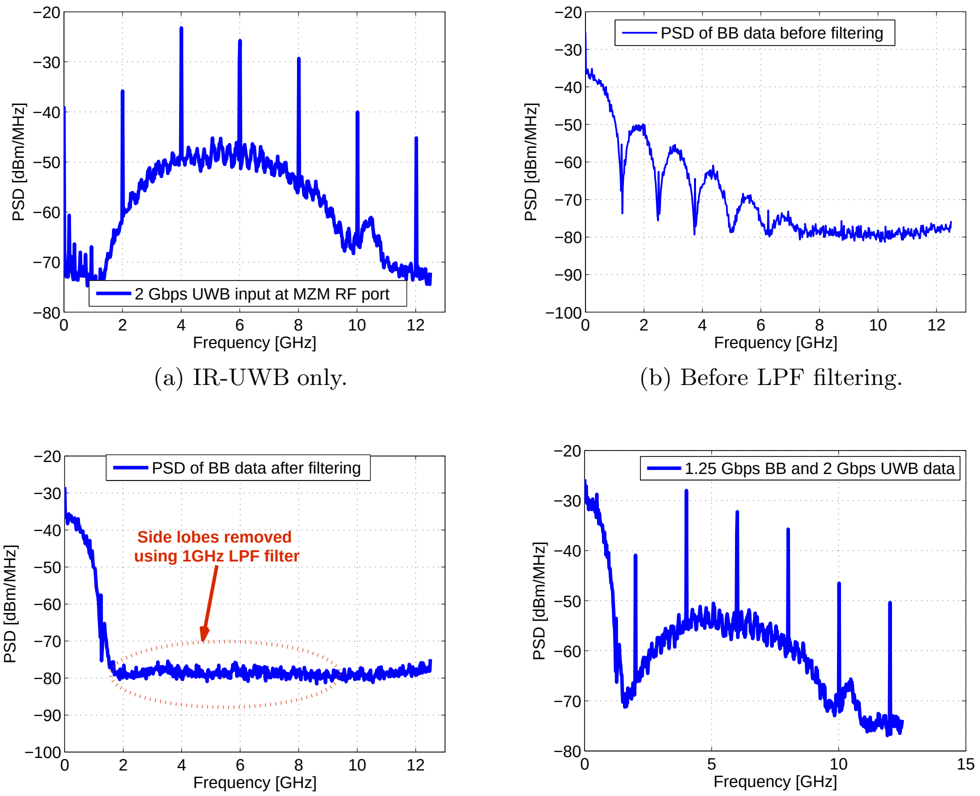

(a) IR-UWB only.

(b) Before LPF filtering.

(c) After LPF filtering.

(d) Combined baseband and IR-UWB.

Figure 5.10: Overview of PSD of 2 Gb/s IR-UWB and 1.25 Gb/s baseband.

services on a single wavelength using a 10 GHz optical system.

Fig. 5.12a shows the spectrum of the received baseband data when the IR-UWB is switched off and on respectively. According to the result shown in Fig. 5.11, the impact of IR-UWB on the baseband data was negligible due to the low spectral component of the proposed pulse as well as optimized power ratios during modulation of the optical carrier. To recover the IR-UWB data, a BPF with frequency response shown in Fig. 5.11 was employed. The response of the BPF had a flat-frequency response with small notch around 9 GHz. However, the rejection ratio for low frequency components (DC-2 GHz) was not significant as can be seen clearly in Fig. 5.11 and hence it caused a small leakage of baseband to IR-UWB port as depicted in Fig. 5.12b. This

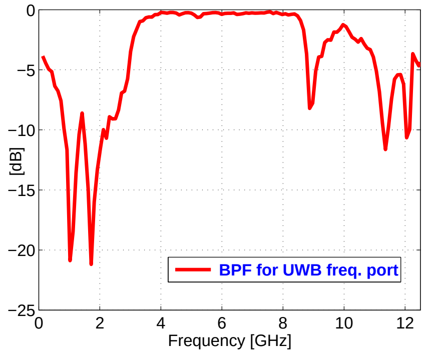

Figure 5.11: Frequency response of BPF.

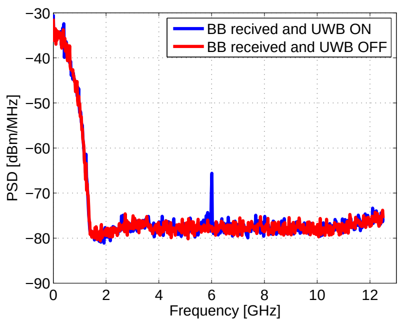

(a) Baseband data.

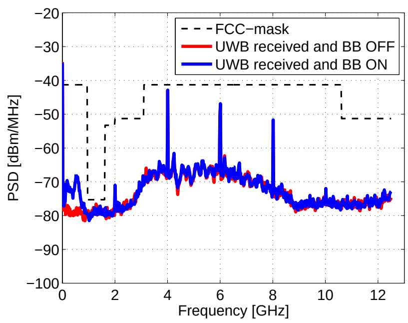

(b) IR-UWB data.

Figure 5.12: Received PSD of 1.25 baseband data and 2 Gb/s IR-UWB.

very small leakage acts as a background noise for the IR-UWB data and hence leads to a noise floor of IR-UWB BER curves as shown in Fig. 5.13a. Note that this small leakage can be eliminated using an optimized BPF $(3.1 - 10.6)$ GHz. The data rate of the baseband data can be increased significantly (to around 10 Gb/s) if FEC limit, spectral efficient modulation such as discrete multitone (DMT) and optimized LPF are considered.

Bit-error-ratio (BER) performance was measured to evaluate the performance of the system. The BER of 2 Gb/s wireless IR-UWB data was subsequently computed using a DSP algorithm in a bit-by-bit comparison between the transmitted and received data. The BER results for IR-UWB transmission are shown in Fig. 5.13a. The power penalty due to the transmission through 1 km SMF fiber was negligible because of high capacity, linearity, low attenu-

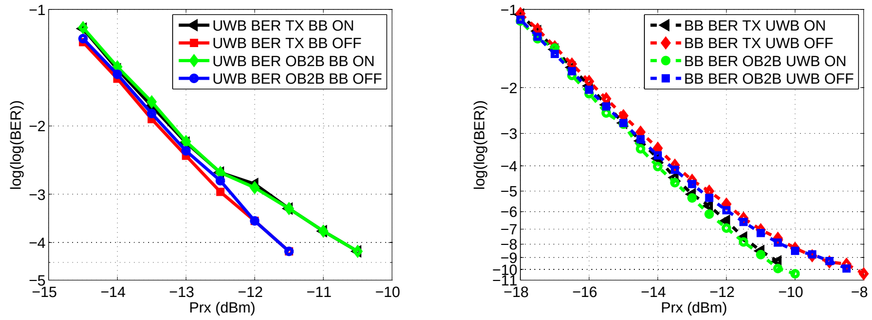

(a) BER of IR-UWB data.

(b) BER of baseband data.

Figure 5.13: BER performance of 2 Gb/s IR-UWB and 1.25 Gb/s baseband data.

ation and negligible chromatic dispersion due to short length of the employed fiber. However, 1 dB power penalty was observed due to the leakage from baseband caused by the poor rejection of the BPF employed in the receiver. The BER results for the baseband data are shown in Fig. 5.13b. There is no power penalty from the transmission through 1 km SMF due to the low bit-rate of 1.25 Gb/s and short reach fiber. However, a noise floor and 1.5 dB power penalty are observed when the IR-UWB is switched-off. This effect is believed to be due to some negligible reflections from the baseband signal caused by impedance mismatch when the AWG is switched off. In general, the experimental results show successful transmission of 2 Gb/s of IR-UWB wireless and 1.25 Gb/s wired services over 1 km SMF-28 fiber over a single optical infrastructure. Hence, the proposed solution has a potential application for low cost, spectral efficient, high capacity and energy-efficient in-building networks.

5.4 Routing of wired/wireless IR-UWB over fiber

5.4.1 Experimental Setup

To realize all-optical routing of integrated wireless IR-UWB and wired services over fiber for future in-building network applications, the experimental setup depicted in Fig. 5.14 was used. The proposed pulse was modulated by OOK modulation using a pseudorandom binary sequence (PRBS) of $2^{13}-1$ data and constructed off-line in MATLAB. Then 2 Gb/s of IR-UWB data was generated electrically by sending the modulated pulse to a Tektronix arbitrary waveform generator (AWG7122B), having an effective RF bandwidth of 9.6 GHz, running at 24 GSamples/s. To achieve this sampling speed, the two ports of the AWG were interleaved and the bandwidth option(zeroing) had been enabled as described in Chapter 4. The generated 2 Gb/s IR-UWB signals were combined with 1.25 Gb/s baseband data generated using $2^{23}-1$ PRBS from a pattern generator. A continuous wave (CW) pump signal at 1557.36 nm (Ch25) was externally modulated using a $LiNbO_3$ modulator biased at the optimal bias point of 3.3 V for hybrid signals. The optical pump signal (Ch25) was generated at the central station called residential gateway (RG), which hosts all local functions and establishes a bridge between in-building network and the access network. Furthermore, the pump signal was boosted by an erbium-doped fiber amplifier (EDFA) at RG in order to compensate the insertion loss of the external modulator. To improve achievable extinction ratio and minimize the ASE noise introduced during the amplification process, a 1 nm tunable optical band pass filter (OBPF) was employed as shown in Fig. 5.14. Two other CW probe signals were generated locally inside the RG using two separate DFB lasers at wavelengths of 1555.75 nm (Ch27) and 1554.13 nm (Ch29). More wavelengths are possible because the solution is in principle scalable to include more than two destinations. Ch25, Ch27 and Ch29 were multiplexed at the RG using an arrayed waveguide grating (AWG) of 200 GHz channel spacing with 2 dB insertion loss. Multiplexed channels co-propagated to the input of wavelength converter SOA for the XGM process. The injected powers into the SOA for Ch25, Ch27 and Ch29 were optimized and set to 5.6, 3.6and 3.8 dBm, respectively, to obtain better conversion performance for respective probe signals. For improved conversion efficiency, the bias current of the SOA was optimized by taking into account the input powers of the optical probe signals. Optimized bias current of the SOA was 125 mA in the experiment. Using the XGM process, the data on Ch25 modulates the two probe signals; Ch27 and Ch29, thereby achieving the multicast wireless IR-UWB and wired services for all-optical routing. Routing of the optical signal to their final destinations was performed by de-multiplexing (DMUX) the optical signals by an AWG followed by distribution using a 1 km $SMF-28$ fiber. The optical signal was detected by a 10 GHz photodetector. The received electrical signals were separated using appropriate filters and then the signal was amplified for processing. The performance analysis was performed using a DSP-based BER measurement for IR-UWB data and using bit-error-tester (BERT) for wired data. A 20 GHz real-time Tektronix DPO72004 digital storage oscilloscope running at a sampling rate of 50 GSamples/s is used for capturing the IR-UWB pulses. The collected IR-UWB data was processed off-line for demodulation and DSP-based BER measurement. Finally, an RF spectrum analyzer was employed to present the electrical spectrum of the pulse and compare it against the FCC-mask requirement. Although, in this experiment, I used the electrical generation of the proposed pulse using AWG, the optical generation of the pulse was also demonstrated as discussed in Chapter 3 and reported in [86]. In addition, the feasibility of generation of modified doublet based on a programmable photonic chip frequency discriminator has been experimentally demonstrated recently and reported in [162].

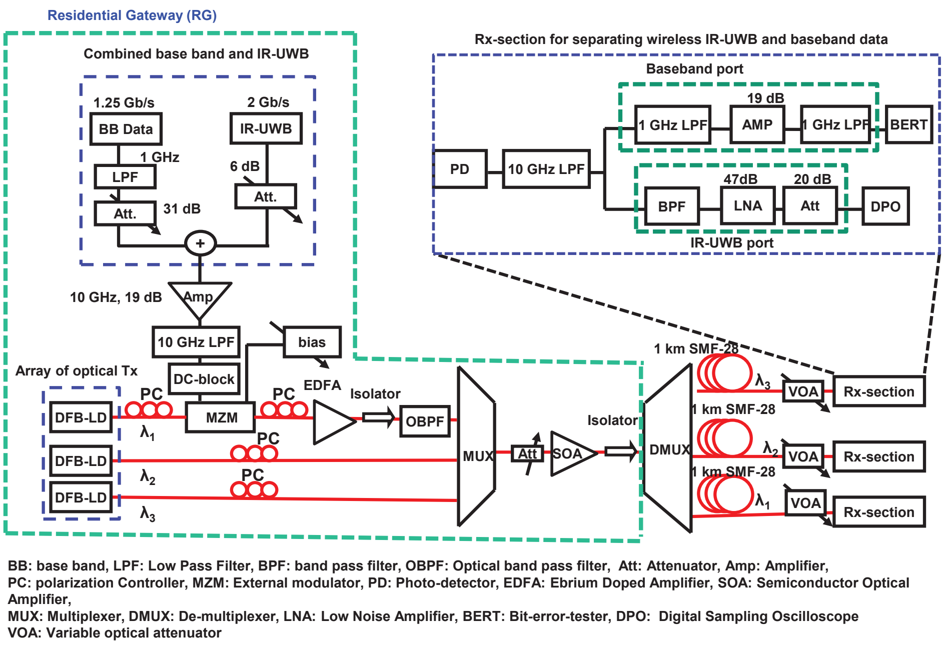

Figure 5.14: Experimental Setup.

5.4.2 Experimental Results

To meet the FCC- mask requirements and efficiently use the available spectrum of IR-UWB, I employed the novel pulse shaping that has a low spectral components below 2 GHz as described above. Fig. 5.15a shows the available

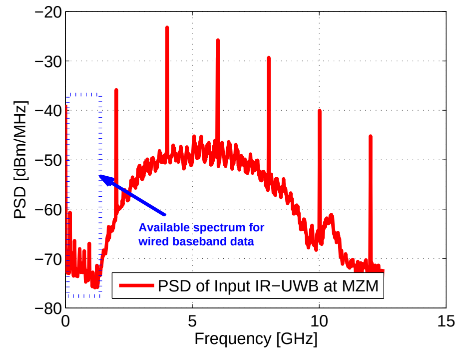

(a) IR-UWB before multiplexing.

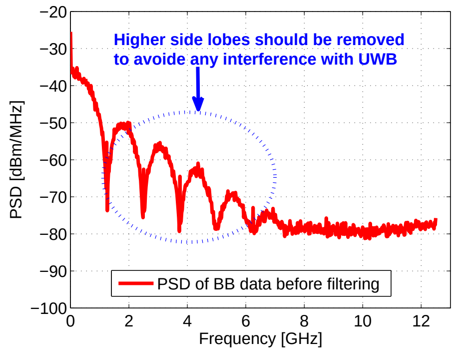

(b) Before LPF filtering.

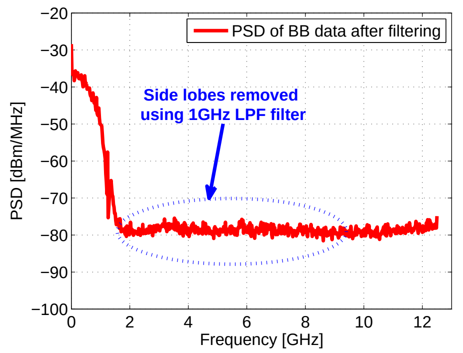

(c) After LPF filtering.

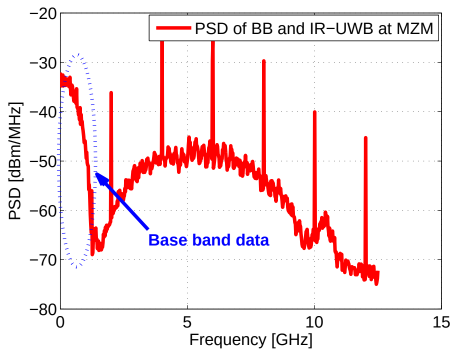

(d) Baseband and IR-UWB.

Figure 5.15: PSD of 1.25 Gb/s wired baseband and 2 Gb/s wireless IR-UWB.

free spectrum (< 2 GHz) of the proposed IR-UWB pulse. The wired baseband data of 1.25 Gb/s is shown in Fig. 5.15b and spectrum was filtered using LPF of 1 GHz bandwidth to limit the bandwidth below 2 GHz to avoid any interference with IR-UWB data. Fig. 5.15c shows the filtered baseband signal. Thus, the LPF suppresses the higher side lobes shown in Fig. 5.15c. Fig. 5.15d shows the efficiently multiplexed 2 Gb/s IR-UWB and 1.25 Gb/s signals with a view to mitigate the impact of interference.

Data carrying channel (Ch25) was multiplexed with probe channels (Ch27 and Ch29) for multi-wavelength conversion using XGM-SOA. Fig. 5.16a presents the optical spectra of all channels and the products from four-wave mixing (FWM) at SOA output. The FWM products were due to the strong opti-

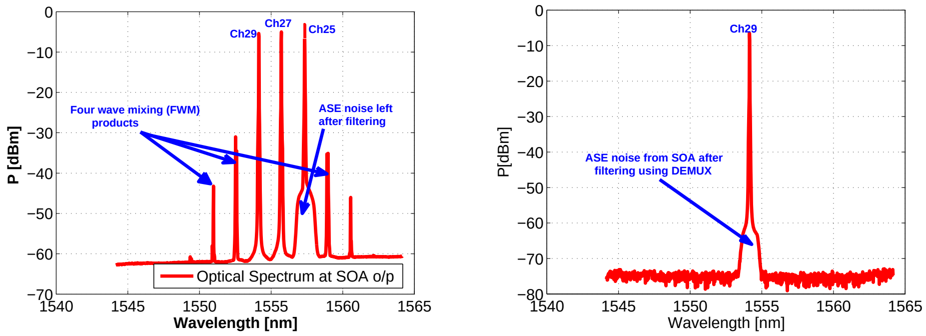

(a) Optical spectrum after SOA. (b) Filtered optical spectrum (Ch29).

Figure 5.16: Optical spectrum.

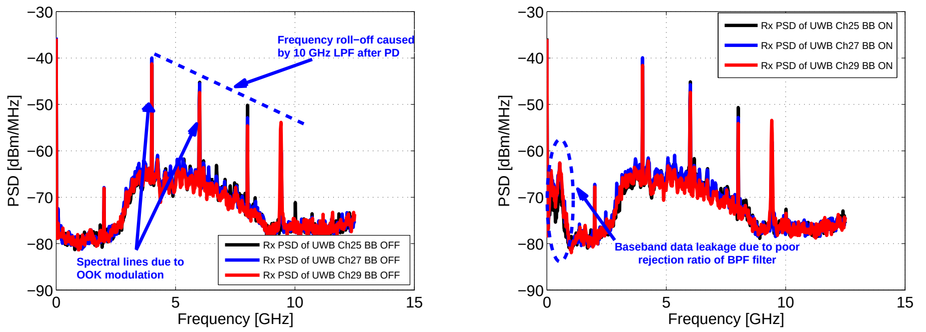

(a) Without baseband data. (b) With baseband data.

Figure 5.17: Received PSD of 2 Gb/s IR-UWB (all channels).

cal signals and the SOA nonlinear effects. These unwanted products were weaker than the desired converted channels and can be filtered out in the de-multiplexer. This removal of unwanted weak FWM products can be seen in Fig. 5.16b in which the probe channel (Ch29) is shown after de-multiplexer output. The received electrical spectra for the baseband data of all the three channels are shown together in Fig. 5.18. This shows that the XGM process has taken place efficiently by modulating the probe channels of Ch27 and Ch29 respectively. A 1 GHz LPF was employed at receiver part to separate the base-band data from wireless IR-UWB data. The results show negligible impact of IR-UWB pulses on the baseband data. To recover the IR-UWB information

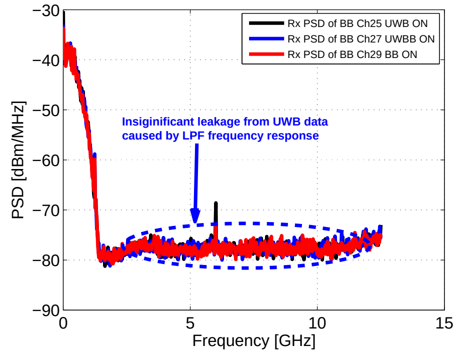

Figure 5.18: RX baseband data with IR-UWB data.

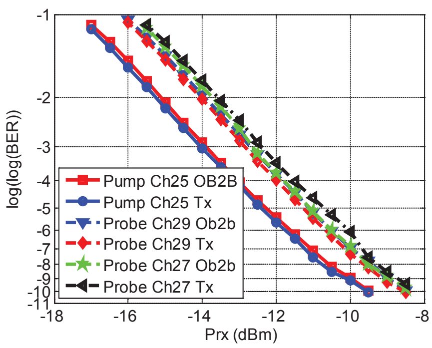

(a) BER of baseband data.

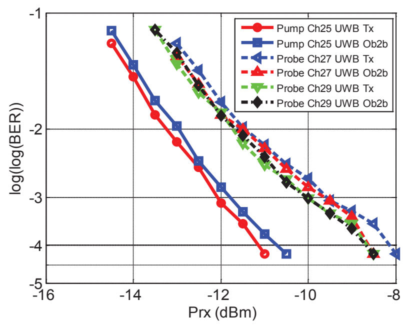

(b) BER of IR-UWB data.

Figure 5.19: BER performance of 1.25 Gb/s wired baseband and 2 Gb/s wireless IR-UWB data.

from the multiplexed electrical signal, a bandpass filter (BPF) with frequency response shown in Fig. 5.11 was employed. As discussed above, the spectrum of the BPF had a flat response with small notch around 9 GHz. However, the rejection ratio for low frequency components (DC-2 GHz) was not high enough to completely suppress the baseband data. Hence, some leakage was observed from baseband to IR-UWB when the baseband is switched off and on, as can be seen in Fig. 5.17a and Fig. 5.17b respectively. This very small leakage acts as a background noise for the IR-UWB information, which leads to a noise floor in the bit-error-rate (BER) curve of all the three channels as shown in Fig. 5.19b. It is important to note that this small leakage can be eliminated using an optimized BPF ($3.1 - 11$ GHz) and the data rate of wired service can be increased to 2.5 Gb/s or even more using an optimized LPF and spectral efficient advanced modulation format such as discrete-multitone provided that the linearity is sufficient.

At the end, the BER performance was measured to evaluate the quality of the routing signals. The BER of 2 Gb/s wireless IR-UWB data was subsequently computed using a DSP algorithm in a bit-by-bit comparison between the transmitted and received data. The BER of the wired data was computed for each channel using a bit-error-rate tester (BERT). The results of BER plots shown in Fig. 5.19a and Fig. 5.19b show a conversion power penalty of less than 2.5 dB for wireless IR-UWB and less than 1 dB for wired respectively. The power penalties were caused due to the combined effect of ASE noise, the cross-gain competition between the probe channels, wavelength-conversion penalty and the nonlinearity of the SOA gain profile. In general, the experimental results confirm the successful routing of wireless 2 Gb/s of IR-UWB and 1.25 Gb/s wired services over 1 km $SMF - 28$ fiber transmission for in-building network application. It should be underlined here that the bit rate of the wired signals can be increased significantly if FEC limit, optimized LPF and spectral efficient modulation (i.e. discrete multitone) is considered.

5.5 Summary

In this chapter, an overview of current in-building networks, future trends therein and the envisaged future integrated in-building with dynamic routing capabilities have been presented. In line with future trends of in-building networks, some networking functions with IR-UWB have been proposed and experimentally demonstrated. A successful experimental demonstration of multicast of IR-UWB over fiber has been described. Successful integration of 1.25 Gb/s wired baseband and 2 Gb/s wireless IR-UWB over 1 km SMF for integrated in-building network has been presented. Finally, routing of an integrated 1.25 Gb/s and 2 Gb/s wireless over 1 km SMF has been elaborated. In general,this chapter for the first time proposed and successfully demonstrated integration of wired baseband and wireless IR-UWB as well as routing of integrated wired baseband and wireless IR-UWB over a single optical fiber infrastructure. The proposed concept has potential applications for low-cost, flexible, high capacity, energy-efficient and smart future in-building networks.

Chapter 6

Ranging/Localization using IR-UWB over Fiber

This chapter discusses ranging and localization using IR-UWB over fiber technologies for in-building/in-home applications. The main objective is to investigate the effect of different fiber types on the achievable accuracy of indoor ranging/localization systems. After the introduction, different radio-based ranging techniques will be described. The wireless channel issues and different receiver architecture will be described. The impact of the fiber onranging and localization under static and line-of-sight (LoS) condition has been studied. Finally, the experimental results for both ranging/localization for LoS conditions will be discussed.[1]

6.1 Introduction

Localization using radio signals has recently attracted an increasing attention in the field of telecommunications and navigation for reasons of safety, emergency and some value added services. The applications that integrate a mobile device's location or position with other information provide location-based services. Traditionally, location-based services (LBS) were designed for supporting typical outdoor applications, for example, GPS navigation. However, traditional LBS do not work inside buildings due to heavy signal attenuation and multipath, while cellular positioning method generally fail to provide a satisfactory degree of accuracy [167]. Therefore, stand-alone solutions are re-

[1] This chapter is based on the results published in [163–166]

quired for indoor environments. Many such solutions utilize technologies like IEEE 802.11 wireless LANs or Bluetooth. However, such technologies have higher complexity and lower accuracy [167]. Hence, researchers started looking for alternative technologies. Due to their very short time-domain pulses, IR-UWB systems are good candidates for ranging/localization systems. The duration of the IR-UWB pulse is inversely proportional to the bandwidth of the transmitted signal. If the arrival time of a pulse is known with little uncertainty, then it is possible to estimate accurately the distance (range) traveled by the pulse from the source. By combining the range estimates at multiple receivers, it is possible to use simple triangulation techniques to estimate the location or position of the source. In general, IR-UWB systems with large bandwidth have the potential to provide high precision ranging/localization.

The interest for indoor localization is due to multiple applications in commercial, health care, public safety and military domains. In the commercial domain, localization has many potential uses in warehousing and in supply-chain management. In the health care domain, there are important uses for tracking/locating patients, medications, and instruments in hospitals, as well as tracking people with special needs such as elderly individuals and individuals with vision and hearing disabilities. In the public safety and military domains precise location can be utilized to assist fire-fighters and military personnel in accomplishing their missions. Therefore, after the theoretical and experimental demonstration on shaping, generating, multi-Gigabit/s transmission and routing of integrated wired/wireless IR-UWB signals over different fibers discussed in Chapter 3, 4 and 5 respectively; the goal of this chapter is to explore the impact of fiber on the ranging/localization accuracy of IR-UWB over fiber systems. This is aligned with the vision of the future in-building network that has a single optical infrastructure that supports both wired and wireless services to provide broadband communication and sensor network applications as described in Chapter 5. Some of the main benefits of using fiber ranging/location with IR-UWB signals are : 1) allow centralized complex processing algorithms (e.g.,in the residential gateway (RG) to be shared among several access points), 2) provide reach extension using a super-efficient high bandwidth, low loss, immunity to EMI and transparent optical medium, 3) provide numerous synchronized access points, which can further relax synchronization mechanisms between mobile device and access points 4) enhance accuracy by deploying many simplified and synchronized radio access points 5) enable energy-efficient networks by exploiting localization information for efficient radiation and traffic management. In general, accurate ranging/localization using IR-UWB over fiber for in-building applications is an attractive solution and the impact of different fiber types should be investigated.

6.2 Radio-based Ranging Techniques

To understand the high-precision ranging/localization capability of IR-UWB signals, position estimation techniques should be investigated first. To estimate the position of a mobile device (called the "target" node) in a wireless network, signals are exchanged between the target node and a number of reference nodes (or radio access points (RAP)) [8, 10]. The position of a target node can be estimated by the target node itself, which is called self-positioning; or it can be estimated by a central unit that gathers position information from the RAPs, which is called remote-positioning (network centric positioning) [8, 10]. Furthermore, depending on whether the position is estimated from the signals traveling between the nodes directly or not, two different position estimation schemes can be considered namely *direct positioning and two-step positioning* [8, 10]. The position estimation can be performed directly from the signals traveling between the mobile device and RAP, which is called direct positioning [168]. On the other hand, in a two-step approach certain parameters are extracted from the signals first, and then the position is estimated based on those signal parameters. Although the two-step positioning approach is suboptimal in general, it can have significantly lower complexity than the direct approach. Also, the performance of the two is usually very close for sufficiently large signal bandwidths and/or SNRs [8, 10, 168]. Therefore, most practical systems adopt two-step approaches, which will also be the main focus in this Chapter. The conceptual representation of both direct and two-step approach is shown in Fig. 6.1.

As shown in Fig. 6.1, the first step in a two-step positioning approach involves measurement of a set of signal parameters related to the position of the target node. These parameters are usually related to the energy, timing and/or direction of the signals traveling between the target node and the reference nodes. Hence, depending on accuracy requirements and constraints on transceiver design, various signal parameters can be employed. Commonly, a single parameter is estimated for each received signal, such as the arrival time or the strength of the signal. However, it is also possible to estimate multiple signal parameters in order to improve positioning accuracy.

In the following, an overview of various techniques for this two-step approach is presented: RSS, ToA, AoA and TDoA.

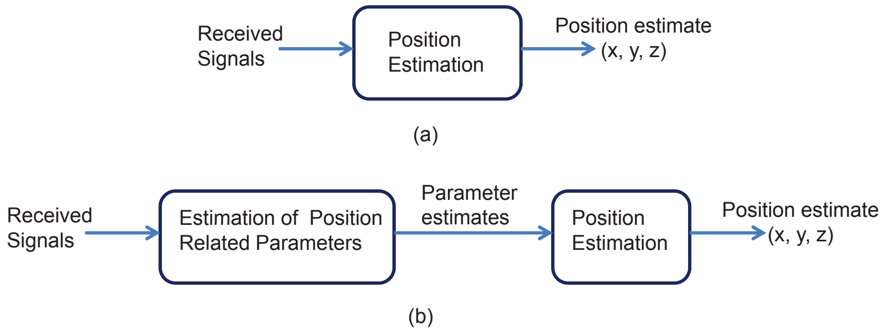

Figure 6.1: (a) Direct positioning and (b) two-step positioning [18].

6.2.1 Received Signal Strength (RSS)

When a signal propagates from a transmitter to a receiver, the amount of energy collected by the receiver depends on the distance (range) between the transmitter and the receiver. Therefore, the RSS can be considered as a parameter that carries position related information. To convert the RSS information into a range estimate, the relation between the distance and signal energy should be known. Knowing such a relation, the distance between the nodes can be estimated from RSS measurements at nodes assuming that the transmitted signal energy is known. Besides, RSS measurements depend on the channel characteristics. Therefore, RSS-based positioning algorithms are sensitive to channel parameter estimations [169].

In general, in the case of two-dimensional positioning under absence of errors, the distance between two nodes provides a circle of uncertainty for the position of the target node as in case-1 shown in Fig. 6.2. However, due to inaccuracies in both RSS measurements and quantification of the distance versus path loss (PL) relation, distance estimates are subjected to errors. Hence, in reality, each RSS measurement defines an uncertainty area as in case-2 shown in Fig. 6.2. As mentioned earlier, one factor that affects the signal energy is called path loss, which refers to the reduction of signal power/energy as it propagates through space [10]. It should be noted that an UWB signal experiences multipath (small-scale) fading, shadowing and PL while traveling from one node to another. A common model for path loss is given as:

$$\overline{P}(d) = P_0 - 10n \log_{10}(\frac{d}{d_0}) \tag{6.1}$$

where n is the PL exponent, $\overline{P}(d)$ is the average received power(dBm) at a distance d and P_0 is the received power (dBm) at the reference distance d_0. For UWB systems, the multipath effects can be mitigated significantly by measuring the sum of the powers of the multipath components (MPCs) [8]. In other words, if the integration interval T in the calculation of the average power,

$$P(d) = \frac{1}{T}\int_0^T |r(t)|^2 dt \tag{6.2}$$

is long enough to include all the MPCs in the received signal $r(t)$, the small-scale fading effect can be mitigated. However, the shadowing effects are usually present in the received power $P(d)$, which are modeled as log-normal variables. In other words, the received power in dBm can be modeled as Gaussian random variable with mean $\overline{P}(d)$ given by Eq. 6.1 and the variance σ_{sh}^2. In short it can be expressed as:

$$10\log_{10} P(d) \sim N\left(\overline{P}(d), \sigma_{sh}^2\right) \tag{6.3}$$

It should be noted that this model can be used in both line-of-sight(LoS) and non-LoS scenarios with appropriate choice of channel-related parameters. From the received power, the Carmer-Rao lower bound (CRLB) for estimating the distance can be expressed as [8]:

$$\sqrt{Var\{\widehat{d}\}} \geq \frac{ln10}{10}\frac{\sigma_{sh}}{n}d \tag{6.4}$$

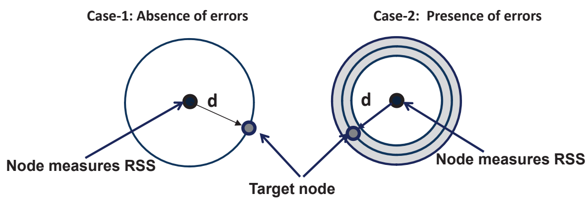

Figure 6.2: Node measures RSS and determine the distance **d** between itself and the target node in the presence and absence of errors.

Note that CRLB is a statistical measure that states that the variance of any unbiased estimator will be not lower than the inverse of Fisher information [8]. For this RSS ranging method it provides a means to access the theoretical best performance of an estimator. Therefore, in Eq. 6.4, $\widehat{d}$ represents an unbiased estimate of d. It can be easily observed from Eq. 6.4 that the lower bound increases as the standard deviation of the shadowing increases, since RSS

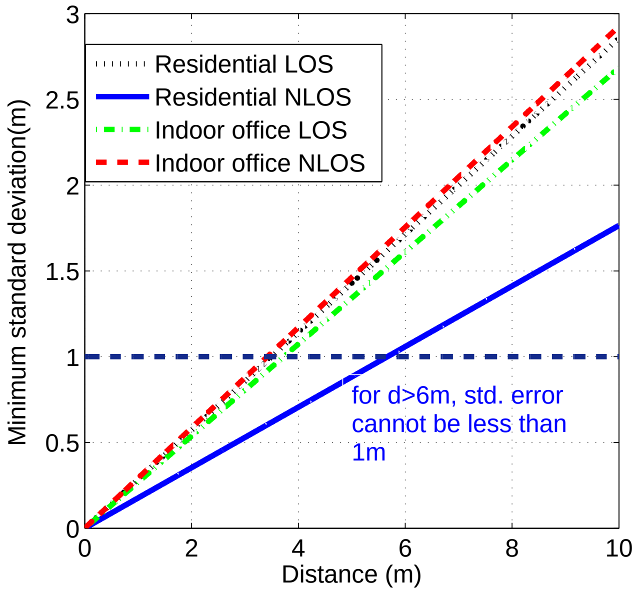

Figure 6.3: RSS ranging accuracy for different channels.

Table 6.1: Channel parameters used for Fig. 6.3 (LoS: Line-of-sight, NLOS: Non-LOS, n: PL exponent and σ_{sh}: standard deviation of shadowing)

Scenario	n	σ_{sh}
Residential LoS	1.79	2.22
Residential NLoS	4.58	3.51
Indoor office LOS	1.63	1.99
Indoor office NLoS	3.07	3.90

measurements vary more around the true average power. In addition, a larger path loss exponent (n) results in a better estimation accuracy, as the average power becomes more sensitive to distance for large n. Finally, the distance dependence in Eq. 6.4 shows that the variance RSS measurements deteriorates as the distance between nodes increase. This is clearly observed in Fig. 6.3, in which the minimum standard deviations are plotted versus distance for various environments according to the IEEE 802.15.4a channel model for which the standard deviation and PL exponent is given in Table 6.1. As observed from the Fig. 6.3, the lower bound increases linearly with distance and also note that the NLoS residential environment has the lowest bound. According to simulation result in Fig. 6.3, the standard deviation of the error cannot be made smaller than 1 m for a distance larger than 6 m. In other words, RSS measurements cannot provide very accurate range estimates for IR-UWB systems.

It should be noted that the accuracy of RSS method is usually poor but can be improved by increasing the number of measurements and averaging the results [16]. As the method is based on the received signal power, no tight synchronization is required between the receivers. However, exact knowledge on the path loss is a vital element for efficient operation of the systems [16]. RSS location techniques are normally feasible for low-cost deployment in cellular networks. However, RSS technique is not suitable for use in multipath fading channels where the variation of the signal strength can be up to 30 dB over a distance of more than half a wavelength [16]. This will make the RSS method more difficult to be used in the UWB systems. Hence, RSS technique is not considered in this thesis.

6.2.2 Time of Arrival (ToA)

Another parameter that provides information about the range between two nodes is the ToA parameter. When the devices are synchronized, the ToA of the signal can be used to obtain a range estimate. If the devices are not synchronized, they can exchange timing information by certain protocols such as the two-way ranging protocol in order to estimate the range [170]. Consider a simple scenario in which the time-delayed version of the transmitted signal arrives at a receiver in the presence of zero-mean additive white Gaussian noise (AWGN). In that case, the CRLB on the standard deviation of unbiased ToA estimator ($\widehat{\tau}$) is given by [170]:

$$\sqrt{Var(\widehat{\tau})} \geq \frac{1}{2\pi\sqrt{2}\sqrt{SNR}\beta} \tag{6.5}$$

where $SNR = \alpha^2 E/N_0$ is the signal-to-noise ratio, α is the channel coefficient, E is denoting the signal energy, $N_0/2$ spectral density white noise and β is the effective bandwidth, calculated as:

$$\beta \triangleq \sqrt{\frac{\int_{-\infty}^{+\infty} f^2 |S(f)|^2 df}{\int_{-\infty}^{+\infty} |S(f)|^2 df}} \tag{6.6}$$

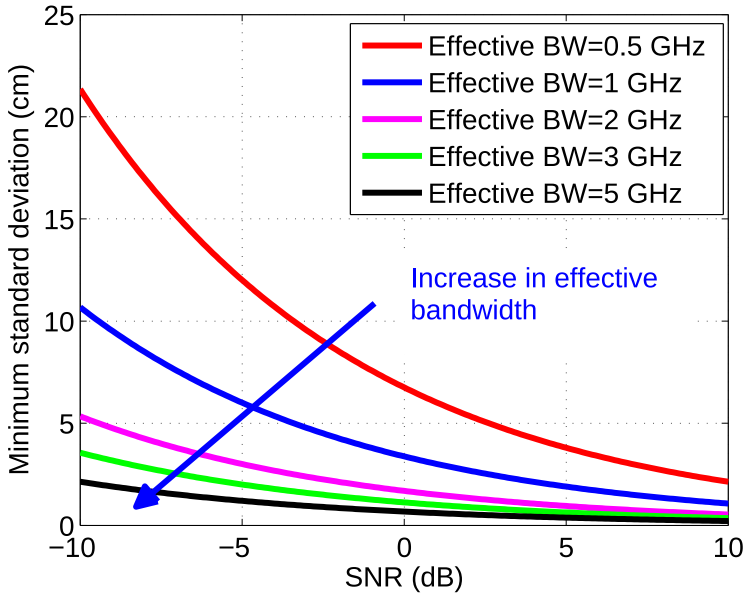

Figure 6.4: Effect of bandwidth on ToA estimate.

and $S(f)$ is the Fourier Transform of the transmitted signal. Note that the precision of the ranging measurement as given in Eq. 6.5 is a function of the received SNR and the effective bandwidth of the signal employed. Moreover, as shown from Eq. 6.5, the CRLB lower bound precision estimate is inversely proportional to the signal effective bandwidth but is inversely proportional to only the square root of the SNR. In general, Eq. 6.5 together with Eq. 6.6 shows us that the lowest achievable variance of the range measurement obtained from ToA is inversely proportional to the effective signal bandwidth, which can be easily seen from Fig. 6.4. For instance, the CRLB for the standard deviation of an unbiased range estimator (obtained by scaling a ToA estimator by the speed of light) is less than 1 cm at an SNR of -3 dB and effective bandwidth of 5 GHz as shown in Fig. 6.4. Notice that, measurement precision is defined as the consistency of a group of observations about the mean value. However, the mean value may be biased. Accuracy is denoted as the closeness of the measurement to the true value. Note that CRLB analysis assesses the theoretical best performance of UWB for ranging but real testing is needed to assess the accuracy of practical UWB ranging. Therefore, ToA technique has been adopted in thesis for studying the impact fiber on ranging and localization using IR-UWB pulses proposed in chapter 3.

6.2.3 Angle of Arrival (AoA)

The AoA parameter provides information about the direction in which the target device resides. A common technique to estimate the AoA parameter is to employ multiple antennas in the form of an antenna array. Then the difference in arrival times of an incoming signal at different antenna elements can be used to obtain the AoA information based on known array geometry [18]. It is important to note that for narrowband signals, those differences in arrival times are represented by phase shifts of the signals. Therefore, the combinations of the phase shifted versions of the received signals at antenna array elements can be tested for different angles in order to estimate the AoA [18]. However, for UWB systems, time differences cannot be represented by phase shifts, hence, time delay versions of the received signals should be considered for AoA estimation [18].

For AoA estimation a uniform linear array (ULA) shown in Fig. 6.6 can be used. When the distance between the transmitting and receiving devices is sufficiently large, the incoming signal can be modeled as a planar wavefront. This results in $l \sin \phi / c$ seconds difference between the arrival times at consecutive array elements, l is the inter-element spacing, ϕ is AoA and c represents the speed of light. Therefore, estimation of the time of difference of arrivals provide angle information. Note that many array structures are possible for AoA based estimation techniques such as uniform circular arrays (UCA) and rectangular lattices, which operate on the same basic principle as the ULA; namely, estimation of time difference between array elements, the geometry of which is known by the receiver.

Assuming that the geometry employed is an ULA, N number of antenna elements, d is the distance between the transmitter and the center of the array at the receiver and l is the inter-element spacing in the ULA. Furthermore, assuming independent white Gaussian noise with zero-mean at different antenna elements, the CRLB for estimating ϕ is given by [8]:

$$\sqrt{Var\{\widehat{\phi}\}} \geq \frac{\sqrt{3}c}{\sqrt{2}\pi\sqrt{SNR}\beta\sqrt{N(N^2-1)}l\cos\phi} \tag{6.7}$$

where SNR is the signal to noise ratio for each element and β is the effective bandwidth defined earlier in Eq. 6.6. It can be easily noted from Eq. 6.7 that an increase in the SNR, effective bandwidth, inter-element spacing or the

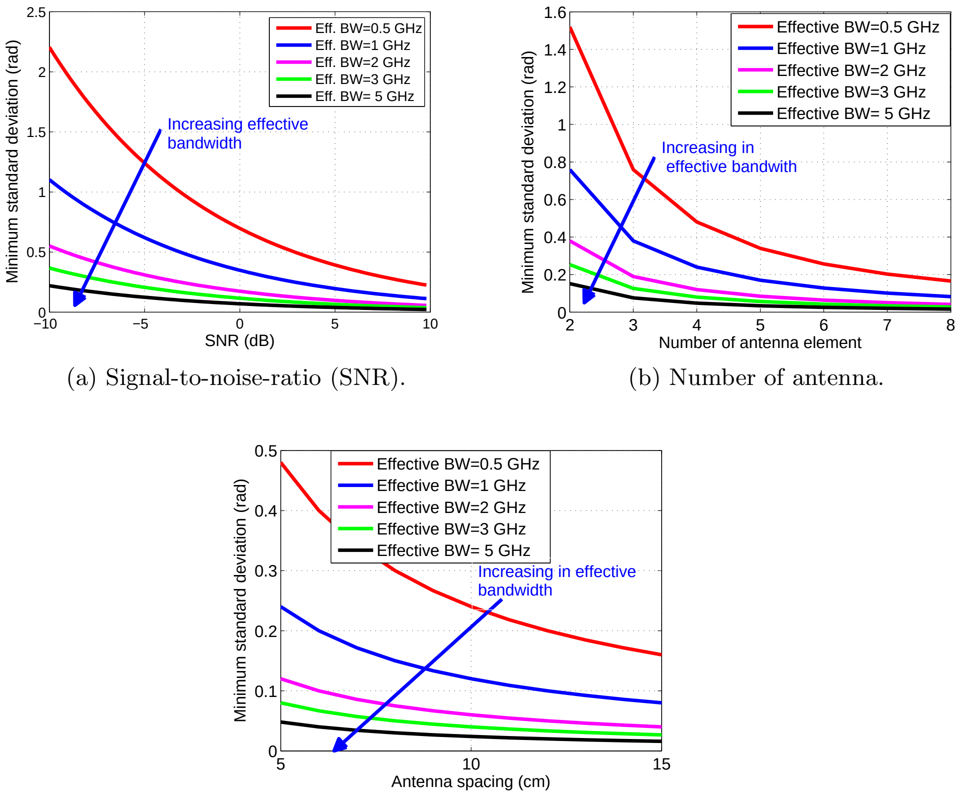

(a) Signal-to-noise-ratio (SNR).

(b) Number of antenna.

(c) Antenna spacing.

Figure 6.5: Effect of system parameters in AOA ranging technique.

number of elements enhances the accuracy of AoA estimation. Therefore, the larger bandwidth of IR-UWB again can facilitate accurate AoA measurements. To show all these effects of the parameters, simulation result is provided in Fig. 6.5. These simulation results show theoretical limits provided in Eq. 6.7, with general parameters $N = 4$, $l = 5$ cm, $\phi = \pi/4$ and $SNR = 5$ dB. In general, observation from the results shown in Fig. 6.5, an increase in SNR or increase in N and increase in β leads to a lower the standard deviation.

In general, in AoA, the signal sent by the target (mobile device) to be positioned is measured at several stationary access points or reference nodes by steering the main lobe of a directional antenna. Each measurement gives a line from the access point to the mobile device. In principle, intersection of two

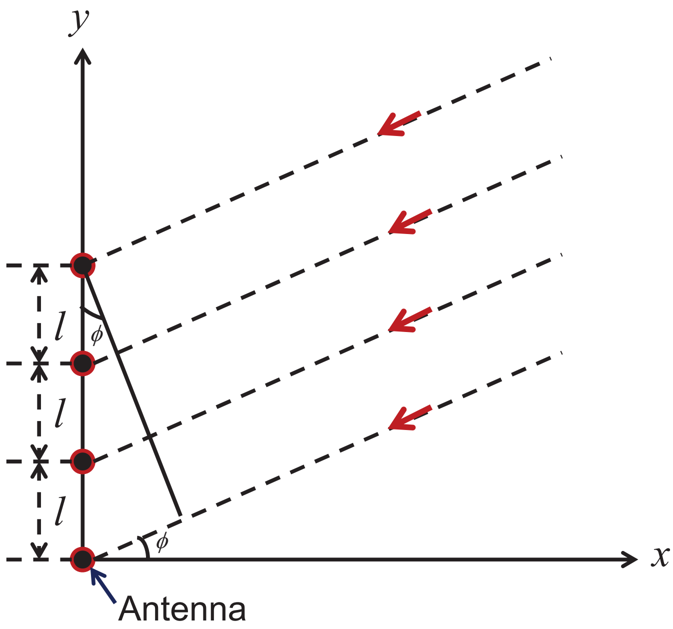

Figure 6.6: A ULA configuration and a signal arriving at the ULA with angle ϕ.

lines is the position of the object. Therefore, in theory only two access points are needed for 2-D localization. However, in practice because of the multipath effects more than 2 access points will be required [16]. The AoA technique has the advantage of not requiring path loss information or synchronization of the receiver (access points) and needs two or more reference nodes to estimate the location. This technique does not need the time reference. However, it requires complex hardware for accurate array calibration. It also suffers from a large AoA spread in microcells [16]. Furthermore, in the absence of LoS or when the distance is large the system will yield a poor performance.

6.2.4 Time Difference of Arrival (TDoA)

The TDoA technique can be employed when there is no synchronization between a given target or mobile device and the reference nodes or access points, but there is synchronization between reference points [169]. TDoA is based on estimating the difference in the arrival times of the signal between the synchronized access points. TDoA does not require knowledge of the absolute time of the transmission. In other words, the TDoA parameters are calculated by taking the difference between the ToA estimates, which remove offset due to the asynchronism between the target device and the access points [170]. Similar to the discussion for ToA given in section 6.2.2, the accuracy of the TDoA parameter increases as the effective bandwidth and/or SNR increases as given in Eq. 6.5 [18].

For two antenna elements, it is easy to see that the difference in signal arrival times restricts the possible transmitter positions to hyperbolas [171]. The intersection of two or more hyperbolas found from additional antenna pairs reveals the transmitted position. The difficulty lies in obtaining a good estimate of the time delay. One way to estimate the TDoA value is to perform cross-correlation between signals coming from a pair of synchronized access points and determine the time difference value corresponding to the peak or maximum cross-correlation function and it is given by:

$$R_{12}(\tau) = E[r_1(t)r_2(t+\tau)], \tag{6.8}$$

where $E[.]$ is the expected value operator, $r_1(t)$ and $r_2(t)$ are the signals received at two antennas, and τ is the time delay. The value of τ corresponding to the peak of the cross correlation function is the TDoA estimate.It should be noted that RoF techniques can produced numerous synchronized radio access points and thus enable TDoA ranging techniques. Once the TDoA ranges have been estimated using IR-UWB signals, then it is possible to obtain the range differences measurement by multiplying the estimated delay with radio speed c. These measurements can be converted into nonlinear hyperbolic equations. The equation of TDoA is:

$$D_{j,k} = \sqrt{(x_i - x_j)^2 + (y_i - y_j)^2} - \sqrt{(x_i - x_k)^2 + (y_i - y_k)^2} \tag{6.9}$$

where $D_{j,k}$ is the range difference obtained from the estimated TDoA. (x_i, y_i) are the coordinates of the target node, (x_j, y_j) and (x_k, y_k) are the coordinates of the RAPs. However, TDoA is not consider in this thesis due to the lack of components. Therefore, ToA technique has been considered in this thesis with proper calibration at distance 1 m.

6.2.5 Hybrid Techniques

In real-time communication, errors due to multipath propagation largely influence the accuracy of ToA and TDoA positioning methods. Besides the multipath effects, the receiver hardware, efficiency in generating the transmission pulses and multiuser interference affects the accuracy of range and delay estimation [16]. To improve the performance hybrid combinations can be used such as RSS with TDoA. This hybrid combination leads to the enhancement of UWB short range positioning with respect to only ToA or TDoA methods [16, 18].

6.3 Overview of UWB channel model

The ultimate performance limits of a communication system are determined by the channel it operates in [172]. Realistic channel models are thus of extreme importance for system design and testing. However, UWB propagation channels show fundamental differences from conventional (narrow-band) propagation in many respects, so that the established (narrow-band) channel models cannot be used [173]. One of the key differences between UWB propagation channels and conventional channels lies in the frequency dependence of the transfer function. Conventional (narrowband) channels show frequency dependence of the local (or instantaneous) transfer functions due to the different runtimes of multipath components; those variations typically occur within a bandwidth of a few MHz. UWB channels show not only these variations, but also variations of the averaged transfer functions; these variations are caused by the different attenuations that different frequency components of the UWB signal encounter [172]. A number of UWB channel models have been proposed in the past. The IEEE802.15.3a group developed a channel model that is valid from 3 to 10 GHz but it is designed only for indoor residential and office environments, and the distance between transmitter and receiver is restricted to less than 10 m.

A more general model for UWB channels, which is adopted for evaluating different ranging/localization systems is provided by the IEEE802.15.4a group [173]. It is valid for a frequency range from $3 - 10$GHz. It is based on measurements and simulations in the following environments: residential indoor, office indoor, built up outdoor, industrial indoor, farm environments, and body area networks. The model is independent of the used antennas. It includes the frequency dependence of the path gain as well as several generalizations of the Saleh-Valenzuela model, like mixed Poisson times of arrival and delay-dependent cluster decay constants. This model can be used for realistic performance assessment of UWB systems. It was accepted by the IEEE 802.15.4a Task Group as standard model for evaluation of UWB system proposals [173]. Hence, using this channel intensive simulations has been carried out by using the proposed IR-UWB pulses in Chapter 3 and the achieved results have been reported in [164]. It should be noted that this chapter focusses only on the experimental results obtained for ranging and localization of IR-UWB over different fiber types under LoS and static environment conditions. For simulation results of different channels scenarios and the effects of parameters on the receiver choice, interested readers are recommended to refer to the work reported in [164].

6.3.1 Line-of-sight (LoS)vs Non-line-of-sight(NLoS) condition

A proper channel model is required for understanding and mitigation of errors to achieve high accuracy in dense multipath propagation environments such as an indoor scenario. It should be noted that, the LOS path between transmitter and receiver devices may be obstructed in the indoor scenario. An LoS path, also some times called a direct path, is a straight line path that connects the transmitter and the receiver. With the absence of an LOS path, the transmitted signal could only reach the receiver through penetrated, reflected, diffracted or scattered paths called non-line-of-sight (NLoS) paths. Note that the NLoS could also include a direct path faded within the bandwidth of the receiver caused by the multipath of short excess delay. The NLoS error is defined as the excessive traveling distance with respect to the direct path. The indoor environments are full of obstacles, walls, and other objects, which affect the transmitted signal and thus the range estimation might be larger than the true distance. Hence, the accuracy of node-location estimates is adversely affected in NLOS scenarios [167].

To cope with NLoS introduced errors, several techniques have been reported in the literature. These can be broadly classified into two main categories: NLoS identification techniques and NLoS error mitigation techniques. The review of these techniques has been reported in [167]. However, as mentioned in the above, this thesis focusses as proof-of-concept on the impact of fiber on ranging/localization accuracy for LoS scenario. Hence, further detailed investigation on NLoS identification and mitigation techniques is out of the scope of this thesis. Interested readers are recommended to read to the work reported in [167] and [8].

6.4 Overview of Receiver Architecture

6.4.1 Direct Sampling

The structure of the receiver obviously depends on the ranging techniques (RSS, ToA/TDoA, AoA) and the requirements in terms of cost of the implementation which can involve some analog front-end processing. In any case the first part of a receiver is composed by an antenna, a band pass filter and a low noise amplifier. After amplification the best way to capture the signal would be to sample and acquire it for the next step which is digital processing. In the digital processing step, the estimation of the time of arrival, the received signal strength or the angle of arrival can be performed in order to get the distance estimation. The implementation of the ranging algorithm, to find out the position of the target node, also is done in this section. However, due to the large bandwidth employed in the order of gigahertz, typical UWB receivers cannot operate at Nyquist rate. Instead, the signal can be captured at lower sampling rates after certain analog front-end processing and using different transceiver architectures [8, 174]. Some of the commonly used receiver architectures are discussed in the following.

6.4.2 Matched Filter (MF)

The optimal receiver for a signal transmitted over an AWGN channel is a correlation or a matched filter receiver, since it maximizes the SNR [20]. The receiver structure basically consists of a low-noise amplifier (LNA), a correlation circuit and a circuit to provide the template waveform for the correlation. Note that to maximize the processing gain and SNR, the template waveform should be the same as that of the to be expected received signal. Such a signal is difficult to generate in practice, since the transmitted pulse is distorted by the antennas and the channel. The need to make the template waveform the same as that of the received signal also makes the receiver circuity complex [20]. One way to avoid this complexity is to approximate the template waveform by using the transmitted pulse or to make a very coarse approximation such as a rectangular pulse.

The correlation circuit consists of an integrator and a multiplier that multiplies the received signal with the template waveform. The result of the multiplier is integrated over the bit duration to maximize the received signal power and to minimize the noise component. Having a train of pulses to integrate over, the correlated signal is raised from the noise and the possible signals of the other users. Therefore, it can be seen that the more pulses there are in a pulse train, the better SNR is attained, since more correlated energy is put into each symbol. However, next to providing an accurate synchronization, performing the correlation at the required speed is probably the biggest issue. Both the multiplier and integrator must be fast enough to process each pulse [20].

6.4.3 Transmitter Reference (T-R)

To solve a clean template as in the case of matched filter, a T-R uses two pulses with a fixed delay. This scheme uses one pulse for the data and the other pulses for template waveform. In other words, in the T-R method the same pulse is transmitted twice through the channel. Both pulses experience the same channel distortion. Hence, the T-R receiver correlates the similarly distorted data pulses, which show high correlation. In general, in the T-R technique each reference pulse acts a preamble for its data pulse, providing rapid synchronization. In addition, T-R receiver has the ability to capture that energy by correlating the received signal with its delayed version which is quite important in low-power IR-UWB systems. Despite its advantage, T-R suffers from some drawbacks such as the performance is poor for low SNR and in the presence of narrow band interference. Another disadvantage is that half of the power is transmitted as template and thus waste of resource.

6.4.4 Energy Detector (ED)

The energy detector receiver is a low cost and low complexity alternative to an MF and TR receiver because it does not require a mixer and a lower sampling frequency is needed. In addition it can be used for both RSS and Time-based ranging as long as the integration window is properly chosen. Note that in non-coherent approaches the enhanced noise terms in the low SNR region become an issue. In particular, noise-square terms for ED and noise-cross-noise terms in the transmit reference (TR) seriously dominate and degrade the detection performance [175]. Therefore, even though a non-coherent approach outperforms the matched filter at high SNR due to better energy capture at sub-sampling rates, it has a poor performance when the noise variance is large.

Note that in conventional communications the transmitted waveform fills up the entire symbol duration, consequently, the receiver is enabled continuously and the observation time period is equal to the symbol duration. However, for IR-UWB the situation is completely different, where the digital information is mapped into extremely short pulses. Therefore, only a small duration is exploited for communications, while only channel noise and interference is received in the remaining part of the symbol duration. Exploiting this feature the noise performance of IR-UWB receivers can be improved by matching the observation time period to the UWB pulse duration [176].

In general, recently, there is an increased interest from the research community in using an ED-type receiver for ranging and localization due to low-cost, low-power consumption, low-complexity and sub-sampling capabilities. Hence, in this thesis an ED receiver has been adopted for ranging/localization using IR-UWB over fiber for in-building network application.

6.5 Location Estimation Algorithm

Due to the limitations of the geometric approaches, statistical positioning techniques are employed in most practical cases [177]. For distance-based positioning algorithms, such as ToA or RSS based schemes, the maximum likelihood (ML) solution can be obtained by a nonlinear least-squares (N-LS) approach, under certain conditions [178]. The N-LS approach requires the minimization of a cost function that requires numerical search methods such as the steepest descent or the Gauss-Newton technique. Such techniques can have high computational complexity and they typically require good initialization in order to avoid converging to the local minima of the cost function [179]. Alternatively, a linear least-squares (L-LS) approach based on the measured distances is initially proposed in [180]. In the L-LS approach, the expression corresponding to one of the reference nodes is subtracted from all the other expressions in order to obtain linear relations in terms of the target node position. Various versions of the L-LS approach are studied in [181] and [182], which subtract different expressions or average of them from the remaining expressions. The L-LS approach is a suboptimal positioning technique, which provides a solution with low computational complexity. However, the accuracy of this kind of algorithms will tend to degrade as the target node moves away from base station assumed as reference [183]. Another approach of linearization technique is using a Taylor series expansion as it has been reported in [184]. A non-linear set of equations needs to be solved, to determine the position the target device can be expressed as:

$$\widetilde{d_i} = \sqrt{(x_i - x)^2 + (y_i - y)^2} \tag{6.10}$$

where $i = 1, 2, ...N$, N is the number of reference nodes in the measurement, (x_i, y_i) are the coordinates of the i^{th} radio access point, (x, y) are the unknown coordinates of the target device and $\widetilde{d_i}$ is the estimated range to the i^{th} radio access point. The set of non-linear equations is linearized using Taylor series expansion. After discarding all the higher order components we can obtain the following equation [184].

$$\widetilde{d} = f(x, y) = f(x_{10}) + \frac{\partial f}{\partial x}|_{x_{10}}(x - x_0) + \frac{\partial f}{\partial y}|_{x_{10}}(y - y_0) \tag{6.11}$$

where $x_{10} = (x_0, y_0)$ is the linearization point. It is chosen as the mean of the radio access point coordinates. $f(x_0, y_0)$ is the value of the non-linear function at the linearization point. $\frac{\partial f}{\partial x}|_{x_{10}}$ denotes the derivative of the function to $x$at x_{10}. Only the terms with x and y are unknown, thus the other terms are included in $\widetilde{d'}$ as represented in Eq. 6.14. The linearized equations are written in matrix form as:

$$A = \begin{pmatrix} \frac{\partial f_1}{\partial x}|_{x_{10}} & \frac{\partial f_1}{\partial y}|_{x_{10}} \\ \vdots & \vdots \\ \frac{\partial f_N}{\partial x}|_{x_{10}} & \frac{\partial f_N}{\partial y}|_{x_{10}} \end{pmatrix} \tag{6.12}$$

$$\widetilde{x_1} = \begin{pmatrix} \widetilde{x} \\ \widetilde{y} \end{pmatrix} \tag{6.13}$$

$$\widetilde{d'} = A\widetilde{x_1} \tag{6.14}$$

The weighted least squares (WLS) solution for the estimated coordinates, $\widetilde{x_1}$ is given by [184]:

$$\widetilde{x_1} = \left(A^T W A\right)^{-1} A^T W \widetilde{d'} \tag{6.15}$$

The weighting matrix $\mathbf{W}$ is a diagonal matrix with the element w_{ii}. The weights are given by $w_{ii} = \frac{1}{\sigma_{d,i}^2}$, $\sigma_{d,i}^2$ is the variance of the estimated distance at location i. $\sigma_{d,i}^2$ is calculated for every RAP of the calibration measurements. Note that the RAPs show different distances and the weights are related to the corresponding distances. On the other hand, the un-weighted LS approach is given by discarding the $\mathbf{W}$ matrix.

The estimated position coordinates at each iteration are used as a new linearization point [184]. This procedure is repeated until the estimated coordinates of the target device converge. Hence, in the following experimental demonstrations the above algorithm as reported in [184] has been adopted because it presents a good trade-off between accuracy and complexity compared to the other linearization techniques.

6.6 Ranging/Localization experiments

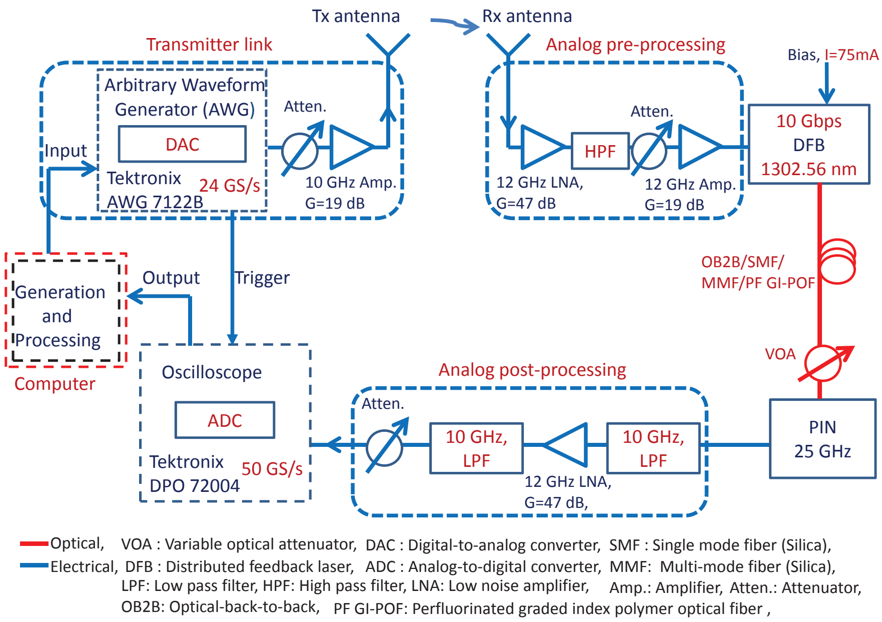

Figure 6.7: Experimental setup.

6.6.1 Experimental Setup

To realize ranging and localization using an IR-UWB over fiber system, the experimental setup depicted in Fig. 6.7 was employed. A personal computer (PC) was used for generating and processing the IR-UWB pulses. The pulses were sent to an arbitrary waveform generator (AWG) for electrical generation. The AWG was set to a sampling frequency of 24 GSamples/s, which was achieved by interleaving its two ports and enabling the large bandwidth option as described in Chapter 4. To meet the FCC-mask requirements, the novel pulse shaping technique, which is based on a linear combination of monocycles with different pulse shaping has been employed as described in Chapter 3 and reported in [83]. Then the generated pulses were amplified using a 10 GHz bandwidth with 19 dB gain amplifier (SHF 100 APP) before radiation. For transmission and reception of the IR-UWB pulses, a commercially available UWB antenna (Skycross SMT-3TO10M-A) at both transmitter and receiver ends was employed. To avoid any inter symbol interference (ISI) caused by multipath signals, a low pulse repetition frequency (PRF) of 5 MHz has been set at the transmitter side. After wireless transmission, the received pulses were amplified using a broadband low noise amplifier (LNA) of 47 dB gain. As shown in Fig. 6.7, a high pass filter (HPF) with cut-off frequency 2.6 GHz and a rejection ratio larger than 60 dB has been employed to minimize the interference caused by existing narrowband services. In addition, to achieve a better modulation depth of the optical carrier, a gain controlled 10 GHz amplifier with 19 dB gain was used after the HPF as shown in Fig. 6.7. As pointed out in Chapter 4, to reduce the cost of the overall optical system, direct modulation of a 10 GHz DFB laser at 1303.36 nm has been adopted. Relevant system parameters are optimized to avoid any distortions introduced by the optical link. Accordingly, the bias of the DFB was set to 75 mA. The modulated optical signal was carried through different types of fibers (SMF, MMF and PF GI-POF) with various lengths and was finally detected using a 25 GHz photo-detector (PD), which has a MMF pigtail with 50 μm core diameter. Furthermore, to avoid any saturation of the PD, the optical input power of the PD was limited only to -5 dBm. The detected signal was eventually post-processed to reduce the noise caused by the optical link as shown in Fig. 6.7. Finally, the received pulses have been acquired by a digital sampling scope (DPO) running at 50 GSamples/s and processed using offline processing using MATLAB at the PC.

Note that before any ranging and localization experiments, extensive simulations have been performed to understand the system parameters using the IEEE 802.15.4a UWB channel model. The results of these system simulations have been reported in [164]. After the simulation and before the actual experiment characterization of each component has been performed to understand the effects of each component. Then the overall system frequency response for different fiber types have been performed as shown in Fig. 6.8. In general, it was observed that the pulse shape of the IR-UWB pulse has changed due to the filtering effects shown in Fig. 6.8. However, given that the selected PRF was low these filtering effects did not cause significant distortion other than ringing of the pulse due to limited bandwidth especially for SI-MMF fibers.

6.6.2 Ranging Experimental Results

As mentioned above, to meet the FCC-mask requirements and simultaneously have higher effective bandwidth by effectively utilizing the available spectrum of IR-UWB from 3.1 – 10.6 GHz at -10 dB, a pulse shaping technique that is based on a linear combination of monocycles discussed in Chapter 3 and

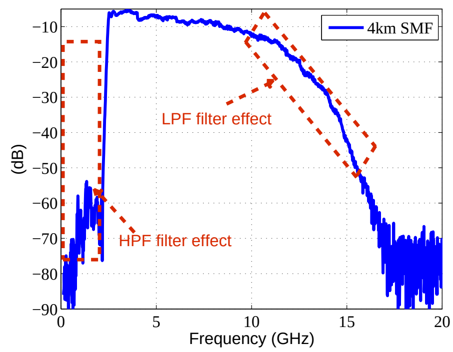

(a) SMF.

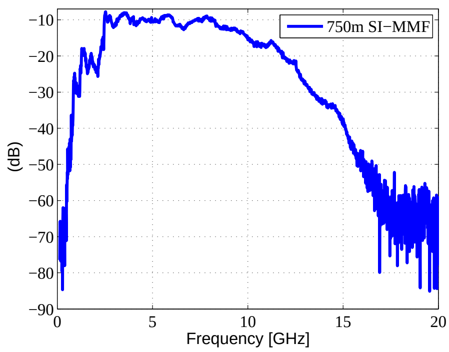

(b) SI-MMF.

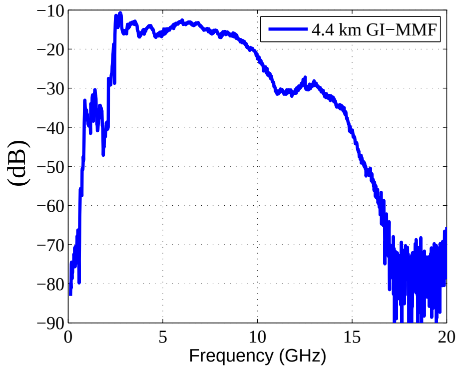

(c) GI-MMF.

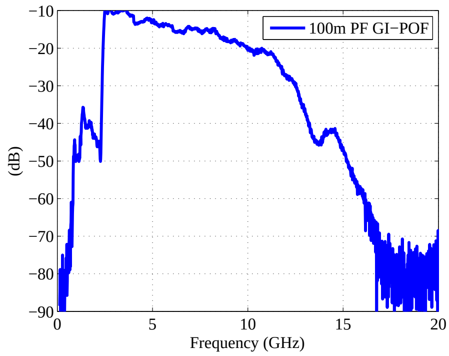

(d) PF GI-POF.

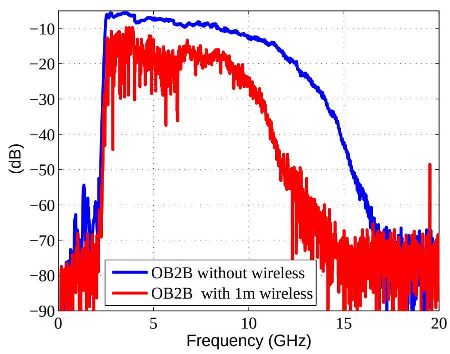

(e) OB2B.

Figure 6.8: System frequency response for different fiber types.

reported in [83] was employed. Note that a high effective bandwidth increases the accuracy of the ToA estimate as described in section 6.2.2 and shown in Eq. 6.5. For simplicity of the setup, a receiver architecture based on energy detector (ED) together with ToA ranging technique to process the received data was implemented. Furthermore, the parameters of the receiver such as integration window width, sampling frequency and threshold are chosen optimally to maximize the ranging accuracy. Accordingly, the effect of the integration window is shown in Fig. 6.9a. If the integration window is larger than needed, then the noise increases and also the leading edge of the first path becomes smoothed out, which introduce a bias to the delay estimation and hence the error increases. The optimal integration found in the measurement is comparable to the width of the pulse we transmitted (i.e., 400 ps) as shown in Fig. 6.9a. Note that a rectangular window has been employed with assumption that for LoS condition, the direct path is usually the strongest path. However, it should be noted that another type of window such as Hamming window which provide side-lobe -43 dB can be implemented especially for inverse filtering deconvolution purpose for characterizing the impulse response of the channel [185]. Note that finding the first path is a challenging task especially for UWB channels due to the fact that the strongest signal is not always the first arriving path [8]. Hence, an adaptive threshold, which considers the noise level and the peak of the signal, is used to detect the leading edge of the first path. The minimum normalized threshold for our measurement is found to be 0.6 as shown in Fig. 6.9b. The sub-sampling frequency capability of ED was investigated as shown in Fig. 6.9c. Note that a sampling frequency of at least 2 GHz is feasible for IR-UWB ranging technique with a root-mean-square error (RMSE) of less than 4 cm. For other channel scenarios, these optimal values could vary due to multipath reflections and external interferences.

After optimizing the parameters for ED-based ToA ranging technique, we perform characterization of different fibers with various lengths. During the measurements, the wireless range between transmitter and receiver is varied from 1 m to 5 m. In each range measurement, 20 points have been considered for each distance, and the separation between the points was fixed to 10 cm. In addition, in each point, 200 realizations have been acquired for averaging purpose. The collected measurement results were averaged to reduce noise effects. The signal was transmitted over PF GI-POF, in addition, measurements over SMF, SI-MMF and GI-MMF were conducted for comparison. Note that for all the measurements processing is done after ensuring direct LoS condition between transmitter and receiver, static environment(with out

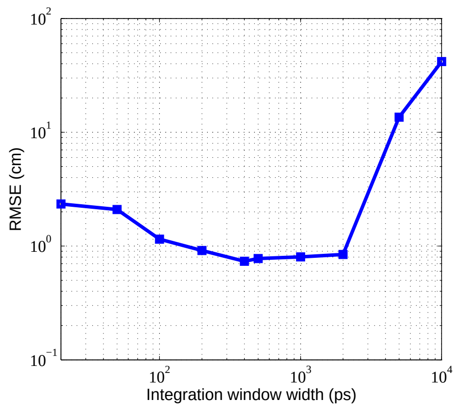

(a) Integration window.

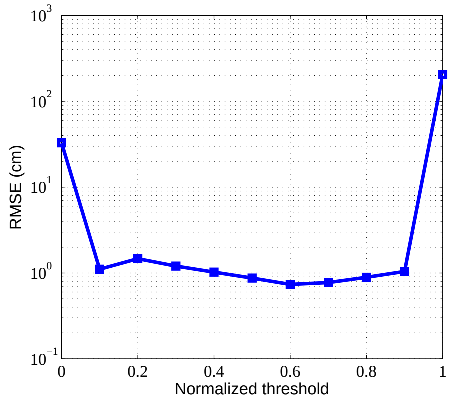

(b) Threshold.

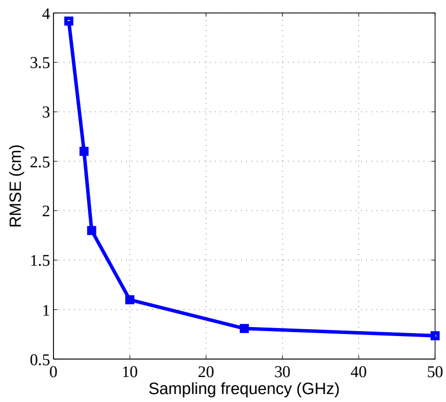

(c) Sampling frequency of received signal.

Figure 6.9: Effect of receiver parameters.

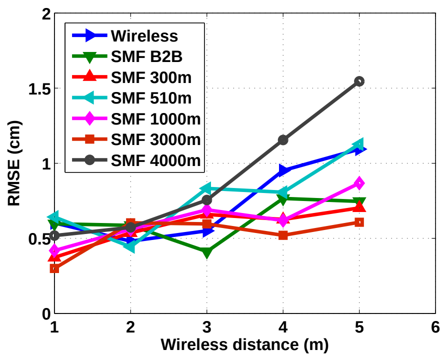

(a) RMSE versus wireless distance.

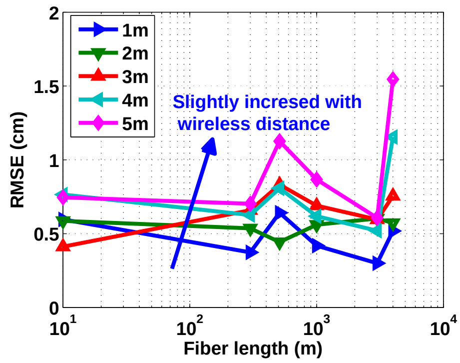

(b) RMSE versus fiber length of SMF.

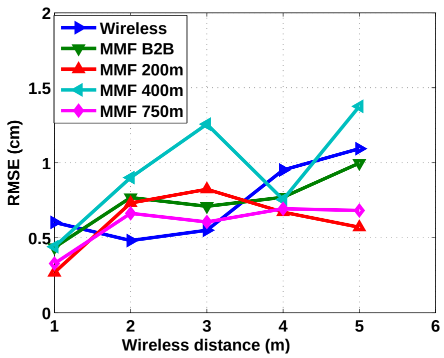

(c) RMSE versus wireless distance.

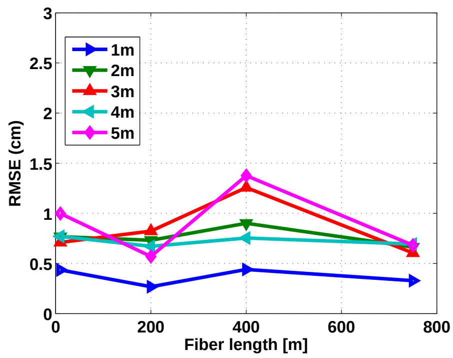

(d) RMSE versus fiber length of SI-MMF.

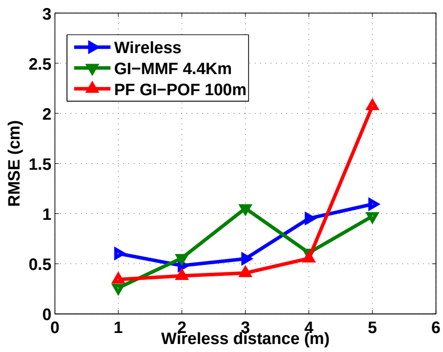

(e) GI-POF and GI-MMF.

Figure 6.10: Achieved ranging accuracy of IR-UWB over different types of fiber.

any movement during measurement) and calibration to all measurements once at distance of 1 m. This scenario has been deliberately selected to avoid any error induced by the channel and triggering. This helps us to understand and isolate the errors introduced by the optical system. Furthermore, all measurements considered the wireless link with optical back-to-back case as reference for evaluating the effect of the fibers. The RMSE of the experimental results is shown in Fig. 6.10. RMSE of less than 2.5 cm is achieved for all types of fiber as shown in Fig. 6.10. However, a random error variation was observed in the multimode fibers both silica and PF GI-POF as shown in Fig. 6.10c and 6.10e. These random variations are caused by the combined effect of modal noise and measurement errors. However, in these all curves, there is a slight increase in the error with respect to the wireless distance, which is attributed by the decrease in SNR as the path loss increases with wireless distance as shown explicitly in Eq. 6.5. In fact, for fixed bandwidth systems, the SNR decrease leads to an increase in error from the theoretical view of CRLB for ToA ranging techniques [8].

6.6.3 Localization Experimental Results

To study the impact of fiber on localization accuracy, all the measurements were performed in a typical office room under line-of-sight (LOS) condition with a rectangular grid of 4 m by 3 m representing the receiver and transmitter positions as shown in Fig. 6.11a. To emulate the four corners of the room ceiling and increased accuracy; the four receivers were chosen and placed each in a corner of the grid. The transmitter moved within the rectangular grid at predefined positions as shown in Fig. 6.11 respectively. A total of 28 points were considered as a position for transmitter antenna as shown in Fig. 6.11. At each point, 200 measurements were collected and processed offline to estimate the position of the transmitter. The collected data have been processed using a two-step processing approach as described above. As a first step, parameter estimation of ToA of the first direct path has been performed using energy detector (ED) based receiver architecture. This receiver architecture has been chosen due to its attractive features: low power consumption, low complexity, and hence low cost. Furthermore, it allows a moderate sampling frequency compared to other type of receiver architectures as described above and shown in Fig. 6.9c. In the second stage, four ToA estimates were combined and hence final position estimation has been carried out using a weighted linear least square (WLLS) estimation algorithm as described in section 6.5. Based on the results observed in Fig. 6.11, the position of the transmitter is estimated

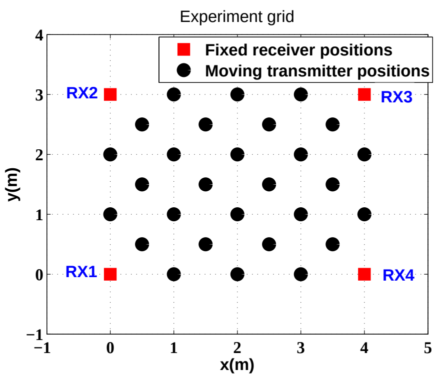

(a) Experimental grid.

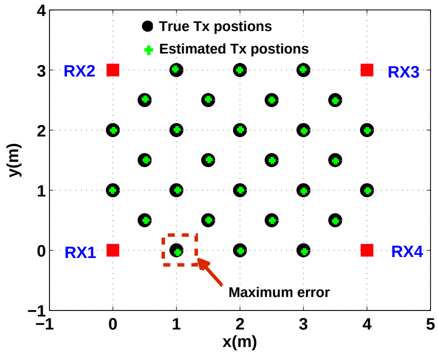

(b) wireless link only.

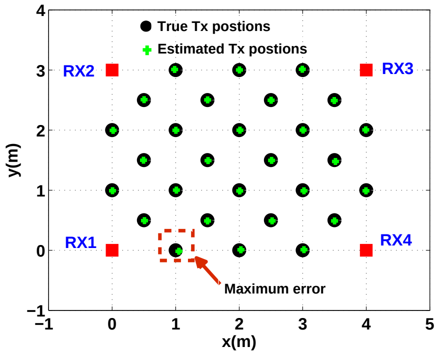

(c) SMF back-to-back case.

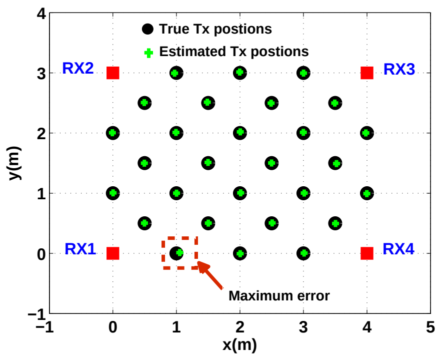

(d) 1km-SMF case.

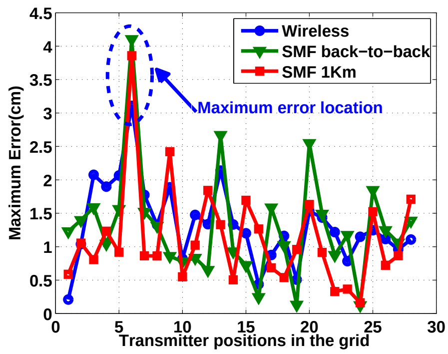

(e) Estimated maximum error.

Figure 6.11: Overview of localization results.

with a high accuracy for the wireless link only and for wireless including 1 km SMF, respectively. The maximum error found at each point in the grid shown in Fig. 6.11d. This high accuracy is achieved due to the combined effect of high bandwidth IR-UWB pulses. ToA based ranging technique, short wireless/fiber links and negligible chromatic dispersion of fiber at 1300 nm. The maximum location error is just 4 cm for the considered rectangular grid. However, the magnitude of this error was found to be dependent on its ambient condition. In general, the achieved accuracy indicates that IR-UWB over fiber is an attractive technology for localization of mobile stations in an in-door environment.

6.7 Summary

In this chapter, an overview of radio ranging techniques have been discussed. In addition, an overview of the UWB channel model, receiver architecture and localization algorithm used in the simulation and experimental demonstrations have been presented. Then the effects of different types of fibers for a ranging and localization system using IR-UWB over fiber technology has been investigated after component and system level characterizations. The experimental results achieved for both glass and plastic optical fibers have been presented. Then localization results using $1km$ SMF have been discussed. All the ranging and localization has been performed by using the TOA concept in which high time resolution is obtained by the narrow pulses of the novel IR-UWB pulses proposed in Chapter 3. Based on the experimental results, the use of 1300-nm wavelength together with short fiber links show insignificant impact on the performance of IR-UWB over fiber ranging/localization systems. Based on the achieved results, IR-UWB over fiber technology has the potential of providing accurate localization for realizing an energy-efficient integrated hybrid optical/wireless communication network for home and in-building scenarios.

Chapter 7

Conclusion and Recommendations

7.1 Conclusion

As discussed in this thesis, the recent years have been characterized by continuously increasing mobile data traffic driven by growing penetration of mobile internet and video via smart phone, tablets, laptops and notebooks. To cope with this data deluge and eventually satisfy the demand of end users, we are witnessing several novel technology trends in the access, in-building and in-home networks. Some of the very clear trends, which lead to high capacity networks are: 1) optical fiber with its super-efficient capacity and transparency is starting to penetrate into the home 2) converged integration of wired and wireless delivery of multi-standard/multi-services is attracting much attention, 3) advanced modulation/coding formats for high spectral and power efficiency are becoming commonly employed, 4) advanced antenna techniques (such as MIMO and beam forming and steering) are also emerging, 5) unlicensed high bandwidth spectrum is becoming important (such as UWB, 60 GHz and wireless optics), 6) low-cost, energy-efficient, context-aware (location-aware) and dynamically routed networks are receiving more interest. All these novel trends together with a single shared optical infrastructure can bring low-cost and energy-efficient solutions for access and in-home/in-building networks in order to provide high capacity, high coverage, mobility, flexibility and reliability for broadband communication and sensor network applications.

On the other hand, to provide high capacity wireless access, the coverage area of radio cells needs to become smaller and smaller. However, this approach requires several hundreds of radio access points to be deployed within a building. All in all, cost-effectiveness, centralization of complex functions and sharing of wireless resources in a dynamic way is becoming crucial. Accordingly, radio-over-fiber (RoF) has been proposed and is playing a crucial role in fiber distributed antenna systems. In addition, the need for accurate indoor positioning in emerging fields such as wireless sensor networks, healthcare, logistics, location-based services, automation, gaming entertainment has driven the attention towards alternative technologies able to overcome the indoor positioning bottleneck. Hence, an unlicensed IR-UWB over fiber has been recognized as an ideal candidate for both communication and sensor networks due to its unique spectral characteristics and the huge signal bandwidth, which localization by IR-UWB makes robust to the challenging indoor propagation conditions.

Therefore, this thesis has focused on IR-UWB over fiber technology for broadband in-building network application. However, one of the key challenges of IR-UWB systems is to meet the FCC-mask requirements with high spectral power efficiency. Hence, in this thesis, a new and novel concept of pulse shaping/generation techniques has been investigated based on simulations and numerous experimental demonstrations. The proposed concepts aim on exploiting existing conventional pulses to make new pulse shape out them, so that the new pulse has many advantageous such as better compliance to indoor FCC emission mask, low complexity, better spectral power efficiency and better wireless coverage than conventional pulses themselves as well as the well-known fifth order derivative of Gaussian pulse. Moreover, a comparison of wireless link power budget of the widely used pulses and the proposed pulses has been performed using realistic assumptions for the path loss model. Based on the simulation results, the proposed pulse outperforms the most commonly used pulses in terms of spectral power efficiency and reach in the wireless link. Another challenge: reach extension. In addition, the simulation results showed that the expected wireless reach for high data rate (> 1 Gb/s) of IR-UWB systems was limited (< 4m). This is one of the reasons why the novel pulse shaping techniques as well as IR-UWB over fiber systems techniques are required for reach extension needed for connecting different WPANs. To reduce complexity and thus cost, a simple and novel optical generation based on the principles of microwave photonic delay line with negative coefficient has been proposed and experimentally demonstrated. Note that the proposed scheme has the capability to be further simplified by photonic integration, which would meet the practical requirements of small size, low-cost and high reliability of IR-UWB communication in short-range applications such as in-building networks.

After shaping, generation and performance evaluation of the proposed pulses, multi-Gigabit/s transmission of IR-UWB over different types of fibers has been investigated for access, in-building and in-home network applications respectively. Accordingly, this thesis has experimentally demonstrated a FEC-limited error-free transmission of 2 Gb/s IR-UWB over 25 km single mode fiber (SMF-28), 4.4 km graded index multi-mode fiber (GI-MMF) and 100 m perfluorinated graded index polymer optical fiber(PF GI-POF). To further reduce the cost of the system, direct modulation of the light source and intensity detection at the receiver has been employed. All these demonstrations show reach extension of high-speed IR-UWB transmission over several orders of magnitude. Furthermore, by centralizing complex functions of shaping, generation and modulation/demodulation in a single station such as within a residential gateway as in the case of in-building (or central office in the case of access networks) low-cost, high capacity and energy-efficient IR-UWB over systems are possible.

To effectively use the optical infrastructure and finally reduce cost of the overall system, an integration of wired baseband data and wireless IR-UWB signals over a single in-building optical network has been investigated. This sharing of a single optical carrier in a shared optical medium has been possible by exploiting the low frequency (DC- 2 GHz)components of the novel IR-UWB pulses. Furthermore, flexible routing of an integrated 2 Gb/s wireless IR-UWB signal and 1.25 Gb/s wired baseband signal using cross-gain modulation (XGM) in a single SOA has been experimentally demonstrated. Therefore, successful routing of three channels has been experimentally achieved at FEC error-free limit for wireless 2 Gb/s IR-UWB data and a BER of 10^{-9} for 1.25 Gb/s baseband data. Note that increasing the transmission capacity of the wired baseband data is feasible using a FEC-limited, optimized low-pass filter and advanced modulation techniques (e.g., discrete multitone (DMT)). In short, the achieved experimental results can be considered as proof-of-principle towards a single infrastructure of integrated wired/wirless services and dynamic routing capability for future in-building networks.

Finally, an attractive ranging/localization technique that makes use of IR-UWB over fiber has been experimentally demonstrated. Utilizing the narrow pulse width of the UWB signals and employing the time-of-arrival ranging technique together with the weighted linear least square estimation algorithm, a cm-level accuracy has been achieved in a rectangular grid of 4 m by 3 m.

Moreover, based on the experimental results using different types of fibers typically for optical in-house/inbuilding networks such as SMF, MMF and PF GI-POF showed no significant impact on the achievable accuracy. In addition, a low cost, low complexity and moderate sampling rate (around 2 GHz) capability of energy detector type receiver did not induce a dramatic increase in the localization error. This is a proof-of-concept demonstration showing that a single in-building fiber network is suitable for sensor network application without significant degradation on the achievable accuracy of indoor ranging/localization techniques.

In general, with all the theoretical and experimental results investigated in this thesis, IR-UWB over fiber technology has the potential of providing medium to high speed wireless data transfer and accurate ranging/localization capability for realizing high capacity,low-cost,energy-efficient and integrated hybrid optical/wireless communication network for smart home/in-building network applications

7.2 Recommendations

As described throughout the thesis, all the experimental work was based on off-line processing. Hence, for real-time applications with reasonable cost and better performance, the following future research topics are recommended:

1. *Component and Transceivers*: To further reduce the cost and power consumption of the system, generation of IR-UWB pulse should be integrated either on optical chips or CMOS chips. Hence, integration of IR-UWB pulse generator is first recommended. The cost of the optical components such as light source can be further reduced using VCSELs. Furthermore, developing low-cost broadband components such as on-chip broadband antenna (with flat gain and linear phase), broadband filters, broadband LNAs and diplexers are recommended as future work.

2. *System-level Transmission*: Multi-Gb/s transmission of IR-UWB over different types of fibers (SMF, MMF and PF GI-POF) was carried out. However, wireless link demonstration should be the next step. It should be noted that the multi-Gigabit/s transmission demonstration was possible due to high bandwidth of fiber and lack of multipath reflections. However, the wireless link could finally limit the achievable data rate. Hence, this work should be extended to study the effect of the wireless channel under different scenarios such as LOS and NLOS conditions. As

ultimate solution, it should be extended to bi-directional wireless data rate transmission for real-time interactive services.

3. *Modulation and Multiple Access Inferences*: In this thesis most of the experimental demonstrations were based on OOK modulation format. However, there are of course other modulation formats possible that can be used to increase the performance of the IR-UWB systems described in the thesis. With some additional complexity on the receiver side, the bi-phase modulation format can be recommended for future work. Furthermore, supporting multiple users and effect of multiple access interference on the performance of the system should be investigated.

4. *Multiple Service and Multi-standard Transmissions* : In this thesis, as a first step, integration of wired baseband data and wireless IR-UWB data was carried out. This can be extended to multi-standard transmission by converging different wireless standards in single in-building optical infrastructure. By using appropriate components such as single or multiple broadband antennas, LNAs, filters and diplexers, integration of LTE, WiFi, IR-UWB and 60 GHz over single optical infrastructure is recommended. This can be realized using either frequency division (up/down-conversion techniques) in the electrical domain or wavelength division multiplexing in the optical domain. This final integration will lead to a highly flexible converged optical infrastructure for broadband communication and sensor network applications.

5. *Application Areas*: In this thesis, as proof-of-concept, the application of IR-UWB for communication and localization was demonstrated. With aim of realizing a smart in-building network, this work needs to be further extended to real-time communication and localization through extensive measurements for wireless channel modeling including NLOS conditions. This work can also be extend further towards beam-forming of IR-UWB signals over fiber for capacity and energy-efficient networks.

6. *Regulation and Standardization Efforts*: It should be clear that without the support of industries to standardize and produce harmonized regulations, the future of IR-UWB over fiber technology is blurred. Hence, single harmonized regulation and support from industry is needed.

.

Appendix A

Overview of IR-UWB modulation schemes

A regular IR-UWB pulse train contains no information and produces energy spikes. In order to transmit information, the IR-UWB pulse train needs to be encoded by data. Information can be encoded in a number of ways, including amplitude, time and phase modulation of the IR-UWB pulses [97]. Note that the modulation needs to reduce energy spikes, thereby satisfy the FCC-mask with better spectral utilization. In addition, the choice of the modulation scheme affects the bit error performance. The most popular modulation schemes developed to date for IR-UWB are described in the following.

Pulse Amplitude Modulation (PAM)

In PAM, a given waveform is sent with different amplitudes corresponding to different data being transmitted [87, 186].The basic PAM signal, composed of a stream of modulated pulses, is given by :

$$y_{PAM}(t) = \sum_{j} A_j x(t - jT_f); \tag{A.1}$$

where $x(t)$ is can be any desired IR-UWB pulse shape such as: monocycle, doublet pulse, 5^{th} order Gaussian derivative and even the proposed pulses in Chapter 3. A_j is the amplitude of the j^{th} pulse corresponding to the symbol represented. More than two amplitude levels can be used to encode more than one bit per symbol [87].

Biphase Modulation (BPM)

In biphase modulation, information is encoded with polarity of the pulses. In other words, the polarity of the IR-UWB pulses is switched to encode a "0" or "1". In this case, only one bit per IR-UWB pulse can be encoded because there are only two polarities available to choose from [87]. Hence, the model for bi-phase is given by:

$$y_{BPM}(t) = \sum_j a_j x(t - jT_f); \tag{A.2}$$

We may have the optimal antipodal case by making, for instance, $a_j = -1$ representing bit "0" and $a_j = +1$ representing bit "1". T_f is the frame duration or pulse-repetition time. In this antipodal case, detection may be performed by a single correlator using as template signal a normalized-energy pulse $x(t)$, which will result in correlation values equal to -1 or $+1$. Its theoretical performance over additive white Gaussian (AWG) channels is the standard performance for antipodal signal [15].

$$P_{b_{antipodal}} = Q\left(\sqrt{2\frac{e_b}{N_0}}\right) \tag{A.3}$$

where $Q(.)$ is the complementary error function.

On-Off Keying (OOK)

This is the simplest form of pulse modulation, in which the transmission of a pulse represents a data bit "1" and its absence represent a data bit "0". The general signal model for OOK is given by [16]:

$$y_{OOK}(t) = \sum_j a_j x(t - jT_f) \tag{A.4}$$

where again a_j is the amplitude of the pulse which can have the values 1 or 0 and T_f is the frame duration.

Pulse Position Modulation (PPM)

PPM is based on the principle of encoding information with two or more positions in time, referred to the nominal pulse position [87]. A pulse transmitted at the nominal position represents a "0" and a pulse transmitted after nominal position with some delay represents "1". Additional positions can be used to provide more bits per symbol. The time delay between positions is typically a fraction of a nanosecond, while the time between nominal positions is typically much longer to avoid interference between the pulses. This type of modulation is the most preferably used modulation because it smoothes the spectrum of the IR-UWB signal [16]. In general, in the PPM, each data symbol is represented by a particular delay in the transmitted pulse. The modulated pulse stream becomes:

$$y_{PPM} = \sum_j x(t - jT_f - \tau_j) \tag{A.5}$$

where τ_j is the delay of the j^{th} pulse corresponding to the symbol represented. In a binary modulation, we have typically $\tau_j = 0$ representing bit "0", and $\tau_j = \delta$ representing bit "1", where $\delta \ll T_f$ is a time delay. Reception of a PMM binary signal can be made using a signal correlator with a special template waveform obtained from the sum of the two possible waveforms or shapes, one of them inverted and delayed by δ :

$$temp(t) = x(t) - x(t - \delta) \tag{A.6}$$

Optimizing δ for minimum (most negative) cross-correlation between the two waveforms, we can achieve positive values at the correlator output for the zero-delayed pulses and negative values for δ-delayed pulses. This maximizes the distance between signals for binary PPM with IR-UWB pulses. The theoretical performance of generic pulses with cross-correlation value r in the presence of white Gaussian noise is [186]:

$$P_{b_{PPM}} = Q\left(\sqrt{(1-r)\frac{e_b}{N_0}}\right) \tag{A.7}$$

M-ary PPM scheme use M different delays to represent the symbols. The choice of these delays is critical, and must be judiciously made.

Pulse Shape Modulation (PSM)

The original idea of PSM consists of an orthogonal binary modulation, where two orthogonal pulses or waveforms are used to represent the data bits. The reception, based on signal correlation, benefit from the time-orthogonality between the waveforms used. The conventional pulses of monocycle and doublet have such property, related to the fact of being, respectively, odd and even time functions. The resulting modulated pulse stream is given by:

$$y_{PSM} = \sum_j x_j(t - j) \tag{A.8}$$

where $x_j(t)$ is the appropriate waveform associated with the j^{th} pulse chosen, depending on the data content. The theoretical performance of binary orthogonal PSM for any set of orthogonal signals in AWG channels is given by:

$$P_{b_{PSM}} = Q\left(\sqrt{\frac{e_b}{N_0}}\right) \tag{A.9}$$

For M-ary orthogonal PSM schemes, we need to use pulse waveforms which are all orthogonal to each other such as modified Hermite functions [15, 16]. Note that, in principle, it is possible to combine different modulation formats. One example is combining the PAM and PPM so that the data is modulated both in the amplitude as well as the delay of the IR-UWB pulses. Therefore, with this type scheme a higher data rate can be achieved. In general, the choice of the modulation format depends on the application, desired performance and complexity of the transceivers.

ACRONYMS

A/D	Analog-to-digital
ALPHA	Architecture for fLexible Photonic Home and Access networks (FP7 project)
AMPS	Advanced mobile phone system
AOA	Angle of arrival
AON	Active optical network
ASE	Amplified spontaneous emission
AWG	Arbitrary waveform generator
AWGN	Additive white Gaussian noise
BB	Base band
B2B	Back-to-back
BER	Bit error ratio
BERT	Bit-error-rate tester
BPD	Balanced photodetector
BPF	Band-pass filter
BPM	Binary phase modulation or Bi-phase modulation
BS	Base-station
BW	Bandwidth
CAT-5	Catalogue 5(cable)
CATV	Cable television
CDMA	Code division multiple access
CMOS	Complementary metal-oxide-semiconductor
CO	Central office
CW	Continuous wave
CWDM	Coarse wavelength division multiplexing
DAA	Detect-and-avoid
D/A	Digital-to-analog
DAS	Distributed antenna system
DC	Direct current

DFB	Distributed feedback (laser)
DIY	Do-it-yourself
DMT	Discrete multi-tone
DMUX	Demultiplexer
DoD	Department of Defense
DPO	Digital phosphor oscilloscopes
DSB	Double side band
DSL	Digital subscriber line
DSP	Digital signal processing
DSSS	Direct sequence spread spectrum
DVD	Digital video disc
DWDM	Dense wavelength division multiplexing
EAM	Electro-absorption modulators
EAT	Electro-absorption transceiver
EC	Electrical circulator
ECMA	European computer manufacturers association
ED	Energy detector
EDFA	Erbium doped fiber amplifier
EOM	Electro-optic modulator
E/O	Electrical to optical
EIRP	Effective isotropic radiated power
EU	European Union
EVM	Error vector magnitude
FBG	Fiber Bragg grating
FCC	Federal Communications Commission
FDM	Frequency division multiplexing
FEC	Forward error correction
FFT	Fast Fourier transform
FIR	Fine impulse response
FM-IM	Frequency modulation to intensity modulation
FP7	Seventh framework program (of European Commission)
FSR	Free spectral range
FTTH	Fibre to the home
FTTP	Fiber to the premises
FWA	Fixed wireless access
FWM	Four wave mixing
GI-MMF	Graded-index multimode fiber
GI-POF	Graded-index plastic optical fibre

GPR	Ground penetrating radar
GPS	Global positioning system
GSM	Global system for mobile communications
HFC	Hybrid fiber coax
HDTV	High definition televison
HPF	High pass filter
HSPA	High speed packet access
ICT	Information and communication technology
IEEE	Institute of electrical and electronics engineers
IF	Intermediate frequency
IFFT	Inverse Fourier transform
IM	Intensity modulation
IM/DD	Intensity modulation and direct detection
IPTV	Internet protocol television
IR	Impulse radio
IrDA	Infrared data association
IR-UWB	Impulse radio ultra-wideband
ISI	Inter-symbol interference
LAN	Local area network
LD	Laser diode
LED	Light emitting diode
LMDS	Local multi-point distribution service
LNA	Low noise amplifier
LO	Local oscillator
LoS	Line-of-sight
LPF	Low pass filter
LTE	Long term evolution
LTE-Adv	Long term evolution advanced
NLOS	Non-line-of-sight
MB-OFDM	Multi-band orthogonal frequency division multiplexing
MC-POF	Multi-core plastic optical fibre
MC-UWB	Multi carrier ultra wideband
MB-UWB	Multi band ultra wideband
MIMO	Multiple-input multiple-output
M2M	Machine-to-machine
MMF	Multi-mode fibre
MOST	Multimedia-oriented system transport
MPC	Multipath component

MP2MP	Multipoint-multipoint
MUX	Multiplexer
MZI	Mach-Zehnder interferometer
MZM	Mach-Zehnder modulator
NA	Numerical aperture
NESP	Normalized effective signal power
NRZ	Non-return-to-zero
OBPF	Optical bandpass filter
OC	Optical circulator
ODSB	Optical double sideband
O/E	Optical to electrical
OEO	opt-electrical-optical
OFDM	Orthogonal frequency division multiplexing
OFM	Optical frequency multiplication
OPLL	Optical phase lock loop
PAM	Pulse amplitude modulation
PAN	Personal area network
PD	Photo-detector
PDA	Personal digital assistant
PF	Perfluorinated
PF GI-POF	Perfluorinated graded index plastic optical fiber
PHY	Physical layer
P-I	Power-current
PIN	Positive-intrinsic-negative(p-type intrinsic n-type)
PL	Path loss
PLC	Power line communication
PM	Phase modulation
PM-IM	Phase modulation to intensity modulation
PMMA	Poly-methyl-methacrylate
POF	Plastic optical fibre
PPM	Pulse position modulation
P2P	Point-to-point
P2MP	Point-to-multipoint
PRI	Pulse repetition interval
PRBS	Pseudo random binary sequence
PON	Passive optical network
PSD	Power spectral density
PSM	Pulse shape modulation

QAM	Quadrature amplitude modulation
RAU	Remote antenna unit
RF	Radio frequency
RFID	Radio frequency identification
RG	Residential gateway
RoF	Radio-over-fibre
RSS	Received signal strength
SCM	Sub-carrier multiplexing
SI-MMF	Step-index multimode fiber
SI-POF	Step-index plastic optical fibre
SMF	Single-mode fibre
SNR	Signal-to-noise ratio
SOA	Semiconductor optical amplifer
SSB	Single-side band
TDM	Time division multiplexing
TDMA	Time division multiple access
TDOA	Time difference of arrival
TFC	Time-frequency code
TH	Time hopping
TOA	Time of arrival
UMTS	Universal mobile telecommunication system
USB	Universal serial bus
UTP	Unshielded twisted pair
UWB	Ultra-wideband
VCSEL	Vertical cavity surface emitting laser
VoIP	Voice over internet protocol
VSA	Vector signal analyser
VSG	Vector signal generator
WBAN	Wireless body area networks
W-CDMA	Wideband code division multiple access
WDM	Wavelength division multiplexing
WDM-PON	Wavelength division multiplexed passive optical network
WiFi	Wireless fidelity (local area networks)
WiMax	Worldwide interoperability for microwave access
WLAN	Wireless local area network
WMAN	Wireless metropolitan area network
WP	Workpackage
WPAN	Wireless personal area network

WWAN	Wireless wide area network
XGM	Cross-gain modulation
XPM	cross-phase modulation
XPolM	Cross-polarization modulation

BIBLIOGRAPY

[1] M. Jacobsson, I. Niemegeers, and S. H. d. Groot, *Pesonal Networks: Wireless Networking for Personal Devices.* Jhon Wiley & Sons, Ltd, 2010.

[2] A. Ng'oma, H. Yang, and J. George, "Integrated fiber-wireless networks: What, Why and How," in *AFRICON*, pp. 1–6, Sept. 2011.

[3] "White paper: Cisco visual networking index: Global mobile data traffic forecast update, 2011-2016," Feb. 2012.

[4] K. David, S. Dixit, and N. Jefferies, "2020 Vision The Wireless World Research Forum looks to the Future," *IEEE Trans. Veh. Technol. Mag.*, vol. 5, pp. 22–29, Sept. 2010.

[5] R. Bendlin, T. Ekpenyoung, and D. Greenstrret, "White paper: Paving the path for wireless capcity expansion," Feb. 2012.

[6] M. Maier and N. Ghazisaidi, *FiWi Access Networks.* Cambridge University Press, 2012.

[7] J. Foerster, E. Green, S. Somayazulu, and D. Leeper, "Ultra-wideband technology for short- or medium-range wireless communications," in *Intel Technol. J.*, pp. 1–11, 2nd quarter 2001.

[8] Z. Sahinoglu, S. Gezici, and I. Guvenc, *Ultra-wideband Positioning Systems: Theoretical Limits,ranging algorithms,and protocols.* Cambridge University Press, 2008.

[9] C. C. Chong, F. Watanabe, and H. Inamura, "Potentials of UWB technology for the Next Generation Wirelss Communications," in *IEEE Int. Symp. on Spread Spectrum Techn. and Appl.*, pp. 422–429, Aug. 2006.

[10] S. Gezici and H. V. Poor, "Position Estimation via Ultra-wideband signals," *Proc. IEEE*, vol. 97, pp. 386–403, Feb. 2009.

[11] A. Yarovoy, "Ultra-wideband systems," in *European Microw. Conference*, pp. 597–600, Oct. 2003.

[12] J. R. Fernandes and D. Wentzloff, "Recent advances in IR-UWB transceivers: An overview," in *IEEE Int. Symp. Cicuits and Syst.*, pp. 3284–3287, June 2010.

[13] M. G. Di Benedetto and G. Giancola, *Understanding Ulta Wideband Radio Fundmantals.* Pearson Education, Inc., USA, 2004.

[14] F. Nekoogar, *Ultra Wideband communications Fundamentals and Applications.* Prentice Hall, 2005.

[15] M. Ghavami, L. B. Michael, and R. Kohno, *Ultra Wideband signals and systems in communication engineering.* John Wiley and Sons, Ltd, 2007.

[16] H. Nikookar and R. Prasad, *Introduction to Ultra Wideband for Wireless Communications.* Springer, 2009.

[17] R. S. Kshetrimayum, "An introduction to UWB communication systems," *IEEE Potentials*, vol. 28, pp. 9–13, Mar. 2009.

[18] S. Gezici, "A survey on wireless position estimation," *Proc. IEEE*, vol. 44, pp. 263–282, Feb. 2008.

[19] X. Chen, S. Xu, H. Yin, and W. Wang, "Potentials of IR-UWB technology for ubiquitous computing," in *Wirelss Commun. Networking and Computing (WiCom)*, pp. 1–6, Sept. 2009.

[20] I. Oppermann, M. Hamalainen, and J. Linatti, *UWB theory and applications.* John Wiley and Sons, Ltd, 2004.

[21] S. T. Abraha, C. Okonkwo, P. A. Gamage, E. Tangdiongga, and T. Koonen, "Routing of power effecient IR-UWB wireless and wired services for in-building networks application," *J. Lightw. Technol.*, vol. 30, pp. 1651–1663, June 2012.

[22] C. Lim, A. Nirmalathas, M. Bakaul, P. Gamage, K. Lee, Y. Yang, D. Novak, and R. Waterhouse, "Fiber-Wireless networks and subystems technologies," *J. Lightw. Technol.*, vol. 28, pp. 390–405, Feb. 2010.

[23] J. Yao, "A Tutorial on Microwave Photonics," *IEEE Photonic Society Newsletter*, vol. 26, pp. 4–12, Apr. 2012.

[24] J. Capmany, B. Ortega, D. Pastor, and S. Sales, "Discrete-time optical processing of microwave signals," *LT*, vol. 23, pp. 702–723, Feb. 2005.

[25] J. Capmany, B. Ortega, and D. Pastor, "A tutorial on microwave photonic filters," *LT*, vol. 24, pp. 201–229, Jan. 2006.

[26] R. A. Minasian, "Photonic signal processing of microwave signals," *TIT*, vol. 54, pp. 832–846, Feb 2006.

[27] T. Berceli and P. Herczfeld, "Microwave photonics-a historical perspective," *Microwave Theory and Techniques, IEEE Transactions on*, vol. 58, pp. 2992–3000, Nov. 2010.

[28] M. G. Larrode, *Radio over Fiber Distributed Antenna systems for in-building broadband wireless services*. PhD thesis, Eindhoven University of Technology, The Netherlands, Mar. 2008.

[29] A. Ng'oma, *Radio over Fiber technology for broadband wireless communication systems*. PhD thesis, Eindhoven University of Technology, The Netherlands, June 2005.

[30] A. Koonen and L. Garcia, "Radio-over-MMF Techniques-Part II: Microwave to Millimeter-Wave Systems," *J. Lightw. Technol.*, vol. 26, pp. 2396 –2408, Aug. 2008.

[31] N. Mohamed, S. M. Idrus, and A. B. Mohammad, "Review on systems architectures for millimetr-wave generation techniques for RoF communication links," in *IEEE Int. RF and Microw. Conference*, pp. 326–330, Dec. 2008.

[32] J. Yao, F. Zeng, and Q. Wang, "Photonic generation of ultra-wideband signals," *J. Lightw. Technol.*, vol. 43, pp. 3219–3235, Nov. 2007.

[33] J. Yao, "Photonics for ultrawideband communications," *IEEE Microw. Mag.*, vol. 10, pp. 82–95, June 2009.

[34] F. Zeng and J. Yao, "An approach to ultrawideband pulse generation and distribution over optical fiber," *IEEE Photon. Technol. Lett.*, vol. 18, pp. 823–825, Apr. 2006.

[35] F. Zeng and J. Yao, "Optical generation and distribution of UWB signals," in *Annual Meetings of the IEEE Lasers Electro-optics Society (LEOS)*, pp. 454–455, Oct. 2006.

[36] F. Zeng and J. Yao, "Ultra-wideabnd impulse radio signals generation using a high-speed electrooptic phase modulator and a fiber-bragg-grating based frequency discriminator," *IEEE Photon. Technol. Lett.*, vol. 18, pp. 2062–2064, Oct. 2006.

[37] F. Zeng, Q. Wang, and J. Yao, "An approach to all-optical UWB pulse generation," in *Int. Topical Meeting on Microw. Photonics (MWP)*, pp. 1–4, Oct. 2006.

[38] F. Zeng, Q. Wang, and J. Yao, "All optical UWB impulse generation based on cross-phase modulation and frequency discrimination," *Electron. Lett.*, vol. 43, pp. 121–122, Jan. 2007.

[39] J. Dong, X. Zhang, J. Xu, and D. Huang, "Ultrawideband monocycle generation using cross-phase modulation in a semiconductor optical amplifiers," *Opt. Lett.*, vol. 32, pp. 1223–1225, May 2007.

[40] F. Liu, T. Wang, Z. Zhang, M. Qiu, and Y. Su, "On-chip photonic generation of ultrawideband monocycle pulses," *Electron. Lett.*, vol. 45, pp. 1247–1249, Nov. 2009.

[41] Q. Wang and J. Yao, "Ultra-wideband gaussian monocycle and doublet pulse generation using a reconfigurable photonic microwave delay-line filter," in *Radio and Wireless Symposium, 2008 IEEE*, pp. 129 –132, jan 2008.

[42] S. Sales, J. Capmany, J. Marti, and D. Pastor, "Experimental demonstration of fiber-optic delay line filters with negative coefficients," *Electron. Lett.*, vol. 31, pp. 1095–1096, June 1995.

[43] Y. Yu, J. Dong, X. Li, and X. Zeng, "Ultra-wideband generation based on cascaded mach-zehender modulators," *IEEE Photon. Technol. Lett.*, vol. 23, pp. 1754–1756, Dec. 2011.

[44] M. Bolea, T. Mora, B. Ortega, and J. Capmany, "Optical UWB pulse generation using an N-tap mircowave photonic filter and phase inversion adaptable to different modulation format," *Opt. Express*, vol. 17, pp. 5023–5032, Mar. 2009.

[45] M. Bolea, J. Mora, B. Ortega, and J. Capmany, "High-order UWB pulse generation based on a micrwave photonic filter using incoherent optical sources," in *Int. Topical Meeting on Microw. Photonics (MWP)*, pp. 462–465, Dec. 2011.

[46] J. Li, S. Fu, K. Xu, J. Wu, J. Lin, M. Tang, and P. Shum, "Photonic ultrawideband monocycle pulse generation using a single electro-optic modulator," *Opt. Lett.*, vol. 33, pp. 288–290, Feb. 2008.

[47] J. Li, K. Xu, S. Fu, M. Tang, P. Shum, J. Wu, and J. Lin, "Photonic polarity-switchable ultra-wideband pulse generation using a tunable Sagnac interferometer comb filter," *IEEE Photon. Technol. Lett.*, vol. 20, pp. 1320–1322, Dec. 2008.

[48] Q. Wang, F. Zeng, S. Blais, and J. Yao, "Optical UWB monocycle pulse generation based on cross-gain modulation in a semiconductor optical amplifiers," *Opt. Lett.*, vol. 31, pp. 3083–3085, Nov. 2006.

[49] B. P. P. Kuo, P. C. Chui, and K. K. Y. Wong, "Tunable repetition-rate ultrawideband monocycle pulse genration by using optical parametric amplifier," in *Photonic Application System Technologies conference*, pp. 1–2, May 2007.

[50] H. Chen, M. Chen, C. Qiu, J. Zhang, and S. Xie, "UWB monocycle pulse generation by optical polarisation time deay method," *Electron. Lett.*, vol. 43, pp. 1–2, Apr. 2007.

[51] H. Chen, M. Chen, C. Qiu, and S. Xie, "A novel composite method for ultra-wideband doublet pulse generation," *IEEE Photon. Technol. Lett.*, vol. 19, pp. 2021–2023, Dec. 2007.

[52] H. Chen, M. Chen, J. Zhang, and S. Xie, "UWB monocycle and doublet pulses generation in optical domain," in *Int. Topical Meeting on Microw. Photonics (MWP)*, pp. 1–4, Oct. 2007.

[53] H. Chen, M. Chen, T. Wang, M. Li, and S. Xie, "Methods for ultrawideband pulse generation based on optical cross-polarization modulation," *J. Lightw. Technol.*, vol. 26, pp. 2492–2499, Aug. 2008.

[54] Q. Wang and J. Yao, "Switchable optical UWB monocycle and doublet generation using a reconfigurable photonic microwave delay line filter," *Opt. Express*, vol. 15, pp. 14667–14672, Oct. 2007.

[55] J. D. McKinney, I. S. Lin, and A. M. Weiner, "Shaping the power spectrum of ultra-wideband radio-frequency signals," *IEEE Trans. Microw. Theory Tech.*, vol. 54, pp. 4247–4255, Dec. 2006.

[56] C. Wang, F. Zeng, and J. Yao, "All-fiber ultrawideband pulse generation base on spectral shaping and dispersion-induce frequency-to-time conversion," *IEEE Photon. Technol. Lett.*, vol. 19, pp. 137–139, Feb. 2007.

[57] M. Dastmalchi, M. Abtahi, D. Lemus, L. A. Rusch, and S. LaRochelle, "Simple and efficient UWB pulse generator," in *Conference on Bragg Gratings Phtosensitivity and Poling in Glass Waveguides (OSA/BGPP)*, pp. 1–2, June 2010.

[58] V. T. Company, L. R. Chen, J. Lancis, and P. Andres, "Incoherent photonic techniques for rf-awg," in *Int. Topical Meeting on Microw. Photonics (MWP)*, pp. 422 –425, oct 2010.

[59] Q. Wang and J. Yao, "UWB doublet generation using nonlinear biased electro-optic intensity modulator," *Electron. Lett.*, vol. 42, pp. 1304–1305, Oct. 2006.

[60] X. Yu, T. B. Gibbon, M. Pawlik, S. Blaaberg, and I. T. Monroy, "A photonic ultra-wideband pulse generator based on relaxation oscillations of a semiconductor laser," *Opt. Express*, vol. 17, pp. 9680–9687, June 2009.

[61] E. Zhou, X. Xu, K. Lui, and K. K. Y. Wong, "High-speed photonic power efficient ultra wideband transceiver based on multiple PM-IM conversions," *IEEE Trans. Microw. Theory Tech.*, vol. 58, pp. 3344–3351, Nov. 2010.

[62] J. D. McKinney, D. E. Leaird, and A. M. Weiner, "Millimeter-wave arbitrary waveform generation with a direct space-to-time pulse shaper," *Opt. Lett.*, vol. 27, pp. 1345–1347, Aug. 2002.

[63] J. Yao, "Photonic generation of microwave arbitrary waveforms," in *OptoeElectronics and Communications Conference (OECC)*, pp. 356–357, July 2011.

[64] Z. Jiang, D. E. Leaird, and A. M. Weiner, "Line-by-line pulse shaping control for optical arbitrary waveform generation," in *Conference on*

Lasers and Electro-Optics and Quantum Electronics and Laser Science Conference (CLEO/QELS), pp. 1–2, may 2006.

[65] Z. Jiang, D. E. Leaird, and A. M. Weiner, "Optical processing based on spectral line-by-line pulse shaping on a phase-modulated cw laser," *IEEE J. Quantum Electron.*, vol. 42, pp. 657–666, July 2006.

[66] S. L. Pan and J. Yao, "UWB-over-fiber communications: Modulation and transmission," *J. Lightw. Technol.*, vol. 28, pp. 2445–2455, Aug. 2010.

[67] S. L. Pan and J. Yao, "Performance evaluation of UWB signal transmission over optical fiber," *IEEE J. Sel. Areas Commun.*, vol. 28, pp. 889–900, Aug. 2010.

[68] H. G. Schantz, "Introduction to ultrawideband antennas," in *IEEE conference on Ultra-wideband Syst. and Tchnologies*, pp. 1–9, Nov. 2003.

[69] X. Yu and I. T. Monroy, "Distribution of photonically generated $5Gbits/s$ impulse radio ultrawideband signals over fiber," *Opt. Lett.*, vol. 36, pp. 810–812, Mar. 2011.

[70] S. L. Pan and J. Yao, "Photonic generation of chrip-free UWB signals for UWB over fiber applications," in *Int. Topical Meeting on Microw. Photonics (MWP)*, pp. 1–4, Oct. 2009.

[71] C. M. Tan, L. C. Ong, M. L. Yee, B. Luo, and P. K. Tang, "Transmssion of ultra wideband radio using multimode signals over fiber system," in *Asia-Pacific Microw. Confernce Proceedings (APMC)*, pp. 1–3, Dec. 2005.

[72] Y. M. Chang, J. Lee, and J. H. Lee, "Ultrawideband doublet pulse generation based on nonlinear polarization rotation of an elliptically polarized beam and its distribution over a fiber/wireless link," *Opt. Express*, vol. 18, pp. 20072–20085, Sept. 2010.

[73] Y. M. Chang, J. Lee, H. S. Lee, L. Yan, and J. H. Lee, "Generation and distribution of $1.25Gbps$ ultrawideband doublet pulses based on the combination of nonliear polarization rotation and parameteric amplification," *J. Lightw. Technol.*, vol. 29, pp. 931–938, Mar. 2011.

[74] M. Hanawa, K. Mori, K. Nakamura, A. Matsui, Y. Kanda, and K. Nonaka, "Dispersion tolerant UWB-IR-over Fiber transmission under FCC indoor spectrum," in *Proc. OFC/NFOEC*, pp. 1–3, Mar. 2009.

[75] M. Abtahi, M. Mirshafie, S. LaRochelle, and L. A. Rusch, "All optical 500 Mb/s UWB transceiver: An experimental demonstration," *J. Lightw. Technol.*, vol. 26, pp. 2795–2802, Aug. 2008.

[76] J. B. Jensen, R. Rodes, A. Caballero, X. Yu, T. B. Gibbon, and I. T. Monroy, "4 *Gbps* impulse radio ultra-wideband transmission over 100m multi-mode fiber with 4 $meters$ wireless transmission," *Opt. Express*, vol. 17, pp. 16898–16903, Sept. 2009.

[77] J. B. Jensen, R. Rodes, M. Beltran, and I. T. Monroy, "Shared medium 2*Gbps* baseband and 2*Gbps* UWB in-building converged optical/wireless network with multi-mode fiber and wireless transmission," in *European Conference on Exhibition on Optical Commun. (ECOC)*, pp. 1–3, Sept. 2010.

[78] X. Yu, R. Rodes, J. B. Jensen, A. Caballero, T. B. Gibbon, and I. T. Monroy, "1*Gbps* impulse radio ultra wideband multi-hope system employing a single mode fiber repeater," in *Annual Meetings of the IEEE Lasers Electro-optics Society (LEOS)*, pp. 697–698, Oct. 2009.

[79] R. Rodes, T. T. Pham, J. B. Jensen, T. B. Gibbon, and I. T. Monroy, "Energy-efficient VCSEL-based multiGigabit IR-UWB over fiber with airlink transmission system," in *Annual Meetings of the IEEE Photonic Society*, pp. 222–223, Nov. 2010.

[80] R. Rodes, X. Yu, A. Caballero, J. B. Jensen, T. B. Gibbon, N. G. Gonzalez, and I. T. Monroy, "Range extension and channel capacity increase in impulse radio ultrawideband communications," *Tsinghua Science and Technol.*, vol. 15, pp. 169–173, Apr. 2010.

[81] T. T. Pham, X. Yu, T. B. Gibbon, L. Dittmann, and I. T. Monroy, "A WDM-PON compatible system for simultaneous distribution of Gigabit baseband and wireless ultrawideband services with flexible bandwdith allocation," *IEEE Photon. J.*, vol. 3, pp. 13–196, Feb. 2011.

[82] T. T. Pham, X. Yu, L. Dittmann, and I. T. Monroy, "Integration of optically generated impulse radio UWB signals into WDM-PON," *IEEE Photon. Technol. Lett.*, vol. 23, pp. 474–476, Apr. 2011.

[83] S. T. Abraha, C. Okonkwo, H. Yang, D. Visani, Y. Shi, H. D. Jung, E. Tangdiongga, and T. Koonen, “Performance evaluation of IR-UWB in short range fiber communication using linear combination of monocycles,” *J. Lightw. Technol.*, vol. 29, pp. 1143–1151, Apr. 2011.

[84] S. T. Abraha, C. M. Okonkwo, E. Tangdiongga, and A. M. J. Koonen, “Experimental demonstartion of 2 Gbps IR-UWB transmission over 100m GI-POF using novel pulse generation technique,” in *European Conference on Exhibition on Optical Commun. (ECOC)*, pp. 1–3, Sept. 2010.

[85] S. T. Abraha, N. C. Tran, C. M. Okonkwo, H. S. Chen, E. Tangdiongga, and A. M. J. Koonen, “Service multicasting by all-optical routing of 1 Gb/s IR-UWB for in-building networks,” in *Proc. OFC/NFOEC*, pp. 1–3, Mar. 2011.

[86] S. T. Abraha, C. Okonkwo, E. Tangdiongga, and A. M. J. Koonen, “Power-efficient impulse radio ultrawideband pulse generator based on the linear sum of modified doublet pulses,” *Opt. Lett.*, vol. 36, pp. 2363–2365, June 2011.

[87] G. R. Aiello and G. D. Rogerson, “Ultra-wideband wireless systems,” *IEEE Microw. Mag.*, vol. 4, pp. 36–47, June 2003.

[88] M. G. Benedetto and B. Vojcic, “Ultra-wideband wireless communications: A Tutorial,” *IEEE J. Commun. Netw.*, vol. 5, pp. 290–302, Dec. 2003.

[89] M. G. DiBenedetto, T. Kaiser, A. F. Molisch, I. Oppermann, C. Politano, and D. Porcino, *UWB Communication Systems A Comperhensive Overview.* Hindawi Publishing Corp., 2006.

[90] X. Chen and S. Kiaei, “Monocycle shapes for ultra-wideband system,” in *IEEE Int. Symp. Cicuits and Syst.*, vol. 1, pp. 26–29, May 2002.

[91] F. Zeng and J. Yao, “Optical generation and distribution of UWB signals,” in *IEEE Int. Conference on Commun. Cicuits and Syst.*, vol. 3, pp. 2024–2029, June 2006.

[92] Q. Wang and J. Yao, “An electrically switchable optical ultrawideband pulse generator,” *J. Lightw. Technol.*, vol. 25, pp. 3626–3633, Nov. 2007.

[93] E. Zhou, X. Zhang, X. Xu, J. Dong, W. Xue, and I. T. Monroy, "Photonic generation of UWB monocycle pulses using a cascaded semiconductor optical amplifier and electroabsorption modulator," in *Proc. OFC/NFOEC*, pp. 1–3, Mar. 2009.

[94] E. Zhou, X. Xu, X. Zhang, W. Xue, Y. Yu, J. Mork, and I. T. Monroy, "Photonic generation of ultrawideband monocycle and doublet pulses by using a semiconductor-optical amplifier-based wavelength converter," *Opt. Lett.*, vol. 34, pp. 1336–1338, May 2009.

[95] H. Shen, P. Orlik, A. M. Haimovich, L. J. Cimini, and Z. Jinyun, "On the spectral and power requirements for ultra wideband transmission," in *IEEE Int. conference on Commun.*, vol. 1, pp. 738–742, May 2003.

[96] B. Parr, B. Cho, K. Wallace, and Z. Ding, "A novel ultra-wideband pulse design algorithm," *IEEE Commun. Lett.*, vol. 7, pp. 219–221, May 2003.

[97] X. Gu and L. Taylor, "Ultra-wideband and its capabilities," *BT Technol. J.*, vol. 21, pp. 56–66, July 2003.

[98] B. Allen, S. A. Ghorashi, and M. Ghavami, "A review of pulse design for impulse radio," in *Proc.UWB Commun. Technol. Syst. Des.*, pp. 93–97, July 2004.

[99] N. C. Beaulieu and B. Hu, "A pulse design paradigm for ultra-wideband communication systems," *IEEE Trans. Wireless Commun.*, vol. 5, pp. 1274–1278, June 2006.

[100] X. Wu, Z. Tian, T. N. Davidson, and G. B. Giannakis, "Optimal waveform design for UWB radios," *IEEE Trans. Signal Process.*, vol. 54, pp. 2009–2021, June 2006.

[101] M. Abtahi, J. Magne, M. Mirshafie, L. Rusch, and S. LaRochelle, "Generation of power-efficient FCC-compliant UWB waveforms using FBGs: Analysis and experiment," *J. Lightw. Technol.*, vol. 26, pp. 628–635, Mar. 2008.

[102] E. Zhou, X. Xu, K. Lui, and K. K. Y. Wong, "A Power Efficient Ultra Wideband Pulse Geneartor based on Multiple PM-IM Conversions," *IEEE Photon. Technol. Lett.*, vol. 22, pp. 1063–1065, July 2010.

[103] M. Mirshafiei, M. Abtahi, P. Larochelle, and L. A. Rusch, “Pulse shapes that outperform traditional UWB antenna/waveform combinations,” in *IEEE Global Telecommunications Conference (GLOBECOM)*, pp. 1–5, Dec. 2010.

[104] X. Luo, L. Yang, and G. B. Giannakis, “Designing optimal pulse-shapers for ultra-wideband radios,” *IEEE J. Commun. Netw.*, vol. 5, pp. 344–353, Dec. 2003.

[105] J. Li, K. Xu, S. Fu, J. Wu, J. Lin, M. Tang, and P. Shum, “Ultra-wideband pulse generation with flexible pulse shape and polarity control using a Sagnac-interferometer-based intensity modulator,” *Opt. Express*, vol. 15, pp. 18156–18161, Dec. 2007.

[106] S. L. Pan and J. Yao, “A Photonic UWB Generator Reconfigurable for Multiple Modulation Formats,” *IEEE Photon. Technol. Lett.*, vol. 21, pp. 1381–1383, Oct. 2009.

[107] S. L. Pan and J. Yao, “Switchable UWB pulse generation using a phase modulator and a reconfigurable asymmetric Mach-Zehnder interferometer,” *Opt. Lett.*, vol. 34, pp. 160–162, Jan. 2009.

[108] S. T. Abraha, C. M. Okonkwo, A. M. J. Koonen, and E. Tangdiongga, “Experimental demonstration of 2 Gb/s IR-UWB over fiber using a novel pulse generation technique,” in *Access Networks and In-house Commun.*, pp. 1–2, June 2010.

[109] S. T. Abraha, H. Yang, C. M. Okonkwo, H. P. A. van den Boom, E. Tangdiongga, and A. M. J. Koonen, “Novel generation and transmission of 2Gbps impulse radio ultra wideband over MMF for in-building network application,” in *Proc. OFC/NFOEC*, pp. 1–3, Mar. 2010.

[110] S. T. Abraha, H. Yang, E. Tangdiongga, and A. M. J. Koonen, “Novel generation and transmission of FCC-compliant impulse radio ultra wideband over 100m GI-POF,” in *European Conference on Exhibition on Optical Commun. (ECOC)*, pp. 1–2, Sept. 2009.

[111] S. T. Abraha, H. Yang, E. Tangdiongga, and A. M. J. Koonen, “Novel generation and transmission of FCC-compliant impulse radio ultra wideband over 100m GI-POF,” in *Int. Topical Meeting on Microw. Photonics (MWP)*, pp. 1–4, Oct. 2009.

[112] T. Koonen, "Fiber to the home/fiber to the premises: What, where and when," in *Proc. IEEE*, pp. 911–934, May 2006.

[113] M. Maier, N. Ghazisaidi, and M. Riesslein, "The audacity of fiber-wireless (fiwi) networks," in *AccessNets, LNICST 6*, pp. 16–35, 2009.

[114] R. Gaudino, D. Cardenas, M. Bellec, B. Charbonnier, N. Evanno, P. Guignard, S. Meyer, A. Pizzinat, I. Mollers, and D. Jager, "Perspective in Next Generation Home Networks: Toward optical solutions?," *IEEE Commun. Mag.*, vol. 48, pp. 39–47, Feb. 2010.

[115] K. Nakajima, K. Hogari, J. Zhou, K. Tajima, and L. Sankawa, "Hole-assisted fiber design for small bending and splice losses," *IEEE Photon. Technol. Lett.*, vol. 15, pp. 1737 –1739, dec. 2003.

[116] P. E. Green, "Fiber to the home: the next big broadband thing," *IEEE Commun. Mag.*, vol. 42, pp. 100–106, Sept. 2004.

[117] Y. L. Guennec and R. Gary, "Optical frequency conversion for millimeter-wave ultra-wideband-over-fiber systems," *IEEE Photon. Technol. Lett.*, vol. 19, pp. 996–998, July 2007.

[118] M. Beltran and R. Llorente, "Dual photonic generation ultrawideband impulse radio by frequency shifting in remote-connectivity fiber," *J. Lightw. Technol.*, vol. 29, pp. 3645–3653, Dec. 2011.

[119] "Arbitrary waveform generators: AWG7000B series data sheet."

[120] Y. L. Guennec, M. Lourdiane, B. Cabon, G. Maury, and P. Lombard, "Technologies for UWB over fiber," in *Annual Meetings of the IEEE Lasers Electro-optics Society (LEOS)*, pp. 518–519, Oct. 2006.

[121] R. Llorente, A. Cartaxo, B. Uguen, J. Duplicy, J. Romme, J. F. Puche, D. Schmertz, Y. Lostanlen, R. Banales, and J. Marti, "Management of UWB picocell cluster: UCELS project approach," in *IEEE Int. conference on Ultra-wideband (ICUWB)*, vol. 3, pp. 139–142, Sept. 2008.

[122] R. Llorente, T. Alves, M. Morant, M. Beltran, J. Perz, A. Cartaxo, and J. Marti, "Ultra-wideband radio signals distribution in FTTH networks," *IEEE Photon. Technol. Lett.*, vol. 20, pp. 945–947, June 2008.

[123] T. Koonen, H. van Boom, and G. D. Khoe, "Broadband access and in-house networks:Extending the capabilities of multiomode fiber networks," in *European Conference on Exhibition on Optical Commun. (ECOC)*, pp. 24–27, Oct. 2003.

[124] N. J. Gomes, A. Das, A. Nkansah, M. Mjeku, and D. wake, "Multimode fiber-fed indoor wireless networks," in *Int. Topical Meeting on Microw. Photonics (MWP)*, pp. 1–4, Oct. 2006.

[125] N. J. Gomes, A. Nkansah, and D. Wake, "Radio-over-MMF techniques-Part I: RF to microwave frequency systems," *J. Lightw. Technol.*, vol. 26, pp. 2388–2395, Aug. 2008.

[126] C. Carlsson, A. Larsson, and A. Alping, "RF transmission over multimode fibers using VCSELs-comparing standard and high-bandwidth multimode fibers," *J. Lightw. Technol.*, vol. 22, pp. 1694–1700, Aug. 2004.

[127] D. Wake, S. Dupont, C. Lethien, J. P. Vilcot, and D. Decoster, "Radiofrequency transmission of 32-QAM signals over multimode fiber for distributed antenna system applications," *Electron. Lett.*, vol. 37, pp. 1087 –1089, aug 2001.

[128] E. I. Ackerman and C. H. Cox, "Sate of the art analog fiber-optic link technology," in *IEEE Int. Symp. Signals Syst and Electronics.*, pp. 372–377, Sept. 1998.

[129] A. Das, A. Nkansah, N. J. Gomes, I. J. G. J. C. Batchelor, and D. Wake, "Design of low-cost multimode fiber-fed indoor wireless networks," *IEEE Trans. Microw. Theory Tech.*, vol. 54, pp. 3426–3432, Aug. 2006.

[130] M. Y. W. Chia, B. Luo, M. L. Yee, and E. J. Z. Hao, "Radio over multimode fiber transmission for wireless LAN using VCSELs," *Electron. Lett.*, vol. 39, pp. 1143–1144, July 2003.

[131] C. Carlsson, H. Martinsson, and A. Larsson, "High performance microwave link using a multimode VCSEL and a high-bandwdith multimode fiber," in *Int. Topical Meeting on Microw. Photonics (MWP)*, pp. 81–84, Jan. 2002.

[132] A. M. J. Koonen, "Bit-error-rate degradation in a Multimode fiber optic transmission link due to modal noise," *IEEE J. Sel. Areas Commun.*, vol. 4, pp. 1515–1521, Dec. 1986.

[133] G. C. Papen and G. M. Murphy, "Modal noise in multimode fibers under restricted launch conditions," *J. Lightw. Technol.*, vol. 17, no. 5, pp. 817–822, 1999.

[134] Y. Koike and M. Asai, "The future of plastic optical fiber," *NPG Asia Mat.*, vol. 1, pp. 22–28, Oct. 2009.

[135] M. Asai, Y. Inuzuka, K. Koike, S. Takahashi, and Y. Koike, "High-bandwidth graded-index plastic optical fiber with low-attenuation, high-bending ability and high-thermal stability for home networks," *J. Lightw. Technol.*, vol. 29, pp. 1620–1626, June 2011.

[136] H. Yang, S. C. Lee, E. Tangdiongga, C. Okonkwo, H. P. A. van den Boom, F. Breyer, S. Randel, and A. M. J. Koonen, "47.4 gb/s transmission over 100m graded-index plastic optical fiber based on rate-adaptive discerete multitone modulation," *J. Lightw. Technol.*, vol. 28, pp. 352–359, Feb. 2010.

[137] J. Lee, *Discrete Multitone Modulation for short-range optical communications*. PhD thesis, Eindhoven University of Technology, The Netherlands, Dec. 2009.

[138] H. Yang, *Optical techniques for broadband in-building networks*. PhD thesis, Eindhoven University of Technology, The Netherlands, Jan. 2011.

[139] Y. Shao, R. Cao, Y. K. Huang, P. N. Ji, and S. Zhang, "112-Gb/s transmission over 100m of graded-index plastic optical fiber for optical data ceneter appliactions," in *Proc. OFC/NFOEC*, pp. 1–3, Mar. 2012.

[140] I. Mollers, D. Jager, R. Gaudino, A. Nocivelli, H. Kragl, O. Ziemann, T. Koonen, C. Lezzi, A. Bluschke, and S. Randel, "Plastic optical fiber technology for reliable home networking: overview and results of the EU project POF-ALL," *IEEE Commun. Mag.*, pp. 58–68, Aug. 2009.

[141] C. M. Okonkwo, E. Tangdiongga, H. Yang, D. Visani, S. Loquai, R. Krudlov, B. Charbonnier, M. Ouzzif, I. Greiss, O. Ziemann, R. Gaudino, and A. M. J. Koonen, "Recent results from EU POF-PULS project: Multi-gigabit transmission over 1mm core diameter plastic optical fibers," *J. Lightw. Technol.*, vol. 29, pp. 186–193, Jan. 2011.

[142] H. P. A. van den Boom, W. Li, P. K. van Bennekom, I. T. Monroy, and G. D. Khoe, "High-capcity transmission over polymer optical fiber," *IEEE J. Sel. Topics Quantum Electron.*, vol. 7, pp. 461–470, May 2001.

[143] S. T. Abraha, P. A. Gamage, A. Crivellaro, E. Tangdiongga, and A. M. J. Koonen, "Converged IR-UWB wireless and wiredbaseband access for in-building network applications," in *Proc. IEEE/LEOS Symp. Benelux Chapter*, pp. 1–4, Mar. 2011.

[144] S. T. Abraha, C. M. Okonkwo, P. A. Gamage, E. Tangdiongga, and A. M. J. Koonen, "Routing of $2Gb/s$ wireless IR-UWB and $1.25Gb/s$ wired services for in-building networks," in *Proc. OFC/NFOEC*, pp. 1–3, Mar. 2012.

[145] M. Popov, "The convergence of wired and wireless service delivery in access and home networks," in *Proc. OFC/NFOEC*, pp. 1–3, Mar. 2010.

[146] A. M. J. Koonen, Y. Shi, N. C. Tran, C. M. Okonkwo, H. P. A. van den Boom, and E. Tangdiongga, "A perspective from europe on in-home networking," in *Proc. OFC/NFOEC*, pp. 1–3, Mar. 2012.

[147] A. M. J. Koonen, H. Yang, H. D. Jung, S. C. J. Lee, E. Tangdiongga, C. Okonkwo, and H. van Boom, "Optical in-building network techniques," in *Annual Meetings of the IEEE Lasers Electro-optics Society (LEOS)*, pp. 622–623, Oct. 2009.

[148] M. Popov, "Everything Converged-a Flexible Photonic Home," in *Int. Topical Meeting on Microw. Photonics (MWP)*, pp. 1–4, Oct. 2009.

[149] A. M. J. Koonen, H. P. A. van den Boom, E. Tangdiongga, and P. Guignard, "Designing in-building optical fiber networks," in *Proc. OFC/NFOEC*, pp. 1–3, Mar. 2010.

[150] I. T. Monroy, K. Prince, A. Osadchiy, N. G. Gonzalez, A. Caballero, D. Zibar, T. Gibbon, X. Yu, and J. B. Jensen, "Converged wireline and wireless signal transport over optical fiber access links," in *OptoElectronics and Commun. conference*, pp. 1–2, July 2009.

[151] "White paper: Raodmap for access and in-building network solutions," Mar. 2011. 212352 ICT ALPHA D1.3p.

[152] H. D. Jung, C. M. Okonkwo, E. Tangdiongga, and A. M. J. Koonen, "All-optical wavelength multicasting of milimeter-wave signals using optical frequency multiplication techniques for in-building networks," in *European Conference on Exhibition on Optical Commun. (ECOC)*, pp. 1–3, Sept. 2009.

[153] S. Zou, C. M. Okonkwo, Z. Cao, N. C. Tran, E. Tangdiongga, and A. M. J. Koonen, "Dyaminc optical routing and simultaneous generation of millimeter wave signals for in-building access network," in *Proc. OFC/NFOEC*, pp. 1–3, Mar. 2012.

[154] W. P. Lin and J. Y. Chen, "Implementation of a new ultrawideband impulse system," *IEEE Photon. Technol. Lett.*, vol. 17, pp. 2418–2420, Nov. 2005.

[155] K. Prince, J. B. Jensen, A. Caballero, X. Yu, T. B. Gibbon, D. Zibar, N. Guerrero, A. V. Osadchiy, and I. T. Monroy, "Converged wireline and wireless access over $78-km$ deployed fiber long-reach WDM-PON," *IEEE Photon. Technol. Lett.*, vol. 21, pp. 1274–1276, Sept. 2009.

[156] S. L. Pan and J. Yao, "Simultaneous provision of UWB and wired service in a WDM-PON network using a cenetralized light source," *IEEE Photon. J.*, vol. 2, pp. 712–718, Oct. 2010.

[157] M. Abtahi and S. LaRochelle, "RoF delivery over PONs of optically shaped UWB signals for Gigabits/s Wireless distribution in the home," *IEEE J. Sel. Areas Commun.*, vol. 29, pp. 1304–1310, June 2011.

[158] S. L. Pan and J. Yao, "Converged IR-UWB wireless and baseband wired access over a WDM-PON," in *European Conference on Exhibition on Optical Commun. (ECOC)*, pp. 1–3, Sept. 2011.

[159] S. L. Pan and J. Yao, "IR-UWB-over-fiber systems compatible with WDM-PON networks," *J. Lightw. Technol.*, vol. 29, pp. 3025–3034, Oct. 2011.

[160] K. K. Wong, G. W. Lu, K. C. Lau, P. K. A. Wai, and L. K. Chen, "All-optical wavelength conversion and multiplexing by cross-gain modulation in a single-stage fiber ampplifier," in *Proc. OFC/NFOEC*, pp. 1–3, Mar. 2007.

[161] A. M. J. Koonen, H. Yang, H. D. Jung, Y. Zheng, H. P. A. van den Boom, and E. Tangdiongga, "Flexible in-building radio-over-fiber networks," in *Proc. NOC European Conference on Networks and Optical Communications*, pp. 195–202, Mar. 2008.

[162] D. Marpaung, L. Chevalier, M. Burla, and C. Roeloffzen, "Impulse radio ultrawideband pulse shaper based on programmable photonic chip

frequency discriminator," *Opt. Express*, vol. 19, pp. 24838–24848, Dec. 2011.

[163] A. Crivellaro, S. T. Abraha, E. Tangdiongga, R. Gaudino, and A. M. J. Koonen, "Remote indoor localization using IR-UWB over fiber techniques," in *Proc. IEEE/LEOS Symp. Benelux Chapter*, pp. 1–4, Dec. 2011.

[164] A. Crivellaro, "Indoor localization using IR-UWB over fiber technology," Master's thesis, POLITECNICO DI TORINO, Italy, 2011.

[165] E. Tangdiongga, S. T. Abraha, A. Crivellaro, C. M. Okonkwo, R. Gaudino, and A. M. J. Koonen, "Accurate Localization Technique for Smart Fiber-wireless In-house Networks," in *Access Networks and In-house Commun.*, pp. 1–2, June 2012.

[166] S. T. Abraha, E. Tangdiongga, A. Crivellaro, R. Gaudino, and A. M. J. Koonen, "Accurate ranging/localization technique using IR-UWB for smart fiber-wireless in-house networks," in *European Conference on Exhibition on Optical Commun. (ECOC)*, pp. 1–3, Sept. 2012.

[167] J. Khodjaev, Y. Park, and A. S. Malik, "Survey of NLOS identification and error mitigation problems in UWB-based positioning algorithms for dense environments," *Annals of Telecommunications*, vol. 65, no. 5, pp. 301–311, 2010.

[168] A. J. Weiss, "Direct positioning determination of narrowband radio frequency transmitters," *IEEE Signal Process. Lett.*, vol. 11, pp. 513–516, May 2004.

[169] A. Roxin, J. Gaber, M. Wack, and A. Niat-Sidi-Moh, "Survey of wireless geolocation techniques," in *Globecom Workshops*, pp. 1–9, Nov. 2007.

[170] H. Soganci, S. Gezici, and H. V. Poor, "Emerging opportunities for localization and tracking: Accurate positioning in ultra-wideband systems," *IEEE Wireless Commun.*, vol. 18, pp. 19–27, Apr. 2011.

[171] D. P. Young, C. M. Keller, D. W. Bliss, and K. W. Forsythe, "Ultra-wideband (UWB) transmiter localization using time difference of arrival (TDOA) techniques," *Signal Sytems and computers*, vol. 2, pp. 1225–1229, Nov. 2003.

[172] A. F. Molisch, "Ultrawideband propagation channels-theory, measurement and modeling," *Vehicular Technology, IEEE Transactions on*, vol. 54, pp. 1528 – 1545, sept. 2005.

[173] A. F. Molisch, D. Cassioli, C. C. Chin, S. Emami, A. Fort, B. K. and J. Karedal, J. Kunisch, H. G. Schantz, K. Siwiak, and M. Z. Win, "A comprehensive standardized model for ultrawideband propagation channels," *Antennas and Propagation, IEEE Transactions on*, vol. 54, pp. 3151 –3166, nov 2006.

[174] I. Guvenc and Z. Sahinoglu, "TOA estimation with different IR-UWB transceiver types," in *Ultra-Wideband, 2005. ICU 2005. 2005 IEEE International Conference on*, pp. 426 – 431, sept. 2005.

[175] I. Guvenc, Z. Sahinoglu, and P. V. Orlik, "TOA estimation for IR-UWB systems with different transceiver types," *Microwave Theory and Techniques, IEEE Transactions on*, vol. 54, pp. 1876 – 1886, june 2006.

[176] T. Krebesz, G. Kolumban, C. K. Tse, and F. C. M. Lau, "Improving the noise performance of energy detector based UWB systems by optimizing the receiver parameters," in *Communications and Information Technology, 2009. ISCIT 2009. 9th International Symposium on*, pp. 1426 –1431, sept. 2009.

[177] S. Gezici and I. G. Z. Sahinoglu, "On the performance of linear least-squares estimation in wireless positioning systems," in *Communications, 2008. ICC '08. IEEE International Conference on*, pp. 4203 –4208, may 2008.

[178] J. J. Caffery and G. L. Stuber, "Overview of radiolocation in CDMA cellular systems," *Communications Magazine, IEEE*, vol. 36, pp. 38–45, apr 1998.

[179] F. Gustafsson and F. Gunnarsson, "Mobile positioning using wireless networks: possibilities and fundamental limitations based on available wireless network measurements," *Signal Processing Magazine, IEEE*, vol. 22, pp. 41–53, july 2005.

[180] J. Caffery, J.J., "A new approach to the geometry of TOAlocation," in *Vehicular Technology Conference, 2000. IEEE VTS-Fall VTC 2000. 52nd*, vol. 4, pp. 1943 –1949 vol.4, 2000.

[181] S. Venkatesh and R. M. Buehrer, "A linear programming approach to NLOS error mitigation in sensor networks," in *Information Processing in Sensor Networks, 2006. IPSN 2006. The Fifth International Conference on*, pp. 301–308, 2006.

[182] Z. Li, W. Trappe, Y. Zhang, and N. Badri, "Robust statistical methods for securing wireless localization in sensor networks," in *Fourth International Symposium on Information Processing in Sensor Networks*, pp. 91–98, Apr. 2005.

[183] I. Guvenc, C. C. Chin, and F. Watanabe, "Analysis of a linear least-squares localization technique in LOS and NLOS environments," in *Vehicular Technology Conference, 2007. VTC2007-Spring. IEEE 65th*, pp. 1886 –1890, april 2007.

[184] T. Gigl, G. J. M. Janssen, V. Dizdarevic, K. Witrisal, and Z. Irahhauten, "Analysis of a UWB indoor positioning system based on received signal strength," in *4th Workshop on Positioning, Naviagtion and Communication (WPNC'07)*, pp. 99–101, Jan. 2007.

[185] G. Bellusci, *Ultra-Wideband ranging for low-compexity indoor positioning applications.* PhD thesis, Delft University of Technology, The Netherlands, Jan. 2011.

[186] J. A. N. da Silva and M. L. R. de Campos, "Spectrally effecient UWB pulse shaping with application in orthogonal PSM," *IEEE Trans. Commun.*, vol. 55, pp. 313–322, Feb. 2007.

Appendix B

List of publications

Invited Papers

1. A.M.J. Koonen, H.D.Jung, H. Yang,C.M. Okonkwo, Y. Zheng, S.T. Abraha, & E. Tangdiongga, "Techniques for flexible radio-over-fibre networks", International Conference on Photonics in Switching, September 2009, Pisa, Italy. (pp. 1-4).

2. E. Tangdiongga , S. T. Abraha , A. Crivellaro , C. M. Okonkwo , R. Gaudino & A. M. J. Koonen, "Accurate localization technique for smart fiber-wireless in-house networks",Proceedings of the Access Networks and in-house communications conference (ANIC), Colardo, June 2012. (AW3A.2 pp.1-2)

Journal Papers

3. H. Yang, E. Tangdiongga, S.C.J. Lee,C.M. Okonkwo, S.T.Abraha, H.P.A. van den Boom, F. Breyer, S. Randel, & A.M.J. Koonen, "Record high-speed short-range transmission over 1-mm core diameter POF employing DMT technique", Optics Letters, 35(5), 730-732.

4. S.T. Abraha, C.M. Okonkwo, H.Yang, D. Visani, Y.Shi, H.D. Jung, E. Tangdiongga, & A.M.J. Koonen, "Performance evaluation of IR-UWB in short-range fiber communication using linear combination of monocycles", Journal of Lightwave Technology, 29(8), 1143-1151.

5. S.T. Abraha, C.M.Okonkwo, E. Tangdiongga, & A.M.J. Koonen, "Power-efficient impulse radio ultrawideband pulse generator based on the linear sum of modified doublet pulses", Optics Letters, 36(12), 2363-2365.

6. S. T. Abraha, C. Okonkwo, P. A. Gamage, E. Tangdiongga , T. Koonen, "Routing of Power effecient IR-UWB wireless and wired services for in-building network Applications", Journal of Lightwave Technology, 30(11), 1651-1663.

International Conferences

7. S.T. Abraha, E. Tangdiongga, A. Crivellaro, R. Gaudion,& A.M.J. Koonen, "Accurate Ranging/Localization Technique using IR-UWB for Smart Fiber-Wireless In-House Networks", Proceedings of the 38th European Conference and Exhibition on Optical Communication, September 2012, Amsterdam, Netherlands. (Accepted)

8. S.T. Abraha, N.C. Tran, C.M. Okonkwo, H.S. Chen, E. Tangdiongga, & A.M.J. Koonen, " Service multicasting by all-optical routing of 1 Gb/s IR-UWB for in-building networks", Proceedings of the Optical Fiber Communication Conference and Exposition (OFC/NFOEC) and the National Fiber Optic Engineers Conference, March 2011, Los Angeles, California. (pp. JWA68-1/3).

9. A.M.J. Koonen, H.P.A. van den Boom, H. Yang, C.M. Okonkwo, Y. Shi, S.T. Abraha, E. O. Martinez,& E. Tangdiongga, "Converged in-building networks using pof : economics and advanced techniques ", Proceedings of the 19th International Conference on Plastic Optical Fibers. October 2010, Yokohama, Japan. (pp. 1-4).

10. C.M. Okonkwo, S.T. Abraha, Y. Shi, H. Yang, H. de Waardt, E. Tangdiongga, & A.M.J. Koonen, "Simultaneous generation and routing of millimetre-wave signals exploiting optical frequency multiplication ", Proceedings of the 36th European Conference and Exhibition on Optical Communication, September 2010, Torino, Italy. (pp. Th.10.B.7-1/3).

11. S.T. Abraha, C.M. Okonkwo, A.M.J. Koonen, & E. Tangdiongga, "Experimental demonstration of 2 Gbps IR-UWB over fiber using a novel

pulse generation technique", Proceedings of the Access Networks and in-house communications conference (ANIC), Karlsruhe, June 2010. (pp. AThA5-1-2).

12. S.T. Abraha, C.M. Okonkwo, A.M.J. Koonen, & E. Tangdiongga, "Experimental demonstration of 2 Gbps IR-UWB transmission over 100m GI-POF using novel pulse generation technique", Proceedings of the 36th European Conference and Exhibition on Optical Communication, September 2010, Torino, Italy. (pp. Th.9.B.2-1/3).

13. S.T. Abraha, H. Yang, C.M. Okonkwo, H.P.A. van den Boom, E. Tangdiongga, & A.M.J. Koonen, "Novel generation and transmission of 2 Gbps impulse radio ultra wideband over MMF for in-building networks application ", Proceedings of the Conference on Optical Fiber Communication (OFC), National Fiber Optic Engineers Conference (OFC/NFOEC), march 2010, San Diego, USA. (pp. OML4-1/3).

14. S.T. Abraha, H. Yang, E. Tangdiongga, & A.M.J. Koonen, " Generation and transmission of FCC-compliant impulse radio ultra wideband signals over 100-m GI-POF " Proceedings of the 35th European Conference on Optical Communication. September 2009, Vienna, Austria. (pp. 6.22-1/2).

15. S.T. Abraha, H. Yang, E.Tangdiongga, & A.M.J. Koonen, "Novel generation and transmission of FCC-compliant impulse radio ultra wideband signals over 100-m GI-POF ", International Topical Meeting on Microwave Photonics, October 2009, Valencia, Spain. (pp. Th4.15-1/4).

Regional Conferences

16. S.T. Abraha, P.A. Gamage, A. Crivellaro, E. Tangdiongga, & A.M.J. Koonen, "Converged IR-UWB wireless and wired baseband access for in-building network applications", Proceedings of the 16th Annual symposium of the IEEE Photonics Benelux Chapter,December 2011, Ghent, Belgium. (pp. 249-252).

17. A. Crivellaro, S.T. Abraha, E. Tangdiongga, R. Gaudino, & A.M.J. Koonen, "Remote in-door ranging system using impulse radio ultra wideband RoF techniques", Proceedings of the 16th Annual symposium of

the IEEE Photonics Benelux Chapter, December 2011, Ghent, Belgium. (pp. 253-256). Ghent, Belgium: Unversiteit Gent.

18. S.T. Abraha, C.M. Okonkwo, A.M.J. Koonen, & E. Tangdiongga, "Optical generation of IR-UWB pulse based on weighted sum of modified doublets", Proceedings of the 15th Annual Symposium of the IEEE Photonics Benelux Chapter, November 2010, Delft, Netherlands. (pp. 201-204).

Acknowledgments

The time has come for me to say many thanks to all those who have directly or indirectly contributed to this thesis.

My deepest gratitude goes first and foremost to my first promotor prof.ir. Ton Koonen for giving me the opportunity to pursue my Ph.D. degree at Electro-Optical Communication(ECO) group and for keeping me on the right track in my research work. I sincerely thank him for his professional supervision, advice, proofreading of hundreds of thesis draft and guidance from very early stage of this work as well as for inspire me with his extraordinary skills. His valuable advice and support lead me to achieve one of the important achievements in my personal life. I am indebted to him more than he knows.

I would like to thank dr. Eduward Tangdiongga, my co-promotor, for his guidance, advice and technical discussions for the past four years. He helped me to improve my experimental skills by preparing a special training program in the first year of my PhD. What is most important, Eduward provided me the right degree of scientific freedom and he was always open for new ideas and discussions.

I acknowledge EU FP7 ALPHA project for funding all my research work. I would like to express my gratitude to prof. Beatriz Ortega from departamento de Communicaciones of Universitat politecnica de valencia for her support and valuable suggestions in improving the quality of this thesis. I am also grateful for prof. Alexander Yarovoy from Delft university of technology for his supervision during my master thesis and also teaching me all the very nice courses. I would also to thank him for his continuous support, in reviewing, commenting and approving this work. I am also very grateful for all other my PhD core committee for reviewing, commenting and approving this work. I appreciate their effort, valuable comments and dedicating time for my PhD defense.

I would like to thank all the members from ECO group, special thanks for dr. H. de Waardt, and ir. Henire van den Boom for the consistent help in the lab with the practical problems, providing necessary equipments and components whenever needed. I am also grateful for prof. Harm Doren for his support, for creating a very stimulating environment within COBRA and his encouragement for my future career. Special thanks to Susan de Leeuw, Jose Hakkens and Jolanda Levering for their kindness and warm assistance to any administrative matters as well as reminding me all the important deadlines. I would like to thank dr. Hejie Yang for his advice and support in the lab as well as for very nice technical discussions about RoF systems. I am also grateful for dr. Chigo Okonkwo for his support, advice and technical discussions during my experimental works as well as in editing all paper works. He also helped me in facilitating and ordering equipments and components for my experimental works. My special thanks go to all the PhD birthday and international dinner party members within ECO group for the nice time and fun after work. I am also grateful for Nikos Sotiropoulos, Cac N. Tran, Abhinav Rohit, dr. Fausto Gomez- Agiz and dr. Aaron Albores for sharing me their components from their experimental setup during my experiments. I am also grateful for sharing my office with Yan Shi, dr. Karen Solis-Trapala, dr. Davide Visani, dr. Shangjian Zhang and dr. Patrick Urban.

Finally, I am particulary indebted to all my families for their love, encouragement and great confidence in me for all these years. My special thanks go to my beloved wife, Tizta Tilahun and my lovely daughter Blen Solomon for their unwavering love and significant support in the difficult time. Last but not least, I owe this thesis to my mother Tamenesh Dori for her unconditional love, support, continuous encouragement, advice and confidence in me since I was a child.

Solomon Tesfay Abraha
Eindhoven, August, 2012
The Netherland

Curriculum Vitae

Solomon Tesfay Abraha was born in Adigrat, Ethiopia on August 03, 1979. In 2003, he received his B. Tech. Degree in Electrical Engineering, with specialization of Communication Technology from Defence University College, Debre Zeit, Ethiopia (*with Very Great Distinction*). He was Assistant Lecturer from 2003 to 2006 at Defence University College in Ethiopia. During 2006 – 2008, he received Netherlands Fellowship Program (NFP) scholarship grant from Delft University of Technology (TU Delft), The Netherlands. In 2008, he received his M.Sc. degree in Telecommunications Engineering from the Faculty of Electrical Engineering, Mathematics and Computer Science of TU Delft. In September 2008, he started working towards his Ph.D. degree in the ECO group of COBRA research institute at Eindhoven University of Technology (TU/e), The Netherlands. His Ph.D. work has been performed inside the EU FP7-ICT ALPHA project. His research focused on Impulse Radio Ultra Wideband (IR-UWB) over fiber techniques for broadband in-building network applications. His research interest also include optical access networks, radio over fiber (RoF) systems, high speed transmission over plastic optical fibers, optical wireless and adaptive digital signal processing for communication applications.

Solomon's work has been recognized with *KIVI-NIRIA Telecommunications Prize 2012* as the best Ph.D research work in the field of telecommunications among the three technical universities in the Netherlands, awarded by the Royal Institute of Dutch Engineers (KIVI-NIRIA). During his Ph.D. studies, he has authored and co-authored more than 15 publications in major journals and international conferences. He has also served as a peer-reviewer for Optics Letters and Optics Express.